Investigating the PKM2-dependent regulation of glycolysis by amino acids

Cassie Messenger

UCL

A thesis presented for the degree of Master of Philosophy in Biosciences

January 2022

Declaration

I, Cassie Messenger, confirm that the work presented in this thesis is my own. Where information has been derived from other sources, I confirm that this has been indicated in the thesis.

Abstract

PKM2 function can be regulated by multiple allosteric ligands and it is not yet well understood how these concurrent ligands come together to illicit one output for PKM2 regulation. Biochemically, amino acids that are PKM2 inhibitors and activators have been used in competition to investigate their combined effect on PKM2 activity, however this has not been monitored in cells including any effects this may have on wider metabolism.

In order to measure glucose metabolism and amino acid concentration within the cell, an LC-MS method was optimised in attempt to improve the current methods using a triple quadrupole mass spectrometer, however this method was not robust or reliable enough for requirements.

This project confirms that changing media conditions with various alanine to serine ratios, influences the intracellular concentration of alanine and serine. Subsequently, using labelled glucose to track how glucose is broken down in high inhibitor (alanine) and high activator (serine) conditions. Data confirm that there is no significant difference in glycolytic intermediate production between these two conditions. A trend of increased carbons metabolised through the serine production pathway in the high inhibitor treatment condition was observed, however this difference was not significant. This trend suggests there may be a build-up of glycolytic intermediates when PKM2 is inhibited, and therefore a higher production rate of serine. Data also suggest that there is an increased rate of TCA cycle intermediate production when cells are treated with a high activator A:S ratio, suggesting this media condition is influencing an increased activity of PKM2 compared to the high inhibitor treatment condition.

Impact Statement

This project will contribute to both the improvement of method capability investigating glycolytic intermediates and amino acids from metabolite extractions of cells and also the knowledge and understanding of metabolic PKM2 regulation within the cell.

Development of a triple quadrupole mass spectrometry LC-MS method for detecting multiple analytes from metabolic extracts would increase specificity and throughput compared to current methods. Generation of such a method would increase data quality in this area. The current standard methods using full scan GC-MS can be variable, are time consuming and destroy samples due to derivatisation. A triple quadrupole LC-MS method would allow sample retention, have increased throughput and specific analyte signatures can remove common issues such as ion suppression. This attempt at method development did not yield a robust method to use for this purpose, however, provides information on how this method can be improved and developed further in the future.

The published material on PKM2 and its metabolic regulation is vast and sometimes contradictory, although literature around PKM2 agree it is a pivotal in many cancers. This project aimed to increase clarity on the relationship between PKM2-activating and -inhibitory amino acid ratios in the cell and any effects on glycolysis, metabolic pathways branching from glycolysis and the TCA cycle. If we can understand this kind of regulation within the cell, it may increase clarity on the metabolic role of PKM2. With greater understanding of an enzyme like PKM2 and its implications in cancer, we can assess PKM2 as a drug target. Molecules such as TEPP-46 have been investigated as a PKM2 activator and have shown *in vivo* regression of tumours. However, greater understanding of PKM2 and its regulation could elude other ways to target PKM2, to increase its metabolic activity and influence it to behave more like its constitutively active isoform PKM1. This would provide a drug that could be used for many cancer types and due to the selectivity of PKM2 expression in cancer cells, would provide a selectivity window for treatment.

Acknowledgements

Firstly, I would like to thank my co-supervisors Dr. Dimitrios Anastasiou, Dr. Jonathan Hutchinson and Prof. Elizabeth Shephard for their guidance and supervision throughout this project. I am grateful to Dr. Dimitrios Anastasiou for allowing me to complete this project within his lab. I would also like to thank Prof. Matilda Katan as a part of my thesis committee for her feedback during my studentship.

I would like to gratefully acknowledge Melanie Leveridge, Dr. Sarah Nickolls and Sapna Desai as my various line managers and department directors at GSK for their support during this study. I would also like to thank GSK for funding this research.

For LC-MS expertise I would like to thank Dr. Bill Leavens and Chloe Tayler from GSK and for GC-MS expertise and measurements I would like to thank the Francis Crick Institute Metabolomics STP, particularly Dr. James Ellis and Dr. James Macrae.

It has been a pleasure to work with Dr. Patricia Figueiredo-Nunes, Natalie Bevan, Aakriti Jain, Dr. Louise Fets, Dr. Fiona Grimm, Dr Agustin Asuaje, Dr. Albert Thommen, Jack Carruthers and Antonia Kasampali within Dr. Dimitrios Anastasiou's lab at the Francis Crick Institute. Everyone provided invaluable guidance and support, especially Dr. Patricia Figueiredo-Nunes and Natalie Bevan.

Finally, I would like to thank my family for providing a support network during this project, with special mention to my partner Thomas Murton, for proofreading, aiding with presentation preparation and overall being my champion.

Contents

a

List of Figures

List of Tables

List of Abbreviations

ATP – Adenosine triphosphate

ADP - Adenosine diphosphate

AMP – Adenosine monophosphate

TCA – Tricarboxylic acid

NADPH – Nicotinamide adenine dinucleotide phosphate

DNA – Deoxyribonucleic acid

RNA - Ribonucleic acid

ROS – Reactive oxygen species

HK - Hexokinase

PFK - Phosphofructokinase

PK – Pyruvate kinase

HIF1α – Hypoxia-inducible factor 1-alpha

LDHA – Lactate Dehydrogenase

G6P – Glucose -6-phosphate

PPP – Pentose phosphate pathway

F6P – Fructose -6-phosphate

F 1,6 BP – Fructose -1,6- bisphosphate

F 2,6 BP – Fructose -2,6- bisphosphate

PEP - Phosphoenolpyruvate

PTMs – Post translational modifications

mTOR – Mammalian target of rapamycin

3-PG – 3-phosphoglycerate

SHMT – Serine hydroxy methyltransferase

GPT – glutamate pyruvate transaminase

GOT – Glutamic oxaloacetic transaminase

OAA – Oxaloacetate

GAP – Glyceraldehyde – 3 – phosphate

TAGs - Triacyl glycerides

UPLC – Ultra performance liquid chromatography

LC-MS – liquid chromatography mass spectrometry

HPLC – high performance liquid chromatography

HILIC – Hydrophilic interaction chromatography

m/z – mass to charge ratio

ESI – electrospray ionisation

MS/MS – tandem mass spectrometry

QQQ-MS – triple quadrupole mass spectrometer

SRM – single reaction monitoring

DP – declustering potential

EP – entrance potential

CE – collision energy

CXP – cell exit potential

FA – formic acid

ACN - acetonitrile

QC – quality control

A – Alanine

S – Serine

R – Arginine

E – Glutamic Acid

D – Aspartic Acid

C – Cysteine

K – Lysine

Q – Glutamine

H – Histidine

L – Leucine

I – Isoleucine

F – Phenylalanine

W – Tryptophan

V – Valine

M – Methionine

Y – Tyrosine

P – Proline

T – Threonine

G – Glycine

N – Asparagine

BSTFA – bistrifluoroacetamide

TMCS – trichloromethylsilane

HCl – hydrochloric acid

NaOH – Sodium hydroxide

MeOH – methanol

FBS – fetal bovine serum

dFBS – dialysed fetal bovine serum

PBS – phosphate buffered saline

PHDGH – phosphoglycerate dehydrogenase

PSAT1 – phosphoserine aminotransferase

PSPH – phosphoserine phosphatase

* - p value <0.05

* - p value <0.01

ns – not significant

Chapter 1:

Introduction

1.1 The dysregulation of macromolecule biosynthesis in cancer

The hallmarks of cancer were first proposed in a review by Hanahan and Weinberg in the year 2000 [1], suggesting characteristics that most, if not all, cancers would possess. These included enabling replicative mortality, sustaining proliferative signalling and activating invasion and metastasis. Over 10 years of research passed when the hallmarks of cancer were revisited by Hanahan and Weinberg [2], detailing the emerging characteristics in more recent literature. The four additional hallmarks described were, avoiding immune destruction, tumour-promoting inflammation, genome instability and mutation and, deregulating cellular energetics. Cancer cells have the ability to rewire their metabolism to promote cell survival, growth and proliferation [3]. It has also been proposed that this metabolic reprogramming is essential to fuel behaviours such as uncontrolled replication [2]. This altered metabolism includes changing the way that glucose is metabolised, commonly by increased glucose uptake and fermentation to lactate, even in the presence of plentiful oxygen and fully functioning mitochondria. This phenomenon is known as the Warburg effect [4].

Otto Warburg hypothesised aerobic glycolysis was the result of faulty mitochondria within the cancer cells [4]. This behaviour of high glucose uptake and lactate secretion is now more commonly described as aerobic glycolysis. This is where two molecules of ATP are generated per glucose molecule broken down in the cytosol, rather than using the tricarboxylic acid TCA cycle and oxidative phosphorylation in the mitochondria to generate ATP (Figure 1.1). Aerobic glycolysis was later confirmed in multiple studies after Warburg's initial discovery, but it has not been confirmed why cancer cells use this process over oxidative phosphorylation to process glucose and generate ATP [5]. These

studies also show that cancer cells have fully functioning mitochondria, contrary to Warburg's original theory [6], [7]. The Warburg effect is not a consistent phenomenon, it is more likely that a dynamic situation exists between aerobic glycolysis and oxidative phosphorylation, and this metabolic flexibility has now been observed in a range of cancers (Figure 1.1) [8], [9]. In some cancers, ATP production via aerobic glycolysis constitutes approximately 17%, with the remaining ATP generated by classical oxidative phosphorylation [10].

There are multiple hypotheses for cells favouring aerobic glycolysis over mitochondrial oxidative phosphorylation, including involvement from the tumour microenvironment. One possibility is that as tumours increase in size, cells become further away from their source of oxygen, nutrients and other growth factors. The distance oxygen can diffuse was modelled in 1919 by Krogh [11] and later confirmed experimentally [12]. The limit was determined to be 150 μm away from blood vessels. One hypothesis is that once cells are this distance from blood supply, they go through a normoxic-hypoxic cycle and only cells that have the capacity to cope with aerobic glycolysis, survive. As only these cells survive, even when oxic conditions arise again, cells retain this capacity for aerobic glycolysis and this phenotype is seen throughout the tumour [13]. Another proposition for this change in glycolytic metabolism is the availability of energy sources. Not only is oxygen in shorter supply, but also glucose, therefore when available to the cell it is used rapidly via aerobic glycolysis, to generate ATP as quickly as possible. A widely speculated contribution of glucose carbons is to biomass production. For two viable daughter cells to be generated by mitosis, the parent cell must double its biomass to allow both daughter cells to have all the contents they need to survive. Although ATP provides energy for biochemical reactions within the cell that are responsible for generating biomass, precursors and other metabolites are also required. Studies have identified that glucose and glutamine are the only metabolites catabolised in any significant quantity, meaning that most building blocks for increased biomass are provided by glucose and glutamine [14]. Therefore, using oxidative phosphorylation to generate ATP, does not fully prepare the cells for proliferation. If, instead, glycolytic intermediates are diverted into macromolecular precursors such as acetyl CoA for fatty acids, to ribose for nucleotides or non-essential amino acids through transamination, then the cell has what it requires

for growth and proliferation. An additional benefit of glucose breakdown, is the generation of nicotinamide adenine dinucleotide phosphate (NADPH), which also supports cell proliferation via its role in DNA synthesis and protection against reactive oxygen species (ROS) [14]. For this to be the case, there must be distinct regulation of aerobic glycolysis, for some cells to survive hypoxic conditions.

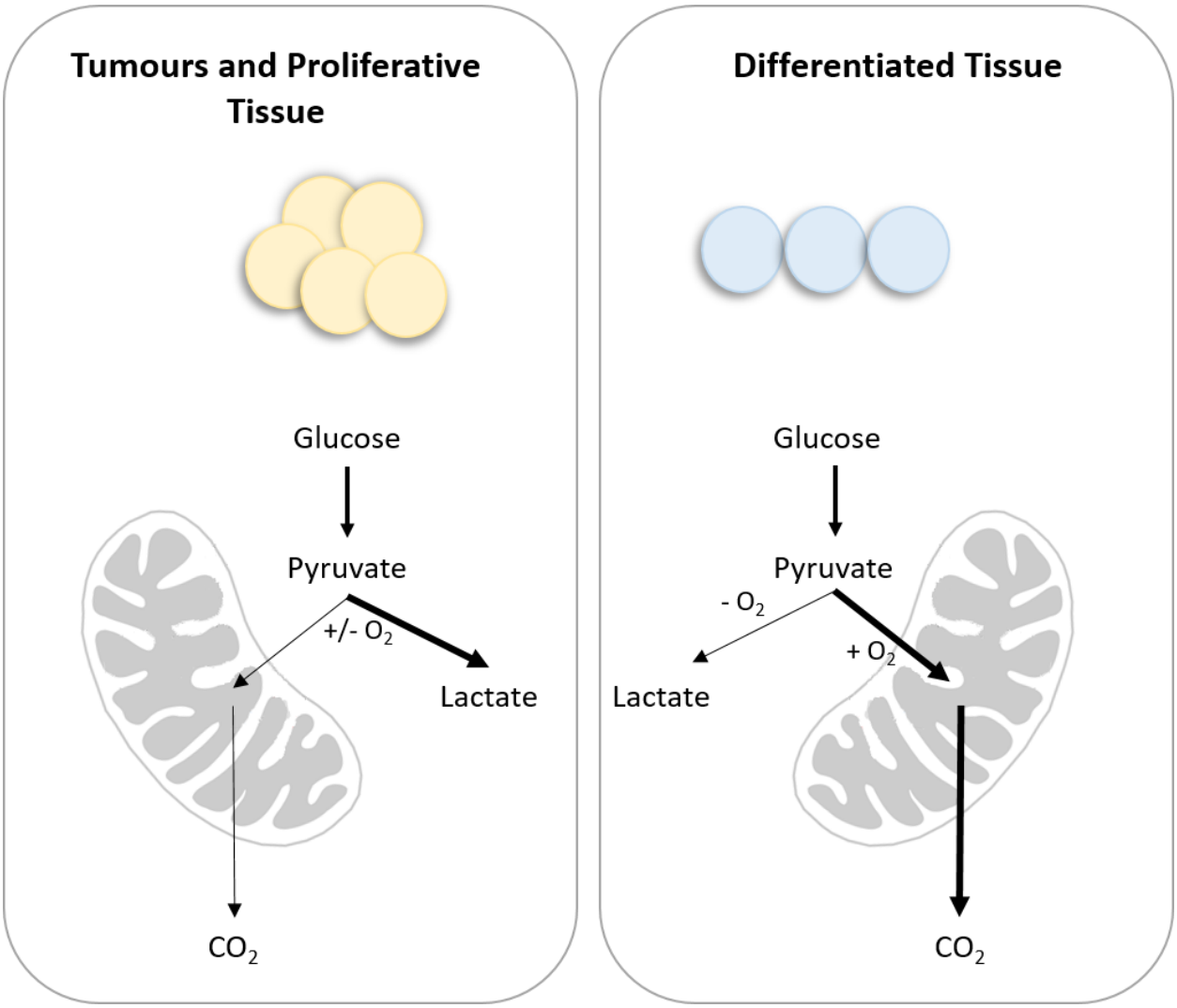

Figure 1.1: Schematic illustration of the balance between oxidative phosphorylation and aerobic glycolysis in normoxic or hypoxic conditions in both differentiated and proliferative tissues, such as tumours. In tumours and proliferative tissue, glucose is taken up into the cells at a higher rate and most of that glucose is fermented through aerobic glycolysis to lactate, rather than pyruvate being transported into the mitochondria for downstream processing. Conversely in normoxic differentiated tissue, most glucose in the cell in converted to pyruvate and transported into the mitochondria for downstream metabolism.

1.2 Glycolytic regulation contributes to the Warburg effect

The Warburg effect demonstrates a potential role of aerobic glycolysis in cancer progression. Therefore, the mechanisms that regulate glycolysis may influence a preference for aerobic glycolysis in cancer cells. Glycolysis provides cellular energy and metabolic precursors for biomass production through 10 enzymatic steps, breaking down glucose into two molecules of pyruvate and contributing to redox balance [15]. It has long been assumed that the key steps of glycolytic regulation relied on the irreversible steps of glycolysis, involving enzymes hexokinase (HK), phosphofructokinase (PFK) and pyruvate kinase (PK). Literature suggests that each of these enzymes acts as a control site and can be regulated by allosteric effectors, covalent modifications and expression regulation (Figure1.2) [16].

Oncogenes are responsible for the differential expression of glycolytic enzymes in cancer cells. Oncogenes that can cause an increase in glycolytic enzymes include hypoxia inducible factor (HIF1α), Ras and Myc. They can affect over 100 downstream genes across the metabolic network. Oncogenes such as these can induce the over expression of glucose transporters GLUT1 and GLUT3, increasing the availability of glucose within the cell [17]. They are also responsible for promoting a high glycolytic rate by converting the available glucose to pyruvate via the increased expression of hexokinase 1 and 2, phosphofructokinase 1, pyruvate kinase M2, and also lactate dehydrogenase (LDHA). LDHA is the enzyme responsible for converting pyruvate to lactate, preventing pyruvate entering the TCA cycle and downstream oxidative phosphorylation. Lactate transporters also have higher expression induced by HIF1α, promoting the secretion of lactate from the tumour to increase the acidity of the microenvironment, facilitating cancer cell invasion and promoting survival [17].

Enzymes are not only regulated by their expression, but activity can be regulated allosterically and via post-translational modifications such as phosphorylation and acetylation. Allostery is a process where proteins can relay the effect of ligand binding at one site to a distal functional site. Different mechanisms of allostery are described, including the model proposed by Monod, Wyman and Changeux in 1965 where pre-existing quaternary states tensed (T) and relaxed (R), undergo a conformation shift upon

ligand binding [18]. Various glycolytic enzymes can be regulated by such mechanisms and consequently affect glycolytic rate.

Hexokinase is the enzyme responsible for the first irreversible step of glycolysis, converting glucose and ATP to glucose-6-phosphate (G6P) and ADP. The reaction is inhibited in a negative feedback manner via product inhibition. High concentrations of G6P signal that no more glucose breakdown is required, which remains the case until enough of the G6P is consumed by conversion to glycogen or oxidation via the pentose phosphate pathway (PPP) [19]. The hexokinase isoform that exists in the liver however, also known as glucokinase, is not regulated by product inhibition. Glucokinase only phosphorylates glucose when it is highly abundant as glucokinase has a binding affinity for glucose significantly less than that of hexokinase. This reaction of phosphorylating glucose is therefore regulated differently depending on the tissue.

Phosphofructokinase (PFK) catalyses the 3rd step in glycolysis, the irreversible conversion of fructose-6-phosphate (F6P) and ATP to fructose-1,6-bisphosphate (F 1,6 BP) and ADP. This reaction has been described as the most important control element of the entire pathway and has multiple regulatory mechanisms that in turn allows regulation of glycolytic flux. High levels of ATP lower PFK affinity for the substrate F6P by binding allosterically. AMP can reverse this inhibition by ATP via competition for the same binding pocket. This competition for the same binding pocket provides tight control of PFK activity as changes in the adenylate pool are responsible, so small changes in ATP concentrations result in magnified changes in AMP concentration. This allows glycolysis to be controlled by the overall energy charge of the cell. PFK has many other allosteric regulators, such as downstream TCA cycle intermediate citrate, allosterically binding to inhibit PFK activity in a negative feedback manner. Another allosteric binding site present on PFK is for allosteric ligand fructose - 2,6 - bisphosphate (F 2,6 BP), which is the most potent allosteric activator of PFK known. F 2,6 BP is generated from F6P and acts in a positive feed forward loop, preparing PFK to increase activity in response to increased glucose being processed [19].

Pyruvate kinase (PK) is the final enzyme in the glycolytic pathway, and due to many possible forms of regulation and non-canonical functions, is thought to play a key role in glycolytic regulation [16].

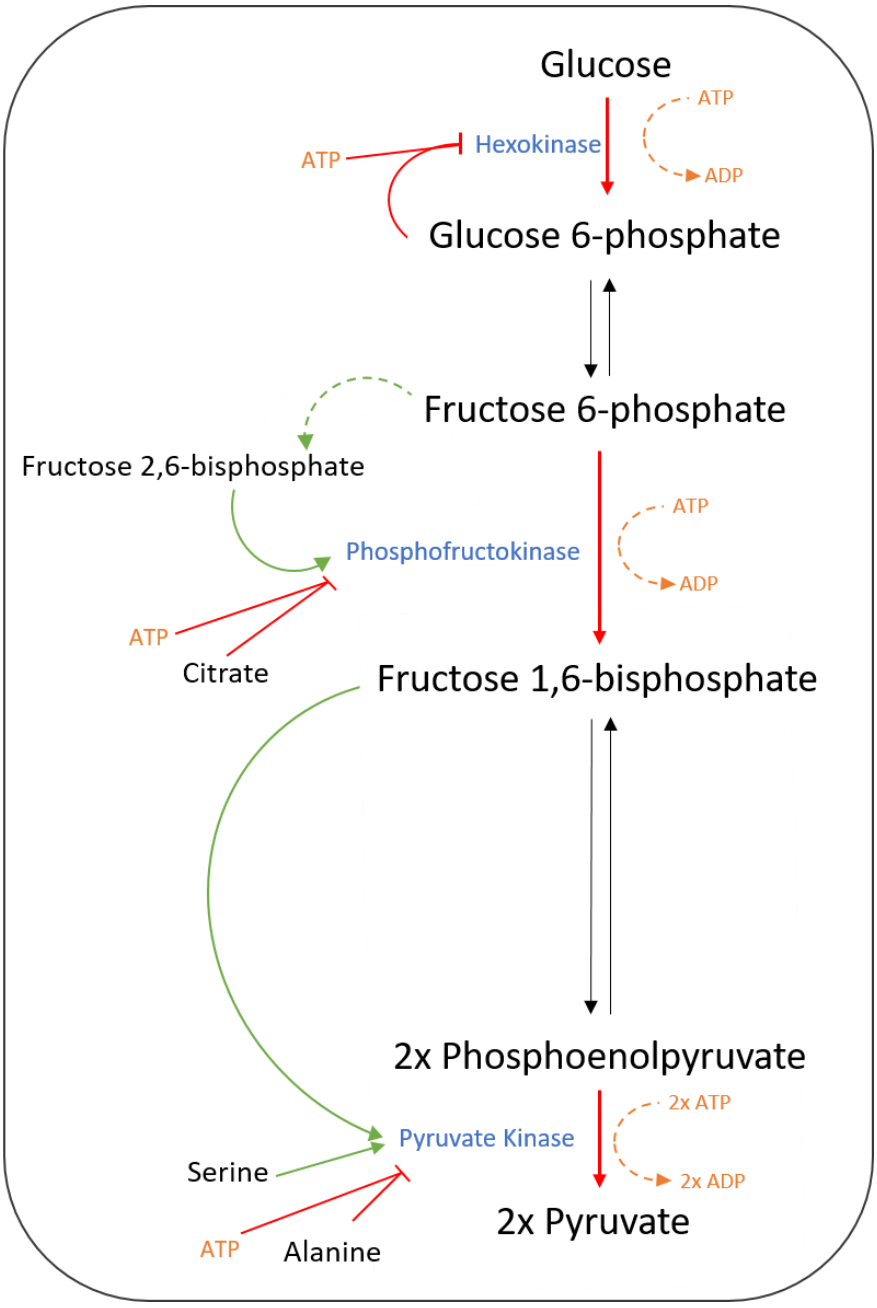

Figure 1.2: Schematic illustration representing the main control points of glycolytic regulation, and how feedback, feedforward and allosteric interactions accelerate or inhibit glycolysis. The illustration identifies Hexokinase as the first point of regulation in the pathway, and highlights the inhibitory action of ATP on this reaction. The second regulatory point highlighted in this pathway is phosphofructokinase (PFK). The green arrows show the feed-forward activation of PFK by fructose 2,6 bisphosphate allosteric binding. The red arrows show the inhibitory action of ATP and citrate on PFK. The final enzyme highlighted is PKM2, where green arrows show the feed forward activating effects of F 1,6 BP and serine, and the inhibitory effects of alanine and ATP.

1.3 Pyruvate kinase activity can be regulated by multiple means including allostery

PK is the enzyme that catalyses the final and irreversible step in glycolysis, converting phosphoenolpyruvate (PEP) and ADP into ATP and pyruvate. Mammalian PK exists as different isoforms encoded by different genes; the *PKLR* gene which encodes the PKL and PKR isoforms of PK, expressed in the liver and blood cells, respectively, and the *PKM* gene, which is expressed in most other tissues such as muscle and the brain. The *PKM* gene itself exists as two splice isoforms, PKM1 and PKM2. The Schematic 1.3 illustrates the exons that are alternatively spliced to generate mRNA for PKM1 or PKM2. This differential splicing causes a difference between the two proteins of 22 amino acids, giving rise to distinct regulatory properties. PKM1 forms a stable constitutively active tetramer, whereas PKM2 activity can be regulated by changes in conformation of the tetramer [20].

PKM2 is preferentially expressed over PKM1 in highly proliferating cells, including in cancerous cells, during embryogenesis and tissue regeneration [21]. Given that PKM2 is expressed in non-transformed cells and during embryonic development, it is likely, the presence of PKM2 influences the metabolic environment in such a way, that is conducive to cancer cell survival. A study has demonstrated that by knocking down PKM2, tumours can still progress and survive, therefore suggesting that PKM2 is not necessary for tumour maintenance. Instead, PKM2 regulation is hypothesised to be pivotal in tumour cell plasticity, regarding metabolism [22]; an increase in PKM2 activity may supress tumour growth [23]. There is plentiful literature published surrounding PKM2, however, the role of PKM2 in cancer is not clear, and more investigation is necessary to understand this important enzyme in cancer metabolism.

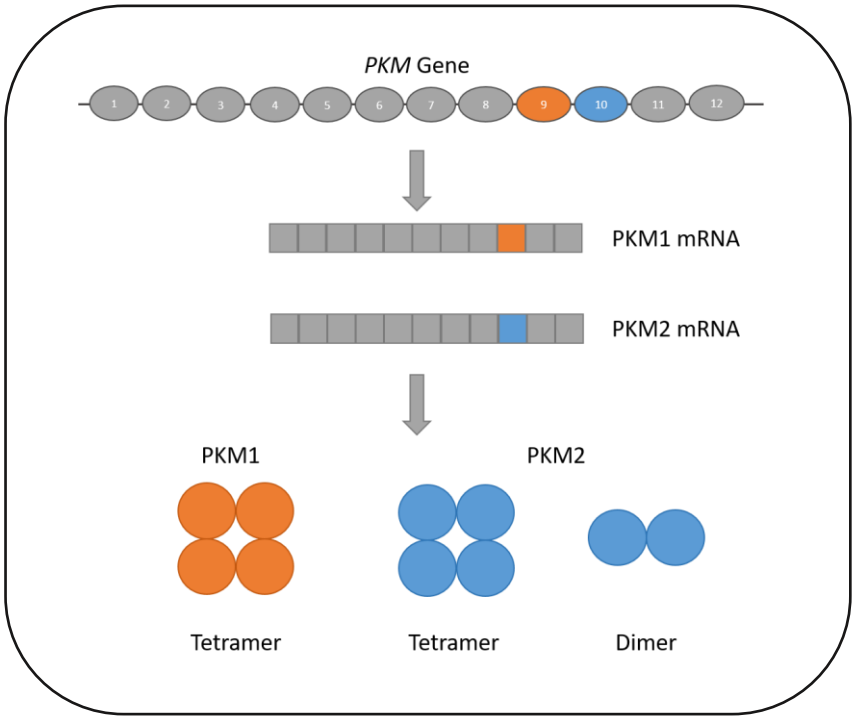

Figure 1.3: schematic illustration to demonstrate the alternative splicing between PKM1 and PKM2. The illustration demonstrates the exclusivity of PKM1 and PKM2 mRNA expression and therefore protein expression. Exon 9 is transcribed and translated for PKM1, highlighted in orange, and exon 10 is transcribed and translated for PKM2, highlighted in blue. This exclusivity generates a constitutively active tetramer for PKM1, and a mixture of highly active tetramers, and poorly active dimers for PKM2.

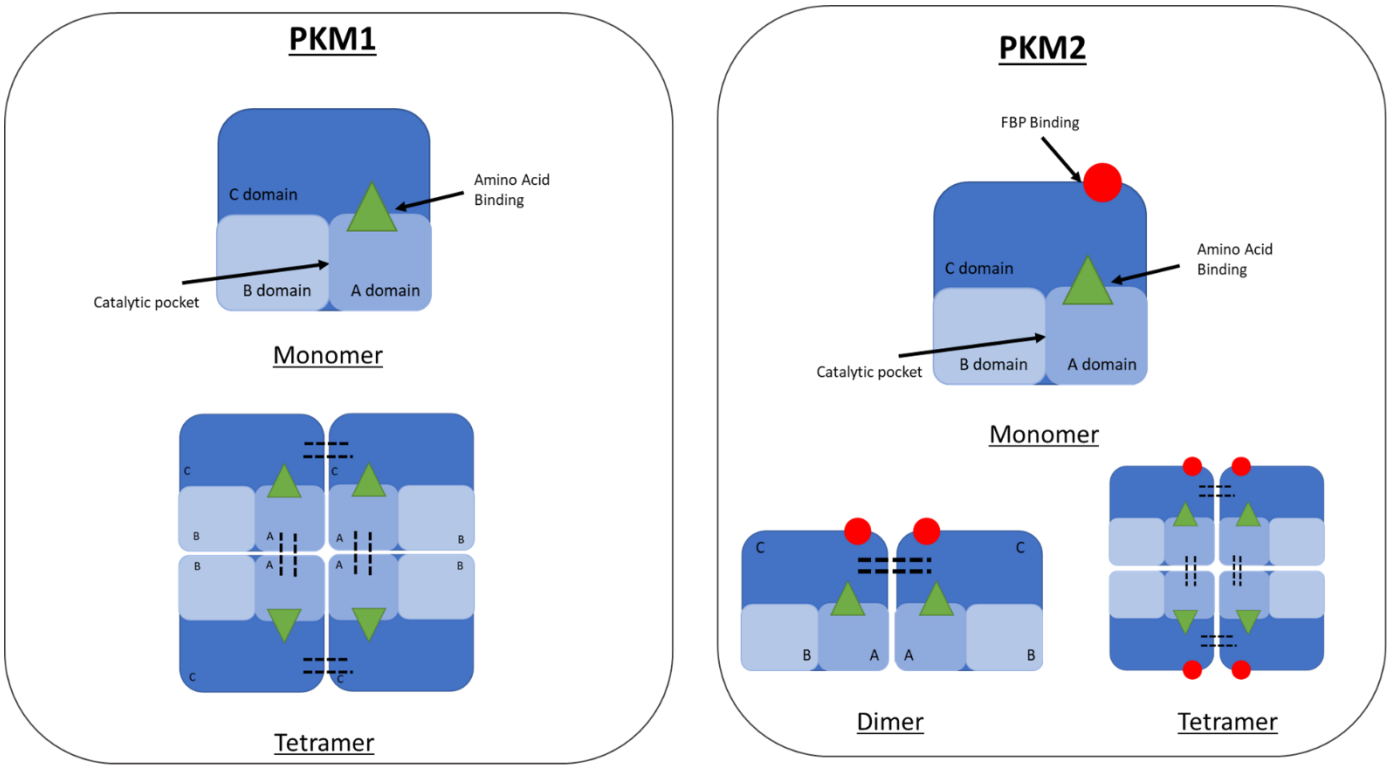

Figure 1.4: schematic illustration to demonstrate the domains of pyruvate kinase and how they differ between isoforms PKM1 and PKM2. The main difference being the presence of the FBP binding pocked in the C domain of PKM2, whereas this is not present on PKM1. Domains are highlighted as well as the FBP, amino acid and catalytic binding pockets. The black dashed lines show the interactions between domains where the A-A interfaces are bound first to generate the dimer, and these dimers come together and interact via the C-C interfaces, which are also identified by black dashed lines. PKM1 exists exclusively as a tetramer, whereas PKM2 can exist as the dimer and monomer, as well as the tetramer [20], [30].

PK consists of four domains (A, B, C and N) and presents as a dimer-of-dimers. The connection between the subunits in the initial dimer consists of intermolecular contacts between the two A domains. Two dimers then come together via interfaces in the C domains, and the active site of PK resides in a pocket between the A and B domains (Figure 1.4) [20]. PKM2 has many means of regulation including allostery and post-translational modifications (PTMs), something not seen for the constitutively active isoform PKM1.

PTMs recorded for PKM2 include phosphorylation, acetylation, oxidation and sumoylation and they affect both canonical and non-canonical functions of PKM2 that support cancer progression. PKM2 can be phosphorylated by oncogenic tyrosine kinases such as FGFR1 and JAK2 at Y105 (A domain). This phosphorylation decreases PKM2 activity and therefore promotes tumour growth [24]. Other phosphorylation events are mediated by serine/threonine kinases, for example ERK2 phosphorylates PKM2 at S37 (N terminal domain) to promote dimer formation of PKM2 and induces the translocation of dimeric PKM2 to the nucleus to complete non-canonical functions, such as behaving as a transcriptional coactivator of β-catenin [24]. This leads to downstream expression of c-myc and therefore increased expression of GLUT-1, LDHA and PKM2 via positive feedback. High concentrations of reactive oxygen species (ROS) cause oxidation of C358 of PKM2, resulting in the dissociation of the highly active tetramer. This oxidation renders PKM2 inactive, therefore causing glycolytic intermediates to accumulate and be forced through the pentose phosphate pathway (PPP), which is sufficient to detoxify ROS, allowing cells to cope with the high concentration of ROS which initiated the cascade [25]. Different isoforms of PKM2 can have different post-translational modifications that can regulate activity; PKL for example, can be reversibly phosphorylated. In the liver, when blood glucose level is low, the glucagon triggered cAMP cascade causes the phosphorylation of PKL, hindering the catalytic activity. This prevents a futile cycle while hepatic gluconeogenesis is required and is reversible when glucose becomes plentiful again [26], [27].

The 22 amino acid difference on the C-C interface between the two isoforms of PKM, contributes to the tight inter-subunit interface and prevents dissociation of the active tetramer through an allosteric binding pocket, which binds F 1,6 BP, an upstream metabolite in glycolysis (Figure 1.4). F 1,6 BP is a feed-forward activator, preparing lower glycolysis for increased flux of glucose carbons. F 1,6 BP shifts the monomer-tetramer equilibrium towards tetramer formation and therefore increasing the activity of PKM2 [28] [20] [29] [30].

F 1,6 BP binding stabilises the highly active R-state by placing the sidechain of Arg342 in an appropriate position to form a hydrogen bond with the helical stretch between Arg294-Glu300 in an adjacent protomer [31]. The formation of this bond primes

the active site to receive a PEP molecule and prevents the dissociation of the tetramer. In this stabilised highly active R-state, the C-C and A-A interfaces are linked by 20-cross interface hydrogen bonds. The poorly active T-state holds a different network of hydrogen bonds across the A-A and C-C interfaces. Inhibitors promote an 11° rotation of the Arg294-Glu300 α-helical stretch compared to the R-state, in which four salt bridges that stabilise the R-state, change to stabilise protomers across the A-A interface in the poorly active T-state. This causes the active site to widen and increase the K_M for PEP (Figure 1.4) [29], [32]. The dynamic regulation between these two states allows a fast response to the environment, rather than the slower mechanism of association and dissociation of the tetramer [33].

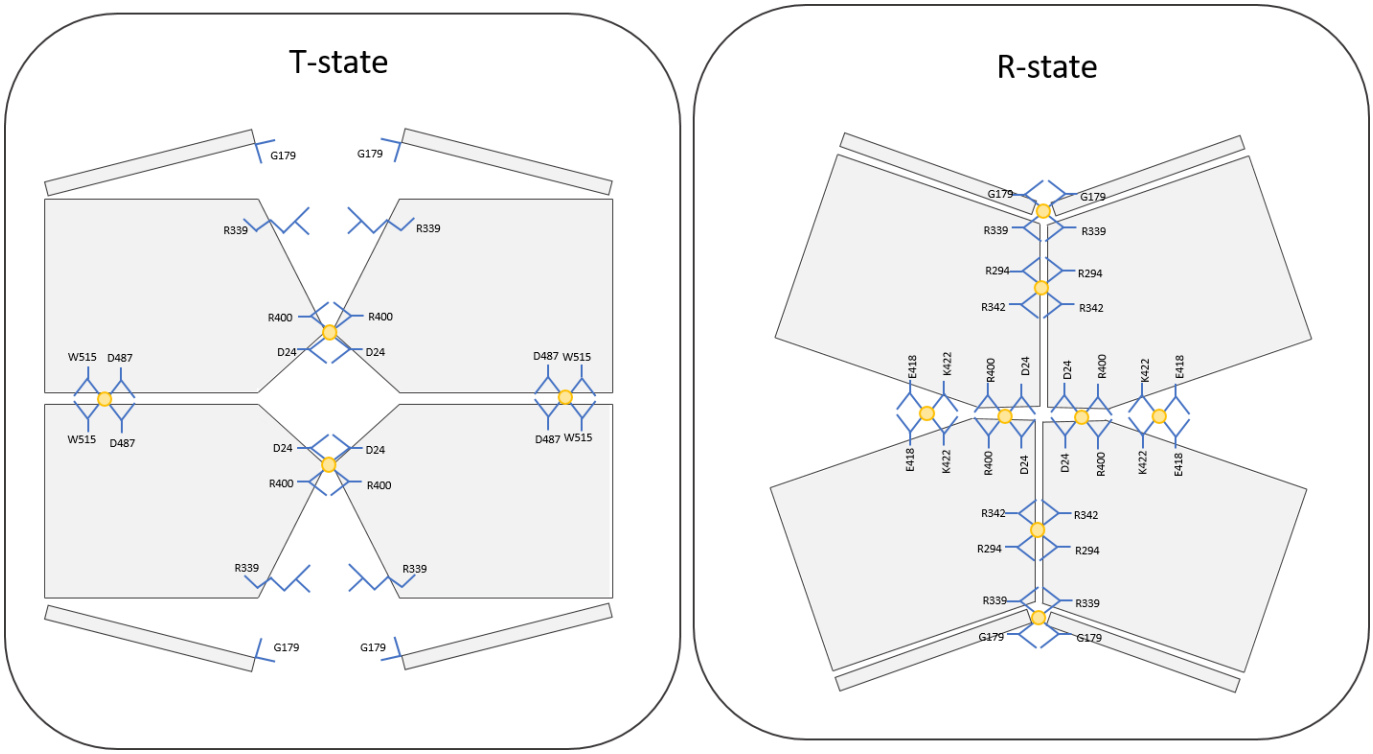

Figure 1.5: Schematic illustration of the T- and R- states of PKM2 highlighting the specific interactions that are involved and change between the two conformation states. Specific amino acid residues involved in the bonds and interactions between the subunits. In the R- state the N-terminus is pulled closer than in the T- state and more interactions completed between the C-C interface.

Various amino acids can bind to an allosteric binding pocket present on both PKM1 and PKM2. Inhibitors including alanine, phenylalanine and tryptophan bind to this pocket on PKM2 and induce the T-state conformation. However, these are not the only amino acids known to bind to and alter the tetramer conformation to cause a change in PKM2 activity. Other inhibitors include valine, methionine and proline [34] [35]. Amino acids can also promote the R-state conformer and therefore increase PKM2 activity, these include serine and histidine which compete with inhibitors such as alanine, for the same binding pocket [36]. This allosteric interaction and change in activity has been demonstrated biochemically where amino acid concentrations are controlled and in excess, however in an intracellular environment, amino acid levels are constantly changing [29], [37].

1.4 Amino acid homeostasis can influence carbon metabolism within the cell

Varying levels of intracellular amino acids can occur via cellular entry and exit of amino acids through transporters, *de novo* synthesis and catabolism of amino acids, and biosynthesis and degradation of proteins (Figure 1.5). All of these factors provide intracellular amino acid concentration homeostasis [38]. There are essential amino acids that cells cannot synthesise, therefore, to increase the intracellular concentration of these amino acids, they must come from broken down proteins, or import into the cell from external sources. The remaining amino acids are non-essential. This means they can be generated within the cell by various pathways.

Transport is vital in ensuring a homeostatic pool of all 20 amino acids inside the cell, not only essential amino acids. Facilitated import into cells is required to increase the intracellular concentrations of amino acids from the circulation provoking the need for specific amino acid transporters. These have been identified based on their physicochemical properties and selectivities for specific amino acids [38], [39]. Many of these transporters require sodium as part of the translocation process for maximal activity and ensure a harmonised mixture of all 20 amino acids within the cell. When one essential amino acid is depleted through protein biosynthesis, signalling or metabolism, it is more likely that amino acid will be imported actively against an abundant intracellular amino

acid. This balance between import and export helps maintain amino acid abundance inside the cell. Alanine, glycine and glutamine are the most abundant amino acids in blood plasma and are all substrates of Na^+ - neutral amino acid transporters. These three amino acids are highly abundant within the cell, and therefore are readily used as exchange currency to drive uptake of other amino acids [37]. Alanine, glycine and glutamine are non-essential amino acids and therefore can be synthesised within the cell for exchange purposes. This synthesis is often triggered by amino acid starvation or restriction. Starvation or restriction also causes the upregulation of other amino acid transporters such as SNAT2 for exchange in the cytosol [40].

Cell starvation of amino acids can activate amino acid biosynthesis, which can trigger cell growth and changes in metabolism. One of the most well studied intracellular amino acid sensors is the mTOR pathway and most specifically the mTORC1 complex. Through amino acid sensing in the cytoplasm, an active mTORC1 complex can increase protein biosynthesis and supress autophagy through downstream signalling [41] . Many amino acids can affect mTORC1 activity, the mechanism of those well understood include methionine, leucine and arginine [38]. mTORC1 is not the sole regulator of amino acid synthesis, other pathways exist to generate new amino acids or cause catabolism. Serine for example, is generated by the serine production pathway, a 3-step process branching from glycolysis and glycolytic intermediate 3-phosphoglycerate (3-PG). Newly-synthesised serine, and imported serine are readily converted to glycine via the enzyme serine hydroxy methyltransferase (SHMT2), which in turn can provide carbons for further metabolism and NADPH to support redox balance [39] [43]. Many amino acids are generated by transaminases or amino transferases, a group of enzymes that generate amino acids from α-keto acids and a nitrogen donor. Alanine transaminase (GPT) is the enzyme responsible for the generation of alanine and α-ketoglutarate from pyruvate and glutamate. There are two isoforms of GPT (GPT1 and GPT2), that are separated by compartmentalisation. GPT1 is localised in the cytoplasm and processes pyruvate generated by glycolysis. GPT2 exists in the mitochondria and processes pyruvate generated by glycolysis and transported to the mitochondria [44]. This allows the generation of alanine in the different locations or cellular compartments where it is required. Many other transaminases exist within the cell including glutamic oxaloacetic

transaminase (GOT), which is responsible for the interconversion of aspartate and oxaloacetate [45]. All 20 amino acids, in some way, contribute to a wide array of cellular metabolic processes, which include biosynthesis of nucleotides, lipids and proteins, as well as glutathione and can provide carbons for the TCA cycle [46]. Newly generated non-essential amino acids and essential amino acids from nutrients can be used in many ways, including behaving as signalling molecules to effect cellular metabolism. Examples of this include modulating intracellular calcium levels and activation of the ERK pathway [47]. Free amino acids are also used up during translation for protein generation, generation of nucleic acids and lipids, all vital during cell growth and proliferation [48].

Both the anabolism and catabolism of amino acids by multiple means, ensures amino acid homeostasis within the cell with constant turnover of amino acids [38]. This careful balance of transport, de novo synthesis and protein translation or degradation keep amino acids at the appropriate level within the cell, depending on the needs of the cell at that time [49].

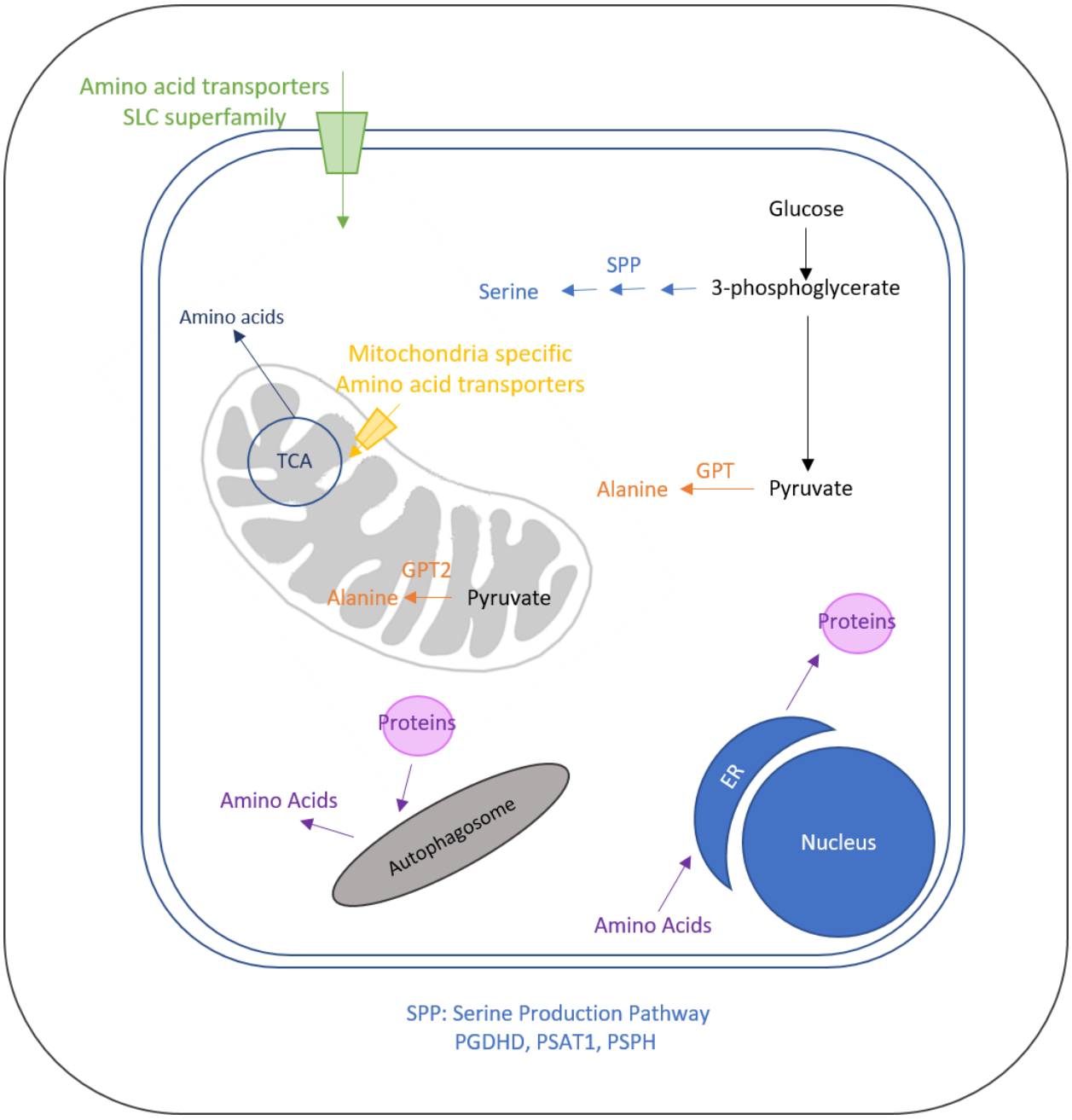

Figure 1.6: illustrative schematic to highlight different mechanisms of amino acid homeostasis. Of many mechanisms that exist within the cell to achieve amino acid homeostasis, transporters, such as the SLC superfamily are highlighted in green to show that amino acids are actively transported into the cell. To highlight that non-essential amino acids can be generated within the cell, the pathways or enzymatic steps to make serine and alanine are shown in blue and orange, which branch off in pathways from glycolytic intermediates. 3-PG and pyruvate, respectively. This diagram also highlights that amino acids can be made in the mitochondria as well as transported in and out of the mitochondria. Amino acids are also used in translation of proteins, but in the same context, can be claimed back in the cell by the degradation of proteins via the proteosome.

1.5 Concurrent regulation of PKM2 via multiple ligands may influence glycolytic flux

Literature shows across many studies that amino acids exist within cells from the high micromolar to millimolar range depending on the state of the cell and the stage of the cell cycle [50], [51]. Cancer cells undergoing proliferation can exhibit large variations in amino acid abundance depending on the stage of the cell cycle and the microenvironment [52]. Amino acids bind competitively to an allosteric binding pocket on PKM2, which alters enzymatic activity, so with such fluctuation in amino acid levels, how do the levels of activating and inhibitory amino acids affect PKM2 activity as allosteric ligands, in combination with F 1,6 BP?

Biochemical studies have shown that amino acids can have an activating or inhibitory effect on PKM2 activity. Inhibitory and activating amino acids are competitive in binding to the same allosteric binding pocket. Once bound, they act collectively to affect substate binding [37]. An inhibitory allosteric ligand such as alanine can bind mutually with the substrate PEP and increase cooperativity, this in turn has an inhibitory effect on PKM2 activity decreasing the V_{max} in specific activity experiments. This happens over a concentration range of high micromolar (800 µM) to low millimolar (3.6 mM), the same concentration range likely within proliferating cells. A concentration dependent response is also seen with the allosteric activator serine, which changes the V_{max} and K_M for PEP resulting in an increase in PKM2 specific activity. [37]. The final effect on PKM2 regulation, results from the competition of activating and inhibitory amino acids for the same allosteric binding site. The same study demonstrates how the effect of serine as an activator reverses the effects of inhibitor alanine to a certain degree, with partial rescue of activity, indicating how multiple ligands come together to regulate PKM2 activity. In this study the approximate intracellular concentration of alanine was measured at 0.5 mM and serine is 0.6 mM, however as mentioned, amino acid abundance can vary within proliferating cancer cells with alanine up to 10-fold higher and serine 2-fold higher than normal tissue. Therefore, depending on the relative concentrations of alanine and serine, and other activating and inhibitory amino acids, PKM2 activity can vary widely [37].

A study investigating the role of specific residues involved in the allosteric regulation of PKM2, modelled how ligands binding to allosteric binding sites would affect

PKM2 activity [53]. The study found that the intracellular concentration of allosteric activator F 1,6 BP, within the cells tested, was high enough to saturate PKM2, rendering it constitutively active, yet in these cells, and other cancer cells, we see the characteristic Warburg metabolism, meaning that PKM2 cannot be constitutively active. However, in this study, the concentrations of activating and inhibitory amino acids, serine and phenylalanine respectively were at intracellular concentrations around their respective K_D values for PKM2 [53]. This led to the hypothesis that it is the ratio of activating and inhibitory amino acids within the cell that regulate PKM2 activity, and by extension glycolysis, even though F 1,6 BP concentrations are high enough to render PKM2 constitutively active.

The complex regulation of PKM2 is proposed to be a part of glycolytic regulation that links back to Warburg metabolism. Firstly, PKM2 activity can be regulated, unlike constitutively active PKM1. PKM2 and its low activity compared to PKM1, favours aerobic glycolysis, processing carbons from pyruvate into lactate for secretion from the cell. Low PKM2 activity should decrease the production of lactate, however we actually observe an increased lactate production, and this is known as the PKM2 Warburg paradox. One proposed mechanism for this involves oxaloacetate (OAA). OAA is a competitive inhibitor of LDHA and the cytosolic concentration of OAA is influenced by PK activity. Glutamine pyruvate transaminase (GPT2), converts pyruvate and glutamate to alanine and α-ketoglutarate (α-KG). α-KG is then converted to OAA through the TCA cycle, which PKM2 activity can also influence. Therefore, if PKM2 activity is low, then there is a lower concentration of cytosolic OAA and therefore lower inhibition of LDHA, increasing the production of lactate and preserving the Warburg effect [54].

If PKM2 activity is decreased, carbons from glycolytic intermediates can be re-routed to generate cellular components required for cell growth and proliferation [55]. Glucose-6-phosphate (G6P) is a substrate for the pentose phosphate pathway (PPP), generating ribulose 5-phosphate which can in turn be used to generate purine nucleotides, in the process also generating NADPH [56]. Glyceraldehyde-3-phosphate (GAP) can be a carbon starting point and combined with acetyl CoA for the generation of triacyl glycerides (TAGs). 3-phosphoglycerate (3-PG) is the first substrate in the serine production pathway where cells can generate de novo serine, and this serine can be

subsequently processed to generate glycine. PKM2 has also been implicated in cellular antioxidant responses. Reactive oxygen species (ROS) cause inhibition of PKM2, causing diversion of carbons from glycolysis through the PPP. This diversion generates sufficient reduction potential to detoxify the increased ROS in the cell [25]. Therefore, by slowing down glycolysis via PKM2, this results in a build-up of glycolytic intermediates that can be used to increase cellular biomass ready for cell growth and proliferation and affect the redox balance of the cell (Figure 1.6) [57].

To track how many glucose-derived carbons are incorporated into macromolecules for cellular growth and increased biomass, labelling studies have been conducted with aim to quantify this. In one study, uniformly ^{13}C labelled glucose was given to cells. After two days incubation, 76% of labelled glucose being secreted as lactate, demonstrating aerobic glycolysis. 9% of those labelled carbons were included into proteins, 7% of those carbons were present in other sugars and glycerol, 4% were incorporated into lipids and only less than 1% was incorporated into purine nucleotides. The hypothesis for the lack of incorporation into purine nucleotides is that glycine can used as an alternative source to glucose. Summarising these data, 22% of carbons from glycolysis are incorporated into biomass, ready to support cell growth and proliferation. The activity level of PKM2, changing between the inactive T-state and active R-state, may be influential in that fast-changing dynamic depending on the cells' needs [58].

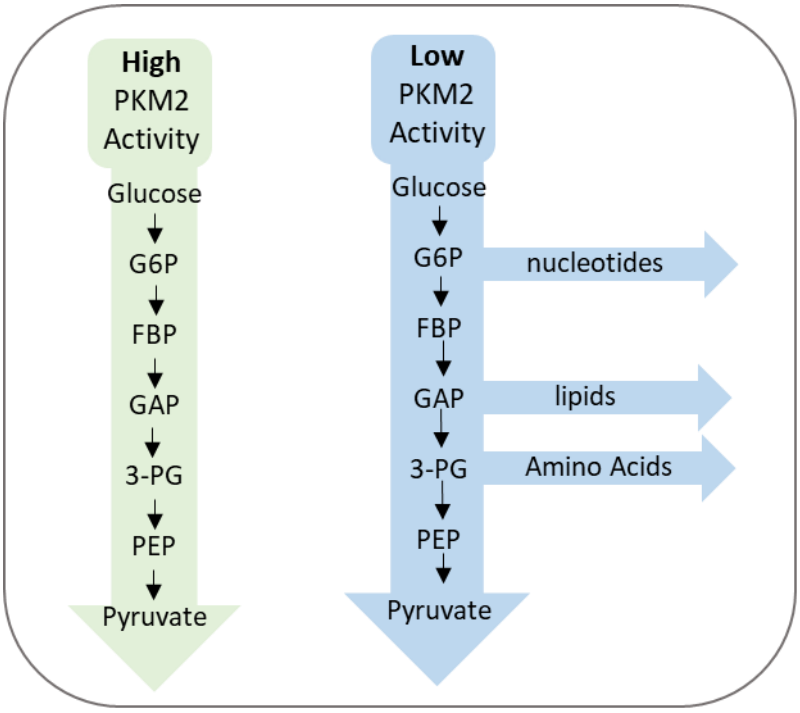

Figure 1.7: Schematic illustration of how PKM2 with high and low activity can cause changes in how carbons from glycolysis are processed. If PKM2 activity is high, then glucose is funnelled very quickly into the production of pyruvate. This is because the final step of glycolysis, the stage PK is responsible for, is very fast, then more glycolytic intermediates are required for this reaction. Conversely, if PKM2 activity is low, then PEP is not required in such high amounts, therefore upstream glycolytic intermediates are not required. Therefore, these unrequired intermediates can be used for other metabolic pathways, such as the generation of nucleotides from accumulated G6P, the generation of lipids from GAP and the production of serine and therefore glycine from 3-PG. The products of these reactions can then be used in increasing the cell biomass for proliferation.

1.6 Project Aims

The above evidence indicates that PKM2 could be a central regulation point for aerobic glycolysis and biomass production in preparation for proliferation. Understanding the effects of multiple intracellular allosteric ligands influencing this regulation is vital in understanding the behaviour of PKM2 in cells.

Previous studies suggest amino acids bind to PKM2 in a competitive manner even in the presence of allosteric activator F 1,6 BP [53]. This raises the possibility that PKM2 activity, and by extension glycolysis, are regulated by the combined action of amino acids and F 1,6 BP binding, rather than F 1,6 BP alone. To test this hypothesis, this project will focus on alanine and serine as model amino acids, as they are known to have competing inhibitory and activating effects on PKM2, respectively.

To investigate this hypothesis, Chapter 2 details the attempt to generate an optimised liquid chromatography tandem mass spectrometry method using a triple quadrupole mass spectrometer, to create a highly specific single reaction method for all analytes of interest. This method will allow the separation and detection of multiple metabolites of interest for quantification using a triple quadrupole mass spectrometer, something not detailed currently in literature for this combination of metabolites.

Chapter 3 will describe the use of the methods investigated in Chapter 2, to determine intracellular concentrations of metabolites, including alanine and serine in LN229 cells. Intracellular amino acid concentrations will be manipulated by altering the media composition, which will contain ^{13}C-glucose as an energy source, in order to investigate downstream metabolites in glycolysis, the TCA cycle, and branching metabolic pathways to monitor cellular metabolism in different media conditions. Data in Chapter 3 will confirm if the intracellular concentrations of alanine and serine can be manipulated by changing media conditions and investigate the effects on intracellular metabolites.

This project will attempt to increase clarity on the complex regulation of PKM2 and the relationship with glycolytic flux. Decoding this complicated system of concurrent regulation by multiple allosteric ligands, contributes to investigating PKM2 as a disease target for multiple cancers.

Chapter 2

Materials and Methods

2.1 Materials and methods for the development and validation of an appropriate mass spectrometry method to detect intracellular analytes

Table 2.1.1 Solid pure materials used for LC-MS assay development and validation, and treatment media generation. All components were made to a 100 mM solution using the solvent stated in the table.

Table 2.1.1		
Component	**Cat. No**	**Solvent**
L-Glycine	G8790	H_2O
L-Arginine	11009	H_2O
L-Asparagine	A4159	H_2O
L-Aspartic acid	A7219	HCl (1M)
L-Cystine	30200	H_2O
L-Glutamine	G3126	H_2O
L-Glutamic acid	G8415	HCl (1M)
L-Histidine	H6034	H_2O
L-Isoleucine	17403	H_2O
L-Leucine	L8000	H_2O
L-Lysine	44208	H_2O
L-Methionine	M9625	H_2O
L-Phenylalanine	P2126	H_2O
L-Proline	P5607	H_2O
L-Serine	S4311	H_2O
L-Alanine	A7469	H_2O
L-Threonine	T8441	H_2O
L-Tryptophan	T0254	HCl (1M)
L-Tyrosine	T3754	HCl (1M)
L-Valine	V0513	H_2O

D-Glucose	G7021	H_2O
U-13C-D-Glucose	389374	H_2O
F16BP	J6625609	H_2O
Pyruvate	BP356	H_2O
Lactate	L7022	H_2O
13C 15N Valine	600148	H_2O
Water	TS-51140	-
Acetonitrile	TS-51101	-
Formic Acid	TS-28905	-
Sodium Bicarbonate	S6014	H_2O
Basal DMEM Powder	D9800-27.10	H_2O
Hydrochloric Acid (HCl)	7647-01-0	-

Table 2.1.2 details the standard parameters of the triple quadrupole mass spectrometer (SCIEX Triple Quad ™ 6500+ system). These mass spectrometer settings were used for all LC-MS assay development and validation.

Table 2.1.2

Component	**Value**
Curtain gas	30 (a.u.)
CAD	9 (a.u.)
Ion spray voltage	4000 V
Temperature	650 °C
QS1	85 PSI
QS2	85 PSI
Collision gas	Nitrogen

2.1.1 Analysis of LC-MS data

Analyst software 1.7.2. Quantitation method wizard was used to analyse the data. A quantitation method was optimised using standards within the sample run to confirm the retention time and applied a peak smoothing factor to all of the peaks. This method was then applied to the rest of the unknown samples and the peak areas for each analyte in each sample were calculated. The peak areas were then plotted in GraphPad Prism

(version 8) for visualisation. QC samples of known concentrations of media or standard mix were analysed alongside the calibration curves and accuracy of the measured QC sample was calculated using the calibration curve. Accuracy was determined by calculating the average measurements for known standards and calculating the deviation of the unknown samples from that measured average.

2.2 Materials and methods used to investigate intracellular metabolite concentrations

2.2.1 Bioinformatics – Identification of cell lines

Gene expression data for the cancer cell line database [69] was filtered to analyse the expression of phosphoglycerate dehydrogenase (PHGDH), phosphoserine aminotransferase 1 (PSAT1), phosphoserine phosphatase (PSPH), GPT and GPT2. These data were then filtered again to isolate cell lines where the gene expression Z score was greater than 3 or less than -3 for any of the enzymes of interest. Z scores indicate the number of standard deviations away from the mean expression of the reference. These data were then clustered based on trends in expression within each enzyme and the data were visualised as a heatmap using R (version 3.6.2) and "pheatmap" (Kolde, 2015).

2.2.2 Treatment media generation

Media for cell treatments were generated as described in section 2.2.5. DMEM powder without amino acids or glucose (US-biological D9800-27), was made as per the manufacturer's instructions with sodium bicarbonate at 44 mM (BP328-1) and adjusted to pH 7.4 using 10M NaOH before filtration. This basal media was stored at 4 °C until use. If required by the media condition amino acids other than alanine and serine, were supplemented in the media to the concentration they are in basal DMEM (Gibco 42430082). Details of each treatment media are in Table 2.2.1.

Table 2.2.1 details the different treatment media used, the basal media and product code for that media, the glucose, alanine, serine and serum contributions to that media. It also details whether amino acids were supplemented to the same concentration of culture media. FBS = foetal bovine serum, dFBS = dialysed foetal bovine serum.

Table 2.2.1

Treatment Name	Base Media	Glucose	Alanine	Serine	Serum	Amino Acid Supplementation
Culture media	DMEM (Gibco 42430082)	-	-	-	10 % FBS	-
Seeding media	DMEM (Gibco 42430082)	-	-	-	10 % dFBS	-
5:1 (w/o) amino acids	DMEM (US biological D9800-27)	5 mM ^{12}C-glucose	500 µM	100 µM	10 % dFBS	-
1:5 (w/o amino acids)	DMEM (US biological D9800-27)	5 mM ^{12}C-glucose	100 µM	500 µM	10 % dFBS	-
5:1 (with amino acids)	DMEM (US biological D9800-27)	5 mM ^{12}C-glucose	500 µM	100 µM	10 % dFBS	Yes
1:5 (with amino acids)	DMEM (US biological D9800-27)	5 mM ^{12}C-glucose	100 µM	500 µM	10 % dFBS	Yes
Labelled 5:1 (w/o amino acids)	DMEM (US biological D9800-27)	5 mM ^{13}C-glucose	500 µM	100 µM	10 % dFBS	-
Labelled 1:5 (w/o amino acids)	DMEM (US biological D9800-27)	5 mM ^{13}C-glucose	100 µM	500 µM	10 % dFBS	-
Labelled 5:1 (with amino acids)	DMEM (US biological D9800-27)	5 mM ^{13}C-glucose	500 µM	100 µM	10 % dFBS	Yes
Labelled 1:5 (with amino acids)	DMEM (US biological D9800-27)	5 mM ^{13}C-glucose	100 µM	500 µM	10 % dFBS	Yes

2.2.3 Culture of LN229 cells

LN229 cells (ATCC CRL-2611), were split every 3-4 days at a 1:5 ratio using DMEM media (Gibco 42430082) and TrypLE (Gibco™ 12604013) to detach the cells, until use of the cells was required. When necessary, cells were counted using a Vi-Cell VR cell analyser (Beckman Coulter), and viable cell count and cell diameter recorded.

2.2.4 LN229 growth in various media conditions

Cells were seeded at 800,000 cells in 3 mL per well of a Nunc 6 well plate (Thermo 140675), in culture media (Table 2.2.1). The cells were incubated at 37 °C for 23 hours to allow the cells to adhere to the surface. The media were removed and replaced with 3 mL of the same media to ensure there is no depletion of any media components and the cells incubated at 37 °C for another hour. The media were then removed from the wells, and each well was treated with different conditions, as detailed in Table 2.2.2 and the plate loaded in to an Incucyte S3 (Essenbio), at 37 °C and 5 % CO_2. The plate was read for confluency every 4 hours for 2 days and 16 hours in total with 9 images taken per well. Data were analysed using the Incucyte S3 software (Essenbio 20192.4.0.0), where

images were exported, and graphical visualisations generated taking the average of the 9 reads per well and plotting average confluency/well against time.

Table 2.2.2 details the plate map of media conditions used to investigate the effect media treatments had on the growth of LN229 cells over time. A= Alanine, S = Serine, FBS = foetal bovine serum, dFBS = dialysed foetal bovine serum.

Table 2.2.2		
A1: Normal Culture media + 10 % FBS	**B1:** 5:1 A:S without amino acid supplementation	**C1:** 5:1 A:S with amino acid supplementation
A2: Normal culture media + 10 % dFBS	**B2:** 1:5 A:S without amino acid supplementation	**C2:** 1:5 A:S with amino acid supplementation

2.2.5 LN229 cell treatment and metabolite extraction for GC-MS analysis

Metabolomics is a desirable way to determine intracellular concentrations of amino acids, glycolytic intermediates and other metabolites. In order to measure various metabolites by GC-MS, published method [66] was used as a guide. LN229 cells were seeded in culture media containing 10 % dFBS at 800,000 cells in 3 mL per 6 cm dish (Nunc 150340) and incubated for 23 hours at 37 °C. 1 hour before treatment, the media was removed, and replaced with fresh media containing 10 % dFBS and returned to the incubator for 1 hour. To begin the time course, cells were treated with various media containing either 5:1 or 1:5 alanine: serine, 10 % dFBS and 5 mM ^{13}C-glucose, Table 3.1 contains the treatment media details. 3 replicates of each condition were plated and treated. At the point of treatment, 3 dishes were left untreated and harvested at that time to be the time zero point for a time course. 3 dishes were also left untreated and counted using a Vi-Cell VR cell analyser (Beckman Coulter) to determine cell number and average diameter of the cells for use in normalisation of metabolite abundances and calculating intracellular concentrations. Treated plates were left to incubate at 37 °C for various time points (15 minutes, 30 minutes, 1 hour, 3 hours and 6 hours, 10 hours, and 24 hours) to monitor various metabolites over time.

When the incubation time was complete, plates were removed from the incubator and cells washed once with 4 °C PBS followed by 4 °C 50 mM HEPES, pH 7.4, 110 mM NaCl, before 725 µL methanol (MeOH) at -20 °C was added to quench the metabolism. From this point, plates were kept on dry ice until the point of extraction. Once the 725 µL MeOH was added, the cells were scraped from the plate into Eppendorf tubes containing the extraction buffer, consisting of 160 µL chloroform and 180 µL water with 2 nmol scyllo-inositol. An additional 725 µL MeOH was used to ensure total harvest of the cells. Eppendorfs were vortexed and sonicated in a water bath at 4 °C for 3x 8 minutes and incubated at 4 °C overnight for extraction. The following day, the tubes were centrifuged at 10,000 g for 10 minutes to pellet and remove the protein content of the extractions. Supernatants were then dried down entirely using speed vac (DNA130-230) and resuspended in biphasic extraction buffer consisting of 1:3:3 chloroform, methanol, water. The resuspensions were vortexed and centrifuged at 10,000 g for 5 minutes at 4 °C. 150 µL of the polar fraction was dried down using a speed vac (DNA130-230), and washed twice with 40 µL methanol, drying down completely between each wash. 20 µL of methoxyamine at 20 mg/ml in pyridine (Thermofischer Scientific), was added and the extractions left to incubate overnight at room temperature. Samples were derivatised with 20 µL bistrifluoroacetamide (BSTFA) + 1 % (v/v) trichloromethylsilane (TMCS) (Thermofischer Scientific B-023) and incubated at room temperature before analysis by GC-MS.

2.2.6 Sample analysis by GC-MS

Measurements were conducted as described in published methods [70] with some modifications, using an Agilent 7890A-5975C GC-MS in electroionisation mode. Standard parameters used for GC-MS measurements are detailed in Table 2.2.3.

Table 2.2.3	
Component	**Value**
Carrier gas	Helium
Flow rate	0.9 mL/minute
Scan range	50-550 m/z
Column	DB-5MS (Agilent)
Temperature Gradients	70 °C (2 minutes) Ramp to 295°C (12.5 °C/minute) Ramp to 320 °C (25 °C/minute) (3-minute hold)

2.2.7 GC-MS Data Analysis

Data acquisition was completed using MassHunter software (versionB.07.02.1938). Metabolites were identified and quantified using standards and ^{13}C labelling estimated as a fraction of the analyte pool after correction for natural abundance. Internal standard scyllo-inositol was used to correct for variations in sampling and metabolite loss through the extraction process. An R-script generated in the Anastasiou lab by Fiona Grimm and modified by Natalie Bevan was used to normalise metabolite abundances to cell number, against the internal standard and correct for natural abundance in labelling. Intracellular concentrations were estimated using volume of cell, with the radius obtained from cell counting using the Vi-Cell VR analyser. Data were then plotted in Prism (version 8) for visualisation purposes and rate calculations. Based on whether the measurements achieve saturation, non-linear regressions were fit. If the measurements begin to plateau, curves were fitted with a one-phase association and if a plateau was not reached then curves were fitted using an exponential growth curve. If the curves were linear, a linear regression was used to calculate the rate of analyte generation. Paired t-tests were used to compare the calculated rates (k) between the two treatment conditions. Where the end point measurements were used to draw conclusions, paired t-tests were used to compare the concentration of analyte between the conditions at 10 hours.

Analyte generation non-linear regressions used:

one-phase association:	$Y = Y0 + (Plateau-Y0) * (1 – exp (- K * x))$
exponential growth curve:	$Y = Y0 * exp (k * X)$

Chapter 3

Generation of an optimised LC-MS method to monitor intracellular amino acid concentration and glycolytic intermediates

3.1 Introduction to ultra-performance liquid chromatography (UPLC) coupled to mass spectrometry

3.1.1 Principles of chromatographic separation in LC-MS

Chromatographic separation results from the specific interactions between analyte molecules, the stationary phase of a chromatography column and the mobile phase. For high performance liquid chromatography (HPLC) and ultra-performance liquid chromatography (UPLC), analytes are separated based on the functional groups packed into a column which can come in a variety of dimensions. Reverse-phase UPLC, usually relies on a non-polar or hydrophobic octadecyl (C18) functional groups to create the separation [59]. On this kind of column, hydrophilic or polar molecules preferentially associate with the mobile phase and therefore elute from the column first. The more hydrophobic the molecule is, the retention time of that molecule increases due to the increased interaction with the hydrophobic column components. Reversed phase is very commonplace in chromatographic methods, however there is an alternative to this method. Hydrophilic interaction chromatography (HILIC) is also used for the analysis of polar analytes. Instead of the mobile phase being extremely hydrophobic like in reverse phase, the initial conditions in HILIC are high in solvent, to allow non-polar molecules to elute first and analytes have an increased retention time if they are more polar, opposite to reversed-phase separation [60].

3.1.2 Component elution from LC-MS columns

Various combinations of polar and solvent mobile phases can be used to elute analytes from the solid phase column. This combination can be run isocratically, at one combination for a set time frame, or run as a gradient running from high to low of one mobile phase. Usually, an isocratic elution is not sufficient to separate out all analytes appropriately and therefore elution gradients are generally used to separate out analytes ranging from weak to strong interactions with the column. An elution gradient can be run stepwise, or continuously and a method can be optimised to generate the best separation possible [56], [58]. In reversed phase chromatography, the organic solvent component of the mobile phase is ramped up over time. In a HILIC method, this is the opposite, the organic component of the mobile phase starts high and is replaced by a more polar component over the run time [60].

3.1.3 UPLC Instrumentation

A UPLC system usually consists of a mobile phase delivery system, an autosampler which injects the sample, an analytical column and means of detection. In this case the means of detection will be a triple quadrupole mass spectrometer. Schematic 2.1 illustrates the typical components of a UPLC system. The difference between HPLC and UPLC is that UPLC can run at increased pressures [59]. This means that the run times are shorter, decreased solvent usage and greater analyte separation. Figure 3.1 illustrates a typical UPLC setup.

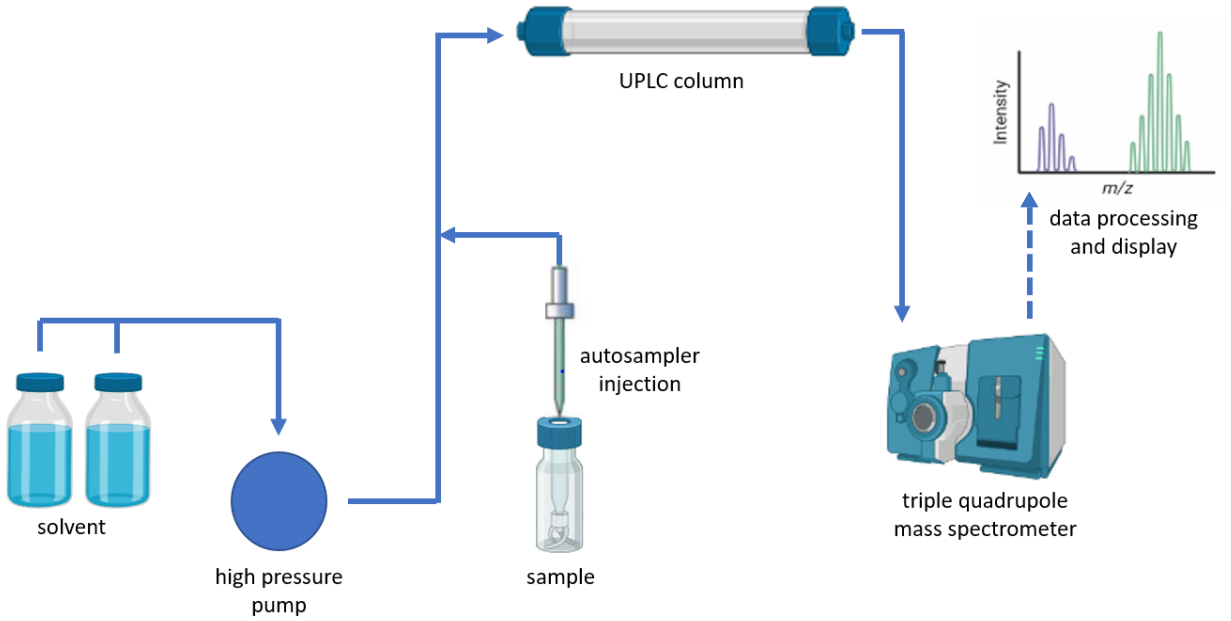

Figure 3.1: schematic illustration of a typical UPLC system including a solvent delivery system, high pressure pump, sample auto injection system, chromatography column and method of detection, in this case a triple quadrupole mass spectrometer. Icons for schematic used from Biorender.

3.1.4 Mass spectrometry basic principles

Mass spectrometry is a widely used analytical tool that can provide both qualitative and quantitative information about known or unknown analytes in a sample. The mass spectrometer measures the mass to charge ratio (*m/z*) of charged particles. These ions and their abundance are recorded, and a mass spectrum is generated allowing the identification of individual analytes [61].

3.1.5 Electrospray ionisation

All mass spectrometers begin by ionising a sample. Samples can be introduced as solids, liquids or gases, but if not gas already, need to be vapourised prior to, or in conjunction with ionisation. There are various methods of ionisation, including electrospray ionisation (ESI). This method ionises a sample eluted from a chromatography column by pumping the liquid sample into a metal capillary and applying a high voltage. This voltage separates the ions based on their charge, and depending on

the polarity and intensity of the electric field. These droplets undergo declustering with the help of a heated gas, such as nitrogen. This allows the loss of the solvent molecules that the analytes are dissolved in eventually generates individual ions in the gas phase. This electrospray process generates ions by the addition of a proton, or removal of a proton, depending on polarity of the ion. This method of ionisation usually produces very few fragments and therefore tandem mass spectrometry is preferable to increase specificity of ion detection [62].

3.1.6 Quadrupole mass analysers

Separation by quadrupole mass filter relies on a flow of single ions based on their *m/z* ratio in a hyperbolic electrostatic field. A quadrupole mass filter comprises of two pairs metal rods parallel to each other. An electric field is generated around these four rods by applying a direct current at a particular voltage across one pair, and the same direct current and the opposite polarity applied to the other pair. With the addition of a radiofrequency voltage to all rods, oscillations can be induced in ions travelling through the center, separating these ions based on their *m/z* ratio. Adjusting this radiofrequency voltage can allow the filtration of ions through this analyser. Figure 3.2 illustrates the components of a typical quadrupole mass analyser.

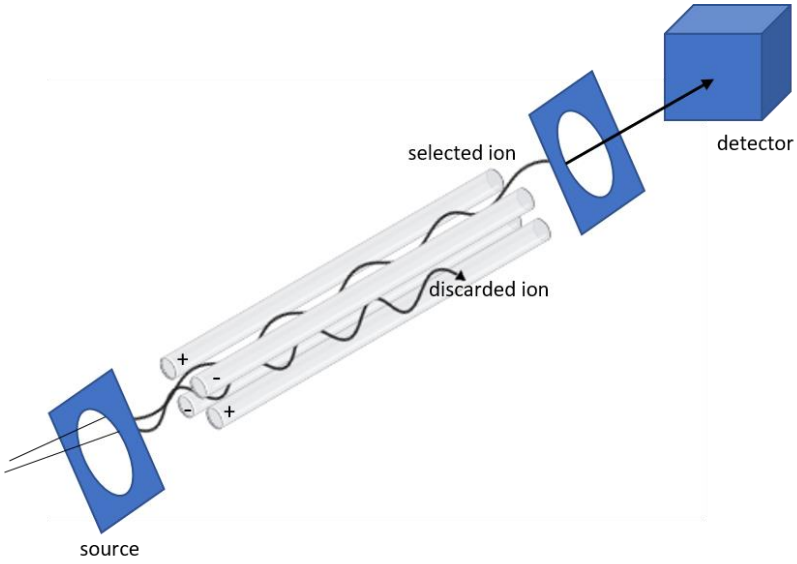

Figure 3.2: illustration of ions travelling through a quadrupole mass analyser. From the initial source, pairs of quadrupoles in opposing directions focus and separate ions based on their mass to charge ratio. The electric field generated by the opposite polarity and parallel metal rods is what causes this separation. A feature of quadrupole mass analysers is that they can be tuned to discard ions that are not of interest.

3.1.7 Triple quadrupole mass spectrometry

Separation of analytes can be improved by fragmenting the precursor ions separated based on their *m/z* ratio, and then filtering those product ions based on their *m/z* in tandem mass spectrometry (MS/MS). Fragments are generated by a gas in a collision chamber before the products are released for filtration based on their *m/z*. This method of mass spectrometry is very sensitive and specific. Figure 3.3 illustrates the two linear mass analysers of a typical triple quadrupole mass spectrometer which are connected by a third quadrupole, also known as the collision cell (Q2). Precursor ions without interest are discarded through the first quadrupole mass analyser (Q1), fragmentation of the ions of interest is completed in Q2, and the third quadrupole (Q3) behaves much like the first, discarding any product ions that are not of interest. This generates a MS/MS spectra, that can be used to qualitatively and quantitatively measure analytes. Single reaction monitoring (SRM) methods can be generated to optimise the voltages applied at various stages of this system that give the highest and most robust

signal for a particular analyte. This involves identifying the most precursor and product ions detected and therefore isolated in Q1 and Q3. The various points of voltage optimisation are the declustering potential (DP), which is the voltage applied to the orifice of the mass spectrometer to aid vapourisation. The entrance potential (EP), is the voltage required to focus the ions into and through Q1. The collision energy (CE), is the voltage applied to fragment the ions in Q2, and the cell exit potential (CXP), is the voltage applied to accelerate and focus ions into Q3 [63], [64].

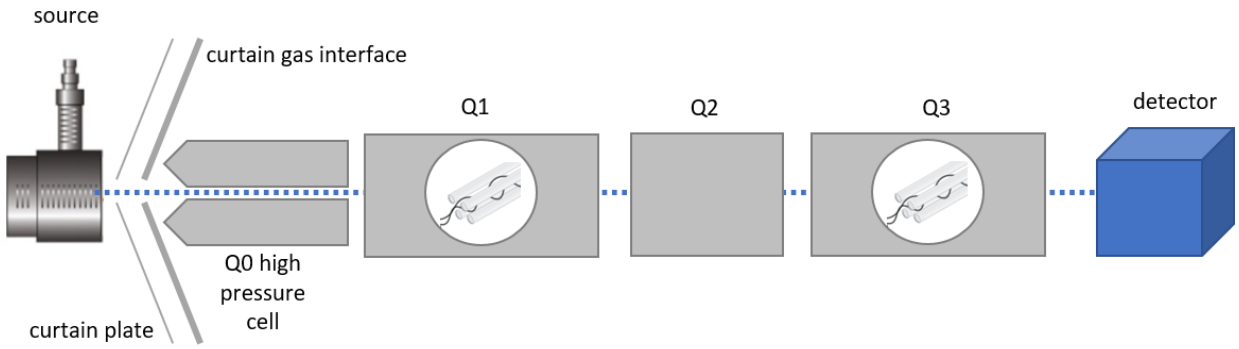

Figure 3.3: illustrative diagram of a triple quadrupole mass spectrometer. Q0 increases pressure and causes ionisation of the analytes. Q1 is the first quadrupole mass analyser and separates out the precursor ions based on their m/z. Q2, also known as the collision cell fragments the precursor ions separated by Q1 and releases the product ions. Q3 is the final quadrupole mass analyser and separates the product ions that were generated in Q2 before they are detected. Icons for generated schematic from Biorender.

3.1.8 Intentions for LC-MS in this investigation

The intention of this study is to generate a highly specific and medium throughput detection method to quantify intracellular amino acid concentration and measure changes in analytes from carbon metabolism in cells treated with various media conditions. An LC-MS/MS method using a triple quadrupole mass spectrometer will be used to generate a highly specific method for detecting these analytes, without the need for derivatisation. This method will be tuned to detect all 20 proteinogenic amino acids, various glycolytic intermediates including glucose, fructose -1,6 -bisphosphate, pyruvate and lactate. This will require optimisation of voltages to determine SRM methods for each analyte, and the development of an LC method to separate and capture all these analytes from metabolic

extracts of cells. Literature demonstrates that all these analytes of interest can be detected by LC-MS, however there is no method that exists to capture all analytes on one LC-MS method using a triple quadrupole mass spectrometer. Therefore, for this study, investigating intracellular amino acid concentration and glycolytic metabolism, one highly specific method to capture all molecules would be highly valuable. In order to do this, two LC columns will be investigated to capture all of these analytes. A Luna NH2 column (Phenomonex), with silica surface beads and attached amino groups to serve as a weak anion exchanger. This offers polar selectivity in reversed phase and HILIC conditions. The other column that will be investigated is an Omega polar C18 column (Phenomonex), the eighteen carbon long ligands on the surface provide hydrophobic interactions, whereas the polar modified particle surface itself allows retention. The combination of these two columns, should capture and separate all of the metabolites of interest.

3.2 Method Optimisation

3.2.1 SRM method optimisation

In order to generate methods on a QQQ-MS, single reaction monitoring methods (SRMs), must be generated. To optimise an SRM method for each analyte, the tune and calibrate method on Analyst software (version 1.7.2 by Sciex) and 1 mM stocks of each analyte in Table 2.1 were used. Each voltage was ramped in increments within full range of this mass spectrometer and each voltage was optimised in combination to achieve the highest and most reproducible ion signals. All optimisations were conducted with mass spectrometry parameters as per Table 2.2. The direct injection flow rate for these optimisations was set at 0.7 mL/min.

3.2.2 LC-MS method optimisation

Method for amino acid separation: Separation was performed using a Nexera X2 system (Shimadzu, Kyoto, Japan). Based on published methods [65], details are contained in Table 3.1 using the following mobile phases composed of A (H_2O + 0.0 1% (v/v) formic acid (FA)) and B (Acetonitrile (ACN) + 0.01 % (v/v) FA). This is the method optimised for amino acid separation using this column for the calibration curves. Various

solvent gradient lengths were applied to determine the best method for analyte separation.

Method for glycolytic intermediates: Separation was performed using the same QQQ-MS parameters. Flow rate was set to 0.2 mL/min and the mobile phase was composed of A (H_2O + 0.01 % (v/v) formic acid (FA)) and B (ACN + 0.01 % (v/v) FA). The final method optimised for glycolytic intermediate separation using this column is detailed in Table 3.1. Various solvent gradient lengths were applied to determine the best method for analyte separation.

Table 3.1

Luna NH2 Column Method		**Polar C18 Column Method**	
Flow Rate	0.4 mL/min	**Flow Rate**	0.2 mL/min
Sample Injection	9 uL	**Sample Injection**	9 uL
Minute	**% B**	**Minute**	**% B**
0	98	0	0
1	98	1	0
15	60	6	10
16	60	6.1	10
16.1	98	6.2	0
17.1	98	7.5	0

3.2.3 Calibration curve generation for sample quantification

In order to quantify amounts of analytes in unknown samples, calibration curves were generated using a standard mixture, where analytes are serially diluted from 900 µM 1:2 for the polar C18 method, and from 625 µM 1:2 for the Luna NH2 method. All dilutions were generated using the LC-MS method starting conditions. Luna NH2 method starting conditions were 100 % B and the Polar C18 starting conditions were 100 % A. All calibration curve points were run according to using the LC-MS method detailed in Table 2.3.

For the Luna NH2 column method, sample accumulation in part of the LC-MS system was seen over time, therefore a wash was introduced into the LC-MS method for the Luna NH2 method. The final optimised LC-MS method was 0.4 mL/min flow rate, mobile phase composed of A (H_2O + 0.01% FA) and B (ACN + 0.01% FA). All test and validation samples measured on LC-MS from section 2.3, used the LC-MS method detailed in Table 3.2 for the Luna NH2 column.

Table 3.2

Revised Luna NH2 column method	
Flow Rate	0.4 mL/min
Sample Injection	9 uL
Minute	**% B**
0	98
1	80
9.5	50
19.5	50
20.5	0
20.6	98
23.6	98

3.2.4 Preparing quality control samples for method generation

In order to determine the method was suitable for use, quality control (QC) samples were prepared. A standard mixture of all analytes generated by combining all metabolites to a final concentration of 1 mM in mobile phases appropriate for the LC method used (for Luna NH2 98 % (v/v) B and for Polar C18 100 % (v/v) A). In order to validate the method and ensure a known concentration in a sample could be detected using a calibration curve, media with the same concentrations as subsequent cellular treatments were used. Media were made using powdered DMEM with no amino acids and no glucose (US Biological D9800-27.10) to the manufacturer's instructions with the addition of sodium bicarbonate at 44 mM (Table 2.1) and pH adjusted to 7.4 using sodium hydroxide (10 M). Media was supplemented with 5 mM glucose, and different ratios of alanine and serine, with either 500 µM or 100 µM of each per condition. To prepare media samples for LC-MS, 200 µL media was sampled and dried down entirely using a speedvac (DNA130-230)

and resuspended in 50 µL mobile phase appropriate for the LC method used (Luna NH2 98 % (v/v) B and for Polar C18 100 % (v/v) A). The 50 µL resuspension was transferred to a 96-well clear PP Greiner (Thermo 651101) plate for the autosampler on the LC-MS system. Quality control samples were run alongside calibration curves for validation purposes as detailed above in the LC-MS method.

3.3 SRM methods optimised for all analytes of interest

To develop the capability for investigating all metabolites of interest for this project using a QQQ-MS, with the eventual aim of calculating an intracellular concentration for these analytes, multiple experiments were completed for optimisation of this method. Firstly, the unique signature each analyte generates in a QQQ-MS must be identified. In order to achieve a highly specific QQQ-MS method for multiple analytes, single reaction monitoring (SRM) methods must be generated for each analyte intended for investigation. Table 3.5 shows the optimised voltages, precursor ion (Q1) and product ions (Q3) used in combination for an optimised SRM method for each analyte. Figure 3.4 shows the DP and CE profiles for alanine optimisation and the difference between a well optimised, and poorly optimised manner. CXP and EP are field voltages that do not require optimisation based on mass of the analyte and therefore the profiles are not shown in this figure. Figure 2.1a and 2.1b show alanine well optimised and the appropriate DP and CE voltages chosen for the optimal Q1/Q3 signal.

Table 3.3 details the precursor and product ions identified as most abundant for each analyte as well as the optimised DP, EP, CE and CXP voltages used for the most reliable detection of each analyte as well we the polarity of the ion being detected.

Table 3.3

ID	Q1 Mass (Da)	Q3 Mass (Da)	Dwell Time (msec)	DP (volts)	EP (volts)	CE (volts)	CXP (volts)	Polarity
Alanine	94.0	44.1	15	60	10	15	12	positive
Histidine	156.0	110.0	15	40	10	20	11	positive
Leucine	132.1	86.1	15	30	10	16	11	positive
Lysine	174.1	84.1	15	40	10	24	10	positive
Proline	116.0	70.1	15	30	10	22	8	positive
Glutamine	147.0	84.0	15	30	10	25	10	positive
Tyrptophan	205.0	146.1	15	40	10	26	8	positive
Tyrosine	182.0	136.1	15	40	10	20	7	positive
Asparagine	134.0	88.0	15	40	10	15	8	positive
Methionine	150.0	104.0	15	30	10	15	10	positive
Phenylalanine	166.0	120.1	15	40	10	21	7	positive
Isoleucine	132.1	86.1	15	30	10	16	9	positive
Threonine	120.0	74.1	15	30	10	16	7	positive
Valine	118.0	72.1	15	30	10	16	8	positive
Glycine	76.0	30.1	15	30	10	20	14	positive
13C 15N Valine	124.0	77.0	15	40	10	17	8	positive
Serine	106.0	60.1	15	65	10	15	20	positive
Arginine	175.1	70.1	15	50	10	32	8	positive
Cysteine	122.0	76.0	15	30	10	30	8	positive
Glutamic Acid	148.0	84.0	15	30	10	20	9	positive
13C-Glucose	192.0	99.0	15	30	10	23	9	positive
Glucose	179.1	89.1	15	-35	-10	-10	-47	negative
Pyruvate	87.1	32.0	15	-10	-10	-12	-15	negative
Lactate	89.0	34.9	15	-40	-10	-14	-15	negative
Aspartic Acid	132.0	88.0	15	-40	-10	-18	-10	negative
Fructose -1,6- bisphosphate	338.7	78.9	15	-20	-10	-76	-21	negative

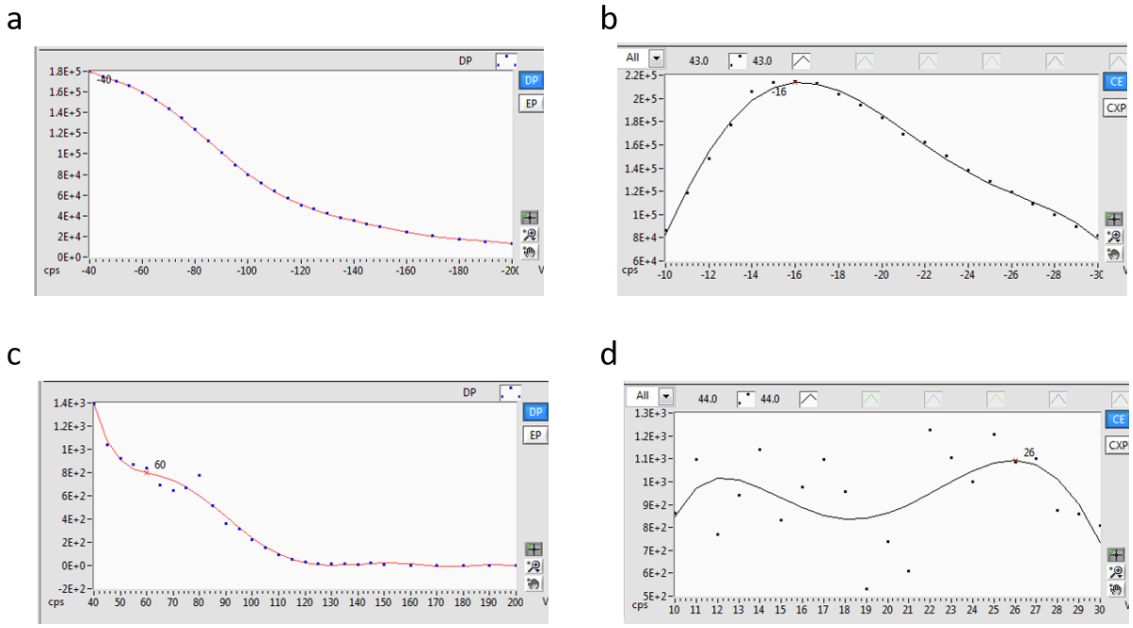

Figure 3.4: Declustering potential (DP) and collision energy (CE) profiles for alanine. DP and CE were ramped in DiscoveryQuant (Agilent) using 10 µM pure standard stocks dissolved in water. a) DP and b) CE profile ramps of alanine when well optimised. The ion peak intensity is on the y axis and the DP or CE voltage is ramped on the X axis. The point highlighted on the curve indicates the voltage at which the highest intensity ion fragment is detected. The profile for c) DP and d) CE for alanine are shown when not well optimised.

3.4 Successful LC separation for all analytes of interest

Once optimised SRM methods were established, to add a level of analyte separation from entire cellular metabolite extracts, liquid chromatography methods were developed to combine with the SRM based detection. In order to capture all the analytes of interest, two LC methods were generated; a Luna NH2 column using a HILIC method and a Luna Omega polar C18 column using a reverse phase method. This is because all analytes, due to their chemical structure, could not be detected by one of these methods alone. Figure 3.5 shows the chromatogram overlays for each LCMS method and the separation achieved with peaks identified as the analyte they represent, and Table 3.6 details the column used and retention times for each analyte. Some retention times are very similar and overlap entirely or slightly, however the combination of the liquid chromatography and the unique SRM method, will still allow identification of each analyte.

In order to calculate an intracellular concentration, a calibration curve should be run to associate peak areas to an amount of analyte. Calibration curves for each analyte were generated using concentrations ranging from 500 µM to 5 nM and diluted in mobile phases appropriate for the LC method. Figures 3.6 and 3.7 show these calibration curves plotted and Table 3.4 contains the R^2 value to determine quality of linearity, the linear range and the limit of quantitation for each analyte. To further the confidence in the calibration curves to be used for intracellular concentration calculations, standard mixtures of analytes were run at six different concentrations to ensure mixing these analytes together would not alter the linearity or linear range of detection for these analytes. By running these calibration curves, it became clear there was some form of analyte accumulation in the system, either on the column or within the sample loop. Figure 3.8 shows the calibration curves of alanine and serine, with one subsequently run after the other. Figure 3.8a shows that the second calibration curve for alanine, gives a higher peak area at each concentration than in the first calibration curve run, although for alanine they are both linear and have R^2 of 0.9951 and 0.9683 respectively, the slopes of these two calibration curves are different, the same is true for serine (Figure 3.8b). In order to resolve this issue of inconsistent slopes between calibration curve repeats, blank samples throughout the run were investigated. The higher concentrations of alanine sampled, more alanine is being detected in blank samples, indicating there is some sample carry-over occurring, until the column is cleaned sufficiently (Figure 3.8c). Therefore, the LC method was altered to include a wash step, dropping to 0 % B for 1 minute to ensure the system is clean before sampling again. The result of this (Figure 3.8d, Figure 3.8e) is a good overlay of subsequent calibration curves with no sample carry-over observed. The final optimised methods are detailed in section 3.2.5 method development.

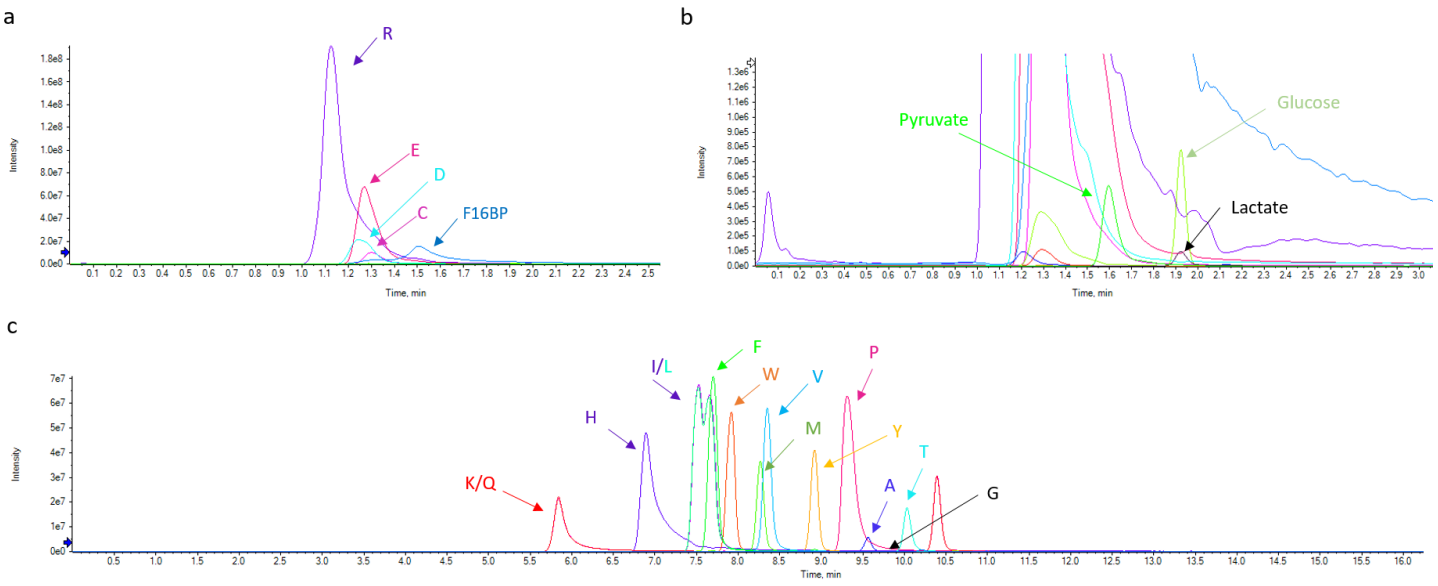

Figure 3.5: Chromatogram overlays of Luna NH2 and Polar C18 LC-MS methods. A mixture of pure standard analytes was generated to a final concentration of 900 µM and analysed via the LC-MS methods detailed in Table 3.3. Chromatograms for a) Omega polar C18 column method showing the peaks for arginine (R), glutamic acid (E) , aspartic acid (D), cysteine (C) and F16BP. b) is the same chromatogram zoomed in to the y axis to highlight the peaks for pyruvate, lactate and glucose. c) is the chromatogram from the Luna NH2 column method, indicating which peak represents lysine (K), glutamine (Q), histidine (H), leucine (L), isoleucine (I), phenylalanine (F), tryptophan (W), valine (V), methionine (M), tyrosine (Y), proline (P), alanine (A), threonine (T) and glycine (G).

Table 3.4 details the column that was used to separate and detect ions of each analyte, the retention time on that column, the R^2 of the plotted calibration curve between the linear range also detailed in this table, and the limit of quantitation (LOQ) for each analyte are also shown.

Table 3.4

Analyte	Column	Retention Time (RT) minutes	R^2	Linear Range	Limit of quantitation (LOQ)
Serine	Omega Polar C18	1.21	0.9966	>350nM-15uM	350nM
Arginine	Omega Polar C18	1.02	0.9873	>350nM-30uM	350nM
Cysteine	Omega Polar C18	1.18	0.997	>350nM-60uM	350nM
Glutamic Acid	Omega Polar C18	1.34	0.9948	>350nM - 115uM	350nM
13C 15N Valine	Omega Polar C18	1.4	0.9936	15uM- 115uM	15uM
Glucose	Omega Polar C18	2.09	0.998	500nM-450uM	500nM
Pyruvate	Omega Polar C18	1.67	0.999	2uM - 450uM	2uM
Lactate	Omega Polar C18	2.09	0.9979	>350nM - 225uM	350nM
Aspartic Acid	Omega Polar C18	1.43	0.9958	>350nM - 60uM	350nM
Fructose-1,6 Bisphosphate	Omega Polar C18	1.51	0.9789	20uM - 450uM	20uM
Alanine	Luna NH2	4.84	0.9933	5nM-200uM	5nM
Histidine	Luna NH2	2.85	0.9956	>5nM - 200uM	5nM
Leucine	Luna NH2	3.27	0.989	>5nM - 200uM	5nM
Lysine	Luna NH2	5.69	0.9973	>5nM - 300uM	5nM
Proline	Luna NH2	4.93	0.9992	>5nM - 150uM	5nM
Glutamine	Luna NH2	2.82	0.9974	>5nM - 300uM	5nM
Tyrptophan	Luna NH2	3.52	0.9965	>5nM - 150uM	5nM
Tyrosine	Luna NH2	4.28	0.9927	>5nM - 20uM	5nM
Asparagine	Luna NH2	3.95	0.9986	5nM - 150uM	5nM
Methionine	Luna NH2	3.95	0.9931	>5nM - 150uM	5nM
Phenylalanine	Luna NH2	3.52	0.9925	>5nM - 150uM	5nM
Isoleucine	Luna NH2	3.27	0.9964	>5nM - 150uM	5nM
Threonine	Luna NH2	5.37	0.9948	>5nM - 200uM	5nM
Valine	Luna NH2	3.94	0.9934	>5nM - 150uM	5nM
Glycine	Luna NH2	5.42	0.9967	>5nM - 150uM	5nM
13C 15N Valine	Luna NH2	3.92	0.9933	>5nM - 150uM	5nM

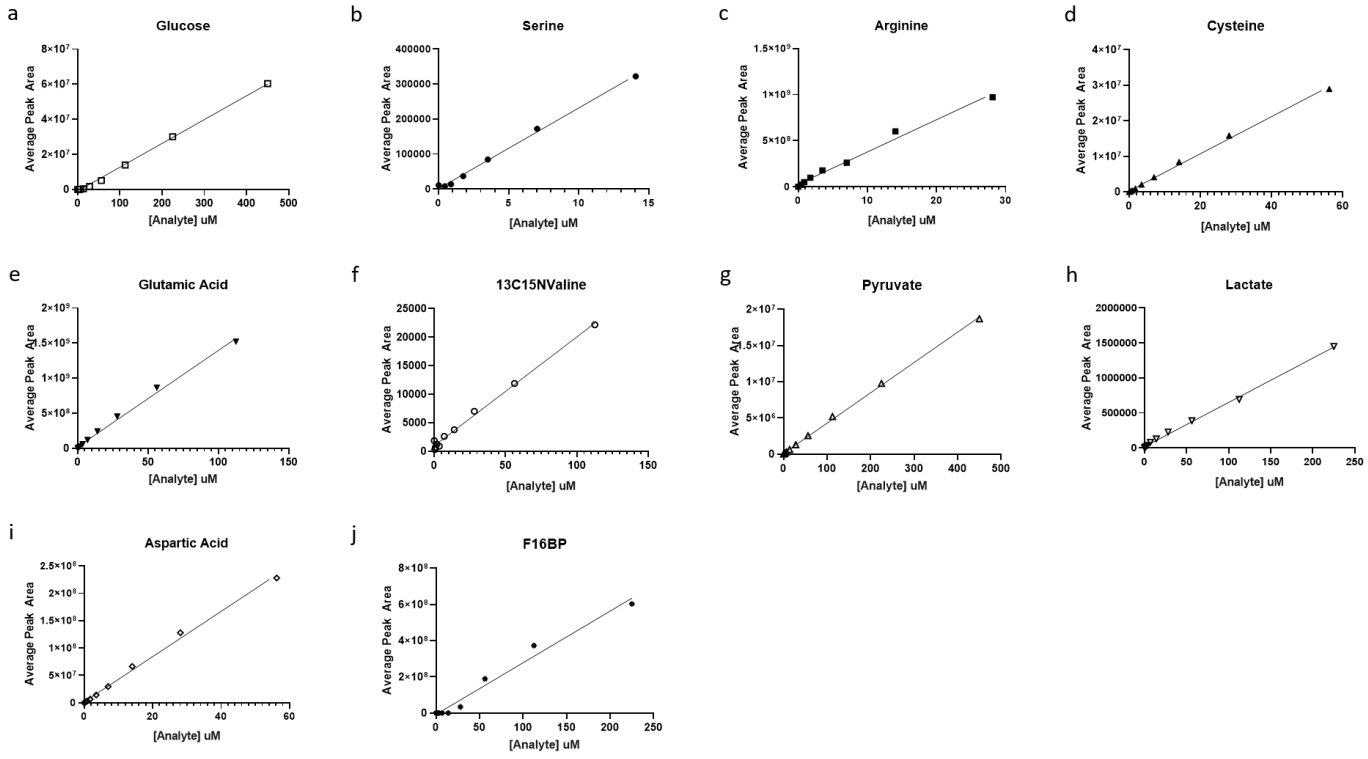

Figure 3.6: Calibration curves for analytes detected on the Omega polar C18 column. Analytes were dissolved in water to a top concentration of 500 µM and serially diluted 1:2 in water down to 350 nM and analysed using the polar C18 method detailed in Table 3.3. Linear regressions were used to fit the data using GraphPad Prism V8.

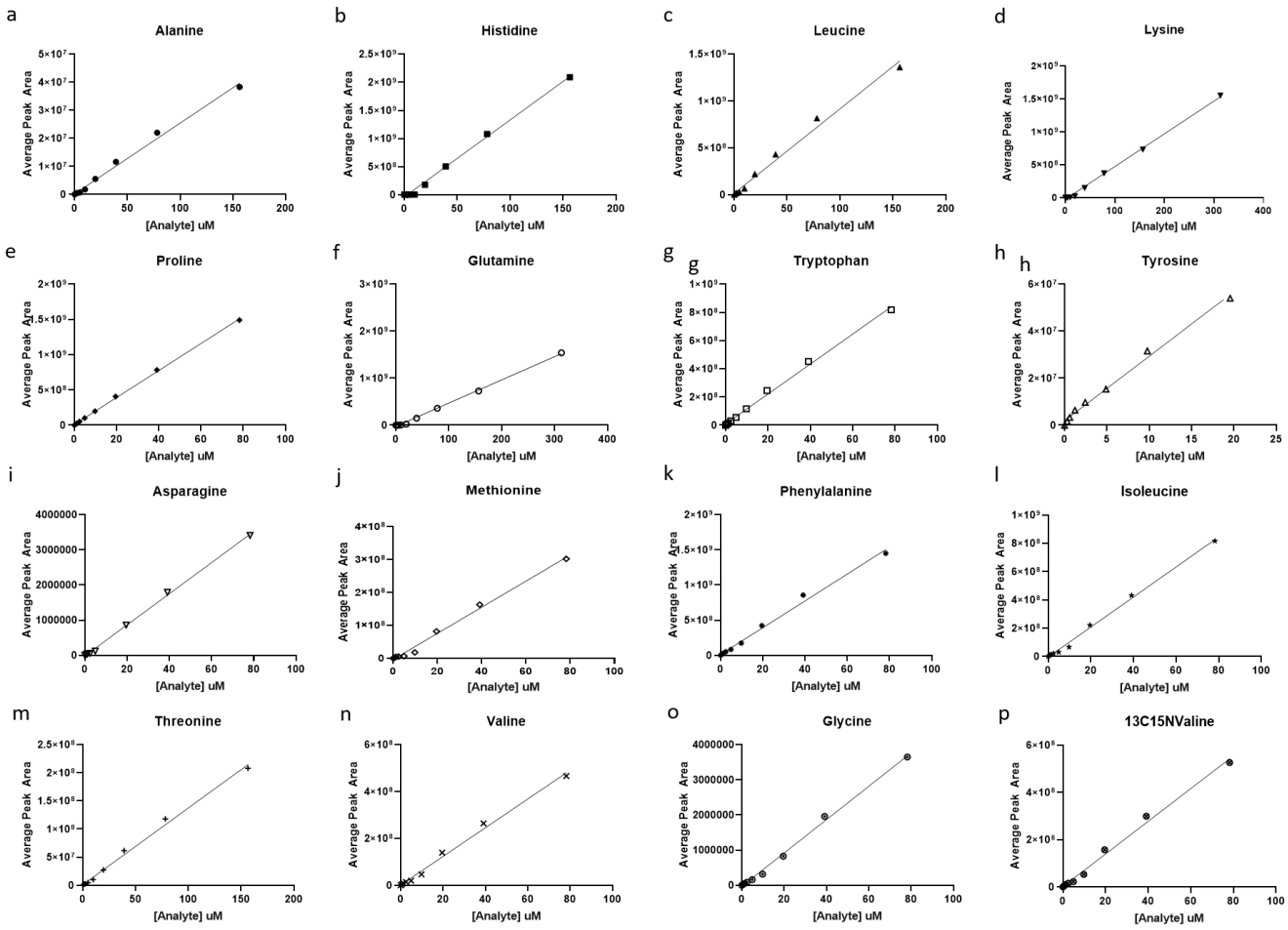

Figure 3.7: Calibration curves for analytes detected on the Luna NH2. Analytes were dissolved in water to a top concentration of 500 µM and serially diluted 1:2 in water down to 350 nM and analysed using the polar C18 method detailed in Table 3.3. Linear regressions were used to fit the data using GraphPad Prism V8.

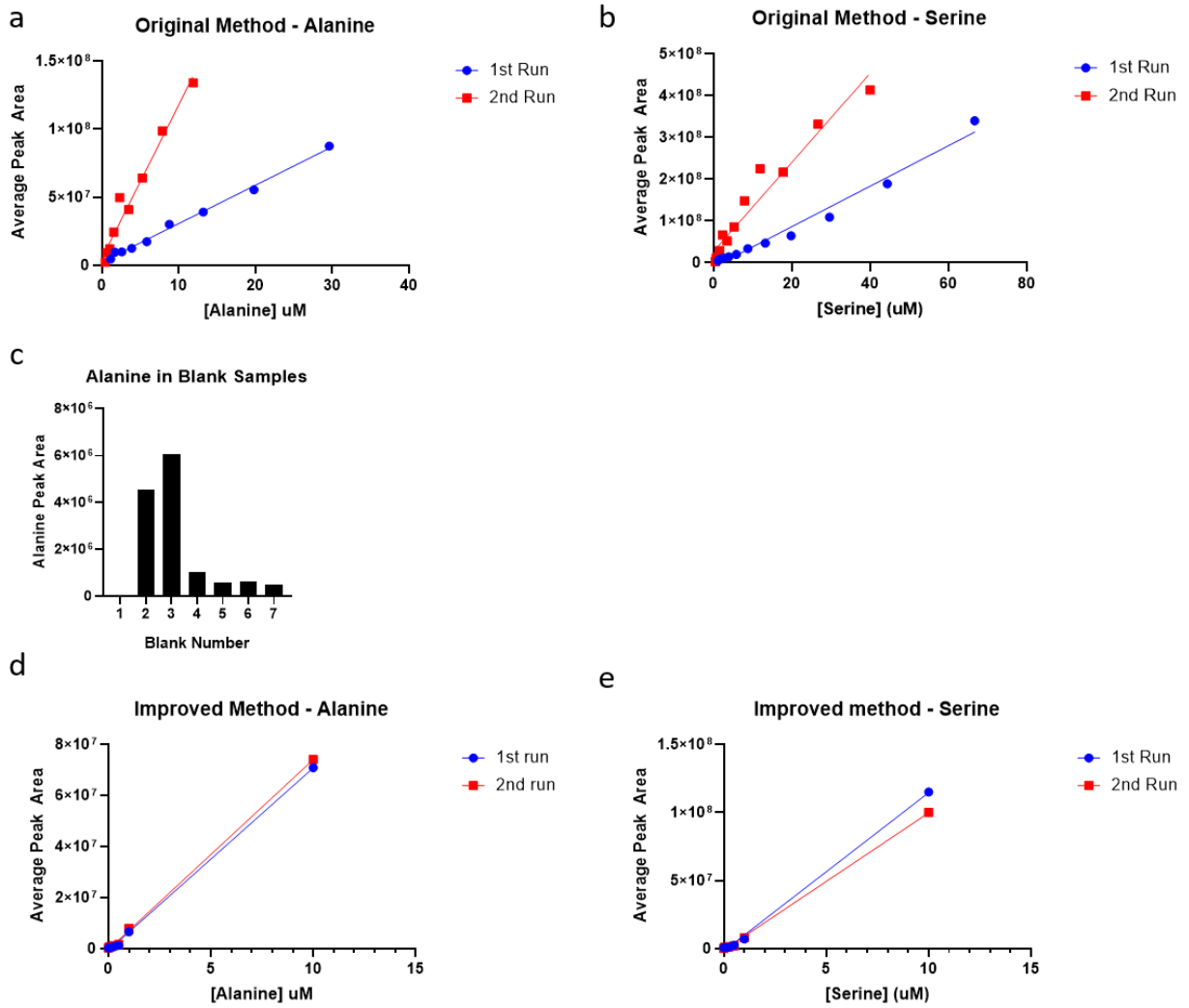

Figure 3.8: Luna NH2 method optimisation was improved with an inclusion of a wash step. Calibration curves of alanine and serine were generated in water from 100 µM serially diluted 1:1.5 and analysed by LC-MS sequentially. Calibration curves for a) Alanine and b) serine are shown with the 1st and 2nd sequential runs of these calibration curves shown in blue and red respectively. Upon interrogation of the data, all measurements for the second run were higher than the first and there was carry over into the blank. c) shows the average peak areas from sequential blank samples within a run. After introducing a wash step in the LC method, detailed in table 3.4, sequential calibration curves overlay. The calibration curves with the 1st in blue and the second in red for a) Alanine and b) serine.

3.5 LC-MS method provides inconsistent measurements between duplicate samples

To validate these methods appropriately, various standard samples were generated and run through these methods with known concentrations of various analytes. These included aliquots of the stocks used to generate the SRM methods, and included in the standard mixtures for calibrations, and media samples containing 500 µM alanine and 100 µM serine, and vice versa. If the sample was not already in a mobile phase appropriate for the LC method used, then the sample was dried down and resuspended in these conditions. Table 3.5 shows the concentration of the prepared QC samples, the measured concentration and the calculated accuracy. For each QC sample, good accuracy was not achieved. Table 3.5 shows that the peak areas and therefore calculated concentration are highly variable between replicates of the same QC sample measured from different positions in the plate and replicates of one sample diluted to various degrees. Due to the variability in this method, the conclusion was made that the methods and this system investigated here, although based on published methodology, are not robust, accurate or reliable enough to calculate intracellular concentrations of various metabolites (3.6 Discussion).

Table 3.5 details the precursor and product ions identified as most abundant for each analyte as well as the optimised DP, EP, CE and CXP voltages used for the most reliable detection of each analyte as well we the polarity of the ion being detected.

Table 3.5

QC Sample	Dilution Factor	Analyte	Expected Concentration (µM)	Calculated Concentration (µM)	Accuracy (%)
Standard Alanine	500	Alanine	300	118	39.3
Standard Alanine	100	Alanine	300	57.5	19.2
Standard Alanine	10	Alanine	300	197	65.6
5:1 Ratio (standards)	500	Alanine	500	217	43.4
5:1 Ratio (standards)	100	Alanine	500	170	34
5:1 Ratio (standards)	10	Alanine	500	246	43.2
1:5 Ratio (standards)	500	Alanine	100	46.4	46.4
1:5 Ratio (standards)	100	Alanine	100	49.1	49.1
1:5 Ratio (standards)	10	Alanine	100	49.9	49.9
Standard Serine	500	Serine	300	213	71
Standard Serine	100	Serine	300	140	46.7
Standard Serine	10	Serine	300	515	172
Standard Serine	500	Serine	100	98.1	98.1
Standard Serine	100	Serine	100	43.2	43.2
Standard Serine	10	Serine	100	106	106
5:1 Ratio (standards)	500	Serine	100	6.55	6.58
5:1 Ratio (standards)	100	Serine	100	266.5	26.5
5:1 Ratio (standards)	10	Serine	100	97.7	97.7
1:5 Ratio (standards)	500	Serine	500	95.9	19.2
1:5 Ratio (standards)	100	Serine	500	181	36.2
1:5 Ratio (standards)	10	Serine	500	321	64.3

In attempt to find another mass spectrometry method to use that was reliable, accurate and accessible to answer the biological questions, a published GC-MS full scan method [66] was investigated. Figure 3.9 shows the percent accuracy of a QC sample containing a mixture of metabolite extractions and internal standard measured 43 times across a sample run with ± 15 % accuracy indicated. Using the published method [66], the internal standard was within 15 % accuracy in 41 of 43 samples tested. Accuracy in this case is a comparison of expected and measured concentration. These data confirmed that the GC-MS method described would be a reliable and accurate method to analyse metabolic extracts.

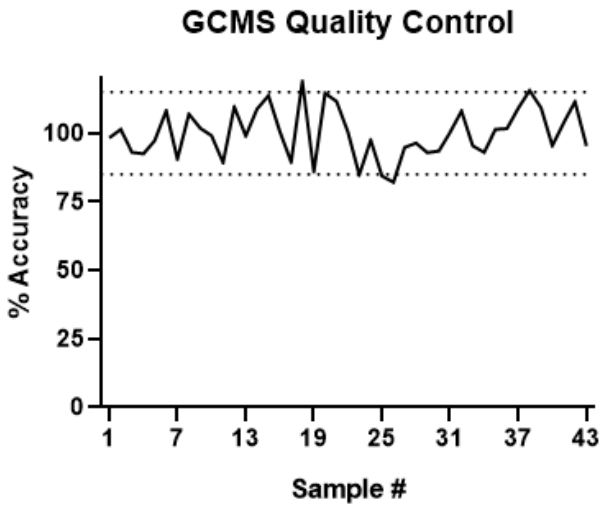

Figure 3.9: GC-MS provides a reliable and reproducible analytical method. A standard mixture of analytes was generated at a set concentration. 5 µL of the mixture was washed with methanol and derivatised as per the method in 2.2.5, this was repeated 43 times. The samples were analysed by GC-MS as per the method in 2.2.7. Data presented in this line graph represent each individual sample measured and the calculated accuracy of that sample around the average of a known standard measured. The dashed lines represent ± 15 % accuracy.

3.6 Discussion

The work in this chapter aimed to generate a single LC-MS/MS method to capture all 20 proteinogenic amino acids and key glycolytic intermediates to analyse cellular metabolite extractions and measure intracellular concentrations. All the analytes to be analysed can be measured by various LC-MS methods [67], [68], but there is no published method using a triple quadrupole mass spectrometer that captures them all. This capture all method using a triple quadrupole mass spectrometer would be advantageous as it is highly sensitive and specific. Although full scan mass spectrometry methods capture all analytes, they can suffer from incorrect assignment of peaks, and highly abundant analytes can supress the signal of analytes with low abundance.

The first step for method generation was to generate selected reaction monitoring (SRM) methods for each of the analytes of interest where DP, EP, CE and CXP voltages were optimised to detect the highest and most reliable fragment ions for each analyte. Once optimised, various LC columns were investigated to determine what solid phase would be most appropriate to capture all the analytes required. The Phenomenex Luna NH2 column was used based on a published method [65], however, this method did not capture any of the glycolytic intermediates required. An Omega polar C18 column (Phenomonex) was tested and did capture the glycolytic intermediates and some amino acids, but not all, including the model amino acid, alanine. Therefore, the decision was made to use a combination of both LC columns, the Luna NH2 and the Omega C18, and the analytes were split between them. If analytes could be captured on both, then the column with the highest quality peak was used. This compromise was made to move forward capturing all analytes across only two LC-MS methods.

Figure 3.5 shows the chromatogram overlays for both methods, some analytes such as asparagine and methionine overlay in LC column retention time. However, an advantage of the SRM methods is that, although their retention time is the same, they have a specific Q1/Q3 signature to distinguish these analytes. The calibration curves in Figures 2.3 and 2.4 gave the linear ranges and limits of quantitation for each analyte, which ranged from 5nM to 500uM. This information helped determine the dilution factor used for samples to be within the linear range of detection. Upon further investigation when multiple calibration curves were run sequentially from lowest to highest

concentration, the second calibration curve had a steeper slope than the first, indicating some sample carry over in the system. Investigating the blank and wash samples throughout the run, it was evident, using alanine as an example, although it was not the only analyte affected, that analytes were being carried over into subsequent samples or blanks. The amount of analyte detected in the blank samples decreased as more blanks were run, however the amount of analyte in the blanks did not decrease to the first blank in the run, before anything was sampled. This carry over, was eliminated in the HILIC Luna NH2 column method by including a wash step of 100 % aqueous before the column was re-equilibrated.

The next stage of method development was validation. This involved using standards of each analyte at set concentrations and media samples to ensure detection of a known concentration of analyte. Different dilution factors were used to probe different sections of the calibration curve, which we would expect to be consistent. However, these data were very variable and ranged from 6 % to 172 % accurate. Even the same QC sample injected at two different times within the same run were not consistent. There was no pattern in this data to suggest that there was a specific reason for this variability. For example, all measurements would be consistently low if there was ion suppression, or subsequent measurements higher than the last may indicate sample accumulation in the system.

Reasons for this variability point to the instrument itself as even replicate samples were being measured differently. One way to monitor this would be to use an internal standard in the QC samples and ensure this is constant through the sampling and use this to normalise the other analytes. Another reason for the media samples tested is that there is a matrix effect. Although the sample is dried down and resuspended in an appropriate mobile phase for the LC-MS method, it may be beneficial to wash the samples with methanol or ACN before resuspension. This may remove any salts or other components that could be causing a matrix effect. However, standard QC samples using the same material as the calibration curves, also showed variability, not only the sampled media, therefore it is unlikely that the variability is due to matrix effects.

In order to improve this method further, more LC-MS options can still be investigated. This could include derivatisation of the samples, possibly using the

AccQTag derivatisation kit by Waters. However, due to the variability in this data, and without significant re-optimisation of the method, or changing the method completely, the decision was made to use a published GC-MS full scan method [66] to detect analytes as accurately and reliably as possible. The advantage of using this method is that most of the analytes desired would be detected, including all amino acids, glucose, some other glycolytic and TCA cycle intermediates. However, it will not identify all glycolytic intermediates, including fructose -1,6- bisphosphate and comes without the many advantages of using a LC-MS/MS method. Data in Figure 3.9 shows that this method can measure appropriately the correct concentration in the quality control samples, accurately and reliably and therefore will be used for all future measurements of metabolic samples.

Chapter 4

Investigating intracellular amino acids and glycolytic metabolism in various media conditions

4.1 Introduction

PKM2 can be regulated by amino acids even when intracellular concentrations of allosteric activator F 1,6 BP are saturating. This led to the hypothesis that it is the ratio of activating and inhibitory amino acids within the cell, that can regulate PKM2 activity and by extension, glycolysis. Alanine and serine were chosen as model amino acids to investigate this hypothesis. Alanine is an inhibitor of PKM2 and was chosen as a model inhibitor because there is plentiful published biochemical data available for the interaction between alanine and PKM2 and because it behaves as an inhibitor via a negative feedback loop. The negative feedback loop occurs through the production of pyruvate from PKM2 and subsequent conversion to alanine by glutamate pyruvate transaminase (GPT). The carbons from glucose breakdown can be tracked into the generation of this known PKM2 inhibitor, alanine. Serine is an activator of PKM2 and was chosen as a model activator because it acts by a feed-forward mechanism. Serine is generated through the SPP from 3-PG and therefore carbons can also be monitored from glucose breakdown into the production of this activator. In order to investigate this hypothesis, we aimed to alter the alanine and serine composition in LN229 cells by providing various ratios of alanine and serine in the cellular media. GC-MS was used to measure the intracellular concentration of alanine and serine. These measurements confirmed the amino acids concentrations can be manipulated by the media composition and the time taken for that amino acid change to reach steady state within the cell.

Following this confirmation, the cells were provided with fully labelled ^{13}C-glucose to monitor the effect on glucose carbons as they are broken down through glycolysis and further processed by the cell. Various metabolites will be compared between conditions with different alanine and serine ratios to create an environment with high PKM2 activator

serine and low PKM2 inhibitor alanine, and vice versa. Cellular metabolite extracts were analysed by GC-MS to determine the intracellular concentration of labelled analytes.

4.2 Published RNA data could be used to identify cell lines for experiments

The COSMIC cell line database was used to investigate RNA expression in cancer cell lines to identify cells that may endogenously have high serine or alanine intracellular concentrations. The enzyme RNA expression investigated were those involved in the serine production pathway, and the generation of alanine from pyruvate. The expression of the RNA encoding the enzymes PHGDH, PSAT1, PSPH, GPT and GPT2 were of interest. Two cell lines were identified as the highest priority to investigate further as having potentially opposite phenotypes. These were LOUCY and KATO-III. The reason that these cell lines were chosen is that LOUCY has very high expression of PHGDH and very low expression of GPT and GPT2. This would suggest this cell line has a high production rate of serine due to the increased expression of PHGDH and a lower rate of alanine production due to the lower expression of GPT and GPT2. This cell line may natively have a high intracellular concentration of serine, and low intracellular concentration of alanine, mimicking the high activator 1:5 A:S conditions used in the experiments described below in Section 4. Alternatively, cell line KATO-III has an increased expression of GPT and very increased expression of GPT2, but a very low expression of PHGDH. The prediction for the phenotype in these cells is an increase in intracellular alanine and a lower intracellular concentration of alanine. KATO-III may therefore mimic the high inhibitor 5:1 A:S condition in the experiment in this chapter. Figure 4.1 contains the RNA expression data from the COSMIC cell line database with the associated cancer cell line. The heatmap in Figure 4.1 can be separated into 4 categories with different predictions on the PKM2 regulation. Bucket A contains cell lines with high PHGDH expression and lower GPT expression, which would predict PKM2-activating conditions. Bucket D contains cell lines that have a very low expression of GPT or GPT2 and would therefore predict PKM2-activating conditions also. Bucket B contains cell lines with high GPT or GPT2 expression, which would predict PKM2- inhibitory conditions. KATO-III and LOUCY could be used to investigate this further without the need for media manipulation to illicit an intracellular concentration change of each amino

acid. The use of these cell lines would allow investigation of the endogenous state of the alanine to serine ratio. Ultimately for the following experiments, LN229 cells were chosen based on the published amino acid and F 1,6 BP concentration data and influence on PKM2 activity [66].

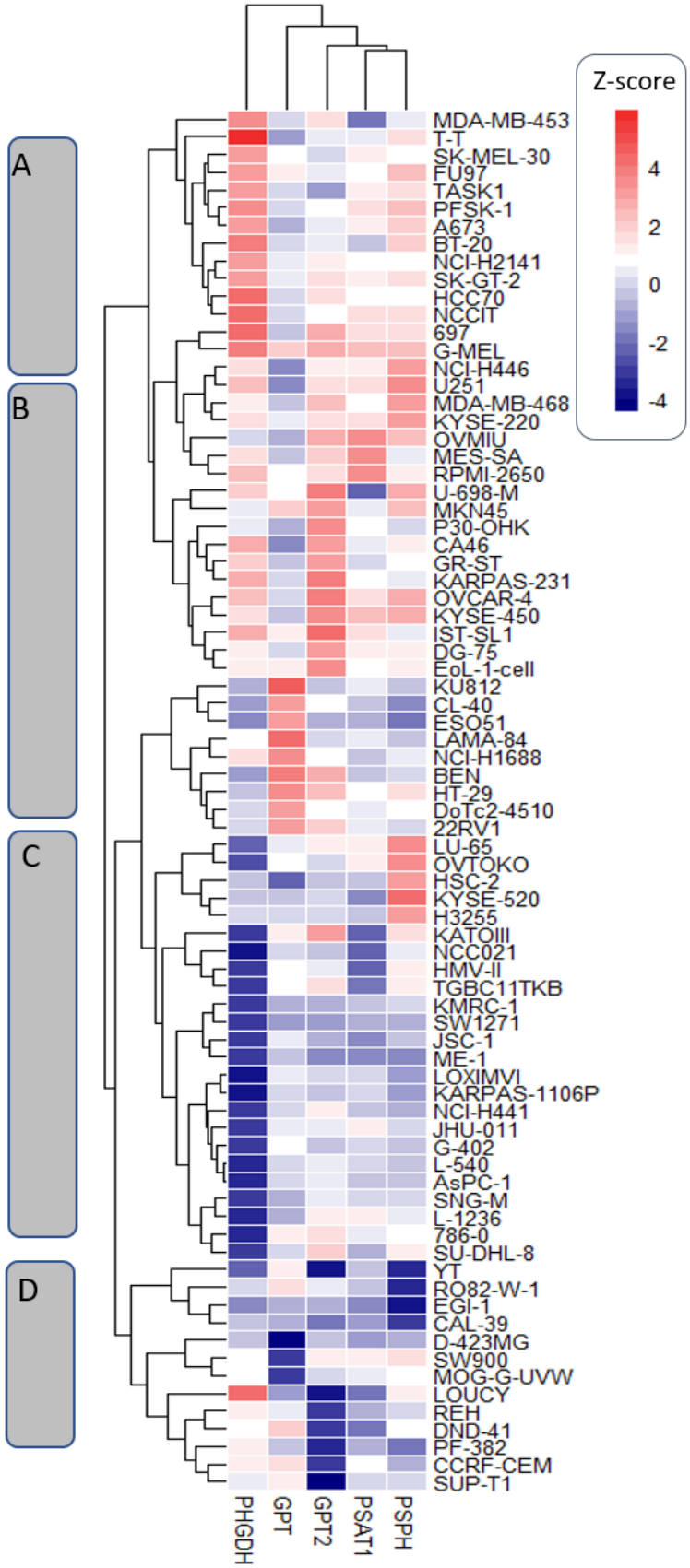
Z-score
4
2
0
-2
-4
A
B
C
D
MDA-MB-453
T-T
SK-MEL-30
FU97
TASK1
PFSK-1
A673
BT-20
NCI-H2141
SK-GT-2
HCC70
NCCIT
697
G-MEL
NCI-H446
U251
MDA-MB-468
KYSE-220
OVMIU
MES-SA
RPMI-2650
U-698-M
MKN45
P30-OHK
CA46
GR-ST
KARPAS-231
OVCAR-4
KYSE-450
IST-SL1
DG-75
EoL-1-cell
KU812
CL-40
ESO51
LAMA-84
NCI-H1688
BEN
HT-29
DoTc2-4510
22RV1
LU-65
OVTOKO
HSC-2
KYSE-520
H3255
KATOIII
NCC021
HMV-II
TGBC11TKB
KMRC-1
SW1271
JSC-1
ME-1
LOXIMVI
KARPAS-1106P
NCI-H441
JHU-011
G-402
L-540
AsPC-1
SNG-M
L-1236
786-0
SU-DHL-8
YT
RO82-W-1
EGI-1
CAL-39
D-423MG
SW900
MOG-G-UVW
LOUCY
REH
DND-41
PF-382
CCRF-CEM
SUP-T1
PHGDH
GPT
GPT2
PSAT1
PSPH

Figure 4.1: Cell lines with predicted endogenous differences in alanine and serine. Heat map of data acquired from the COSMIC cell line database to indicate RNA expression of enzymes PHGDH, PSAT1 and PSPH in the serine production pathway, and GPT1/2 those responsible for alanine production. Data was filtered using a Z score threshold of > 3 or < -3 to identify cell lines with significant over or under expression of these genes. Cell lines were then ordered by hierarchical clustering. Buckets of cell lines are indicated by labelled boxes. Z scores indicate the number of standard deviation away from the mean reference expression.

4.3 Cells deprived of most amino acids are still viable after 24 hours

To determine that over time cells in various media conditions are still viable, cells were incubated for 60 hours, and their confluency measured over time using an Incucyte. The percentage confluency increases over time in all conditions until approximately 24 hours (Figure 4.2). At this point, cells with only alanine and serine provided as amino acids in the media slow down growth, which stays constant at roughly 75% confluency for the remainder of the time measured. The culture media and conditions supplemented with all amino acids continue growing until they reach 100 % confluency and remain there. Cell growth is not slowed by using dialysed fetal bovine serum (dFBS) and supplemented amino acids. The slopes at the exponential growth phase of each condition are similar, therefore the condition with basal DMEM, 10 % dFBS, 5mM ^{13}C-glucose, and 500 µM : 100 µM alanine : serine and vice versa, without additional amino acid supplementation were chosen for the later metabolomics time course experiments.

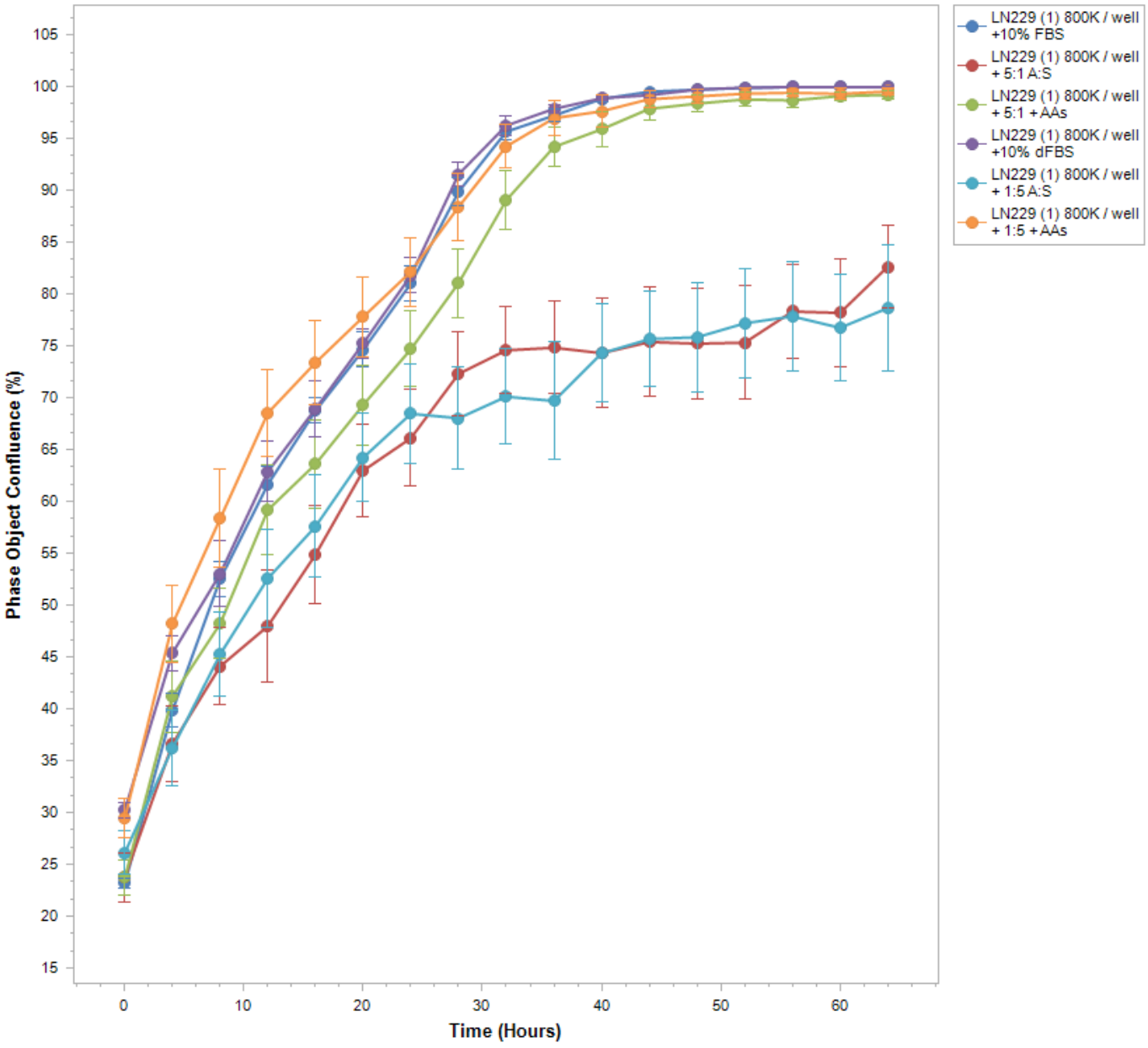

Figure 4.2: LN229 cell growth curve in various media. Incucyte growth curve experiment where LN229 cells were seeded at 800,000 cells in a 6-well plate in different media conditions, and left to incubate for 60 hours. Confluency measurements were taken every 4 hours. Conditions include culture DMEM + 10 % FBS (dark blue), culture DMEM + 10 % dFBS (purple), DMEM with 5:1 or 1:5 alanine: serine and no other amino acids given (red and pale blue respectively), DMEM with 5:1 or 1:5 alanine: serine with all other amino acids supplemented to the same concentration as DMEM culture media (green and orange respectively.)

4.4 The intracellular concentrations of alanine and serine can be altered by manipulating growth media

To determine if a change in intracellular concentration of amino acids, that can influence PKM2, affects glycolysis and downstream metabolism, we must first confirm that we can manipulate the intracellular concentration as intended. To do this, LN229 cells were treated with media containing a 5:1 or 1:5 ratio of alanine and serine. Using the volume of the cell calculated using the cell radius, the intracellular concentrations of alanine and serine were calculated. The high inhibitor, 5:1 alanine to serine condition had a measured intracellular ratio of 10:1 A:S, indicating that the intracellular amino acid ratio manipulation in this condition was achieved (Figure 4.3). In the high activator, 1:5 alanine to serine condition, the measured intracellular ratio achieved was 1:2 A:S (Figure 3.3). In these tested conditions, an intracellular ratio of 5:1 or 1:5, as in the media is not achieved. However, in each media condition, the amino acid intended to be at the higher concentration, was measured to be at a higher concentration, compared to the opposing amino acid. The concentration of these amino acids reached steady state within 15 minutes of treatment and is constant for 6 hours. Therefore, it is possible to manipulate the alanine to serine ratio within the cells by manipulating the media given to the cells.

a

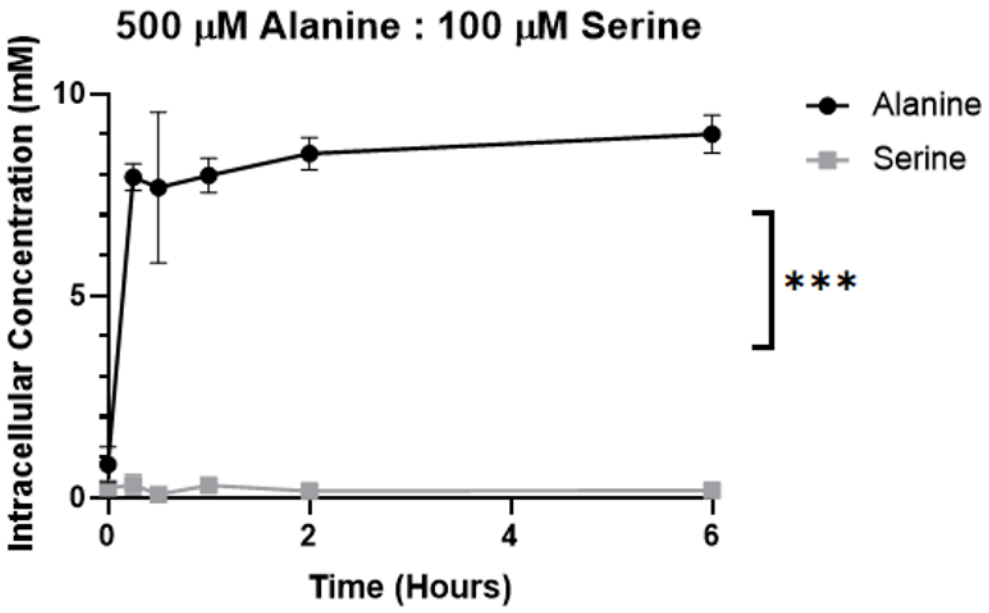

b

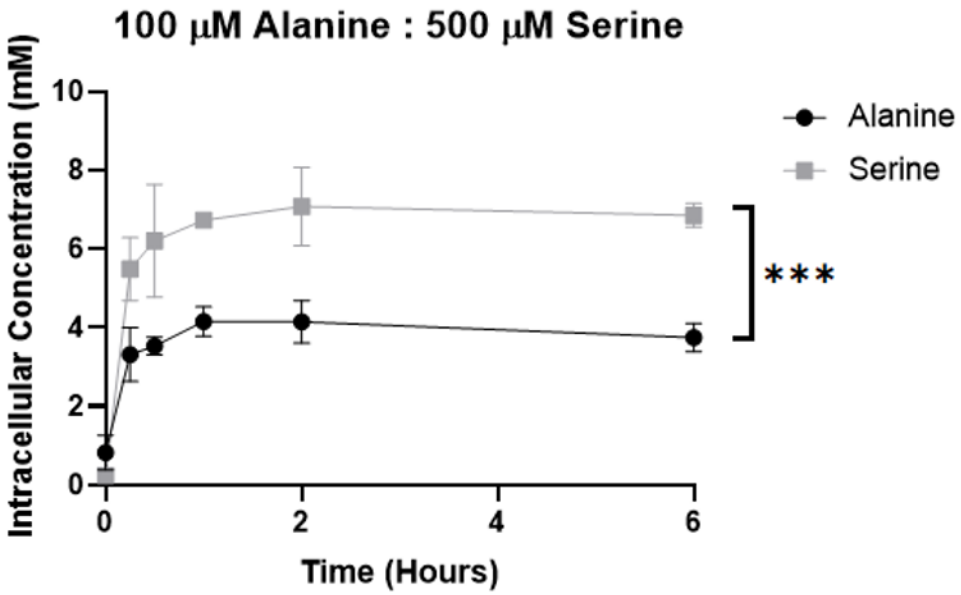

Figure 4.3: Intracellular concentrations of alanine and serine in different treatment conditions. LN229 cells seeded at 800,000 cells per well were treated with a 5:1 or 1:5 ratio of alanine to serine in media and metabolism quenched and extracted at various time points over 15 minutes, 30 minutes, 1 hour, 2 hours and 6 hours. Extractions were analysed by GC-MS. Intracellular concentrations of alanine (black) and serine (grey) in LN229 cells after 6 hours with media containing a) 500 µM alanine and 100 µM serine or b) 100 µM alanine and 500 µM serine. *** = p value < 0.001. t-test compared the plateau of the curve fit as the established, stable concentration.

4.5 Alanine is the inhibitor with the highest measured intracellular concentration and lowest binding affinity

Alanine and serine are not the only amino acids within the cell that can influence PKM2 activity. Only alanine and serine are given in the media and dFBS is used to allow starvation of other amino acids, and avoid them binding to PKM2. Other amino acids still exist in the cell from general amino acid metabolism, although not all are available in the cytosol to bind PKM2. The amino acids within the cell at time zero are plotted in Figure 4.4a. PKM2 activator, histidine is below the lower limit of detection and therefore is unlikely to be contributing to any PKM2 effects. Other PKM2 inhibitors such as phenylalanine do exist in the cell at detectable levels at time zero and therefore could influence PKM2 activity. Published affinity measurements of all inhibitory amino acids and their inhibition constants (K_i) were determined using a system with purified protein [37]. The authors determined the K_i for alanine was the lowest of all of the inhibitors at 62 µM. The intracellular concentration of alanine within 15 minutes of treatment is within the mM range (Figure 4.3), therefore this will be saturating PKM2. The study also determined a K_i of 205 µM for phenylalanine, and 225 µM for tryptophan. The intracellular concentration of these inhibitors was measured to be higher than the K_i in all cases (Figure 4.4b). However, as stated, within 15 minutes of media manipulation, the intracellular concentration of alanine is 8- and 5- fold higher than tryptophan and phenylalanine respectively, which will outcompete the other inhibitors present in the cytosol.

a

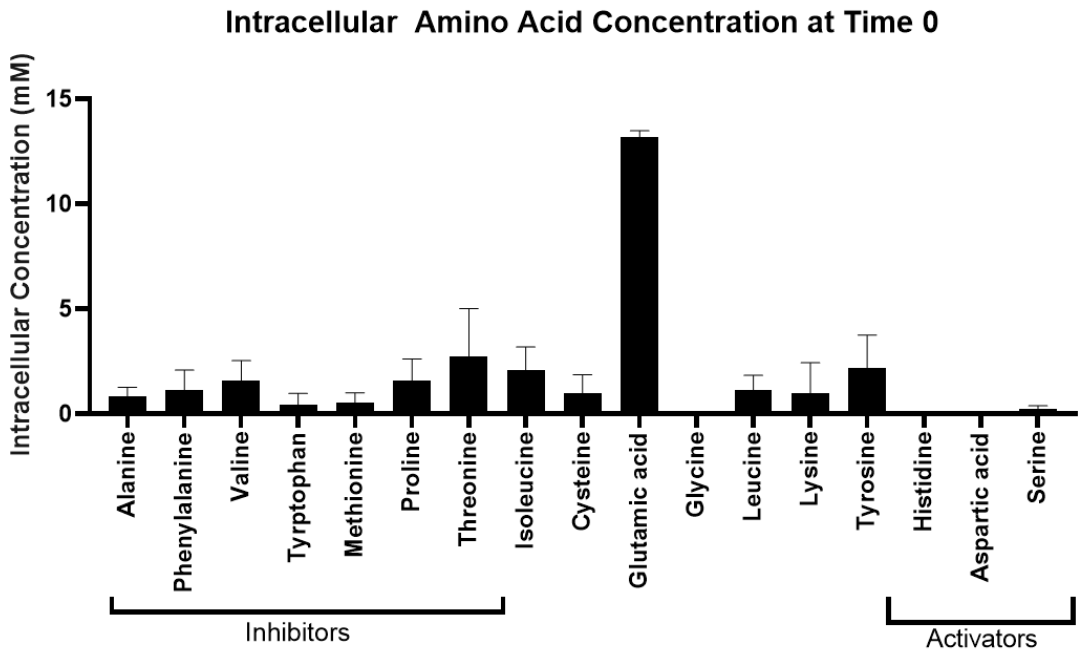

b

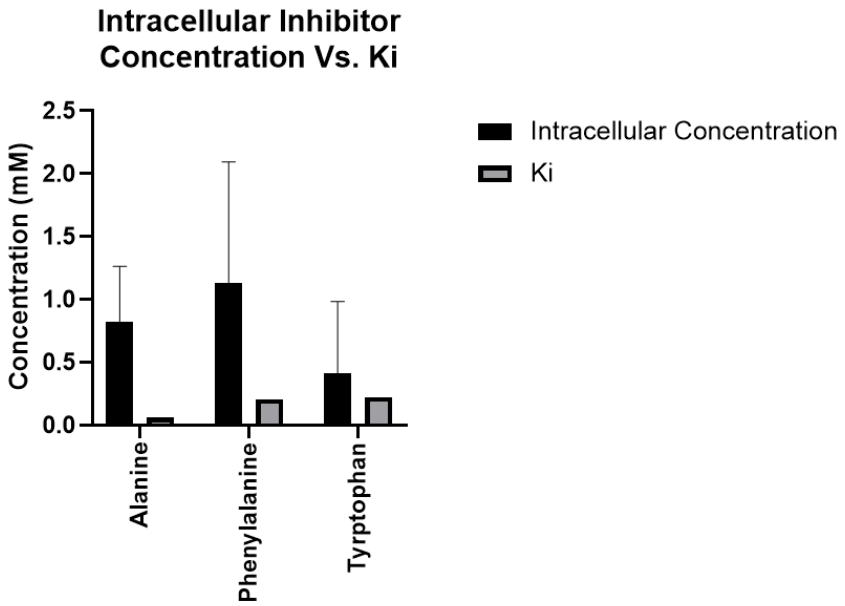

Figure 4.4: Intracellular amino acid landscape at the point of treatment. LN229 cells seeded at 800,000 cells per well and left to incubate for 23 hours. Media was replaced and cells incubated for another hour before metabolism was quenched and harvested before any further treatment. Extractions were analysed via GC-MS. a) Intracellular concentration of each amino acid at time zero before treatment. Amino acids with documented PKM2-activating or -inhibitory effects are highlighted. b) Measured intracellular concentrations of PKM2 inhibitors compared to the measured Ki for these amino acids against PKM2 from published data [35]

4.6 Amino acid ratios have no effect on glycolytic intermediates

As it has been demonstrated that the intracellular amino acid concentration can be manipulated within the cell, next we investigated any changes in glycolytic and downstream metabolism. In order to do this, the cells were given ^{13}C-glucose and treated with the PKM2-inhibitory 5:1 A:S and PKM2-activating 1:5 A:S media conditions and left to incubate for 6 hours, with various time points harvested in between. Metabolism was quenched and metabolites extracted and analysed on GC-MS and intracellular concentration of metabolites calculated. A 6-hour incubation was used in this case to determine a difference between treatment conditions and if an isotopic steady state of labelled metabolites is reached in this time.

The effects on glycolytic intermediates were investigated initially. The absolute intracellular concentration of glucose decreases over 6 hours and there is no difference between the two treatment conditions (Figure 4.5a). The fractional labelling of glucose achieves steady state for the time course at 75 % within 15 minutes and remains stable (Figure 4.5c). The fractional labelling of glucose is maintained between the two treatment conditions. The next glycolytic intermediates that can be detected using this method are glucose – 6 – phosphate (G6P) and fructose - 6 - phosphate (F6P). Both of these metabolites reach an isotopic steady state within 15 minutes and are maintained at 75 % fractional labelling (Figure 4.5f and Figure 4.5i). 3 - phosphoglycerate (3-PG), further down the glycolytic pathway reaches 75 % fractional labelling within 15 minutes and remains at steady state (Figure 4.5l). The final metabolite of glycolysis is pyruvate, which is another analyte for which the intracellular concentration can be detected. Pyruvate is one of the products of PKM2 alongside ATP, and investigating this metabolite might shed light on the regulation of PKM2 between the two conditions. The absolute concentration of pyruvate spikes within 15 minutes, but then decreases over the 6-hour time course (Figure 4.5p). However, the amount of labelled pyruvate increases over time up to 6 hours (Figure 4.5n). The fractional labelling of pyruvate increases to a maximum of 40 % and a clear plateau is not reached, indicating the isotopic labelling of pyruvate has not yet reached steady state within 6 hours (Figure 4.5o). There is no significant difference in pyruvate labelling between the high activator and high inhibitor treatment conditions.

Regarding the last step of aerobic glycolysis and the conversion of pyruvate to lactate, the concentration of labelled lactate increases across 6 hours (Figure 4.5q). The fractional labelling of lactate does not reach steady state within 6 hours and there is no difference between the two treatment conditions (Figure 4.5r). There is no significant difference in the absolute concentrations, labelled concentrations or fractional labelling of glucose, G6P, F6P, 3-PG, pyruvate or lactate between the high activator and high inhibitor treatment conditions. These data also show that glucose, G6P, F6P and 3-PG reach an isotopic steady state in 6 hours, however, pyruvate and lactate do not. Therefore, it would be beneficial to extend the time course, to attempt to achieve an isotopic steady state for these analytes.

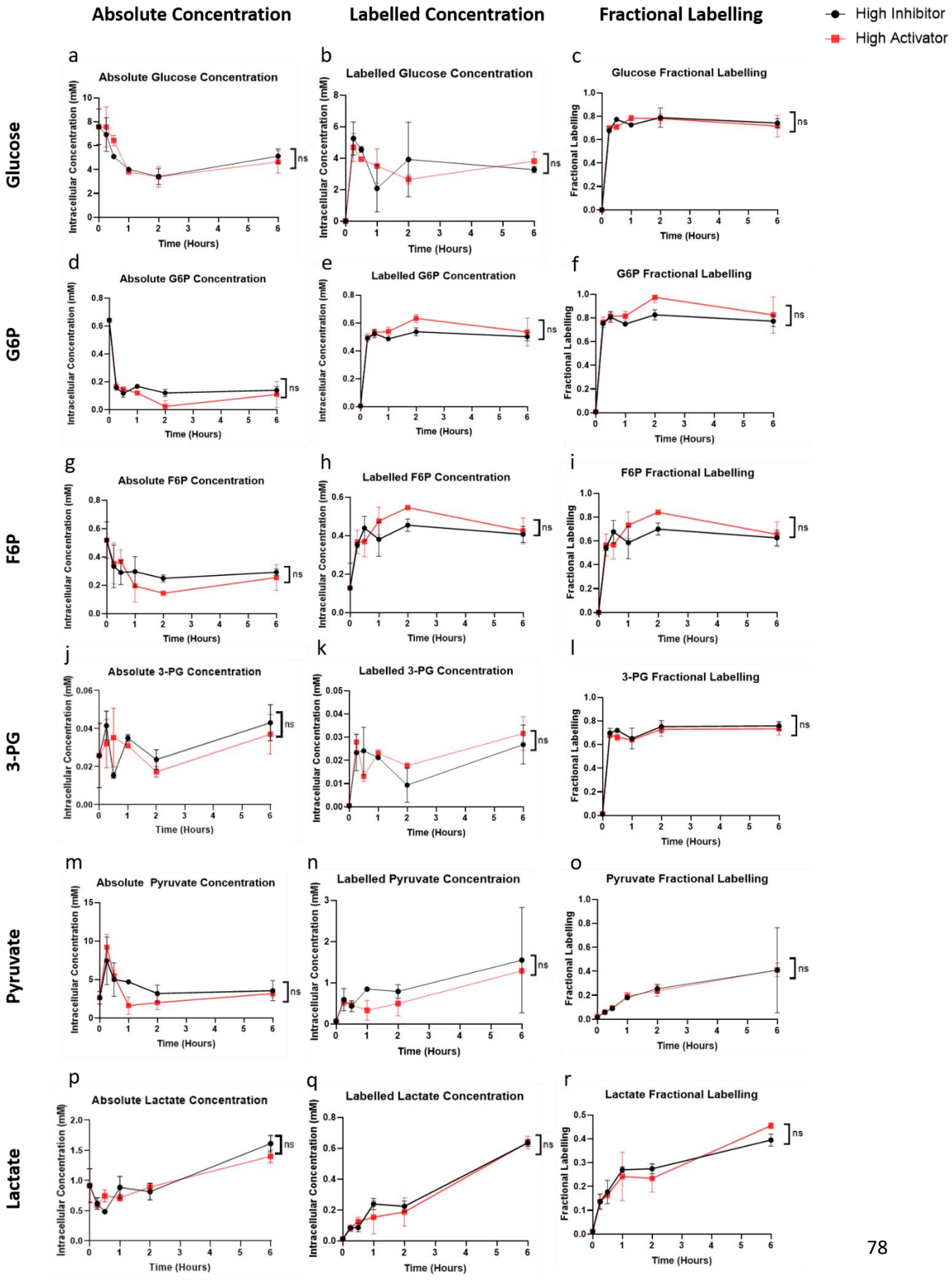
Absolute Concentration
Labelled Concentration
Fractional Labelling
High Inhibitor
High Activator
Glucose
G6P
F6P
3-PG
Pyruvate
Lactate
a
Absolute Glucose Concentration
b
Labelled Glucose Concentration
c
Glucose Fractional Labelling
d
Absolute G6P Concentration
e
Labelled G6P Concentration
f
G6P Fractional Labelling
g
Absolute F6P Concentration
h
Labelled F6P Concentration
i
F6P Fractional Labelling
j
Absolute 3-PG Concentration
k
Labelled 3-PG Concentration
l
3-PG Fractional Labelling
m
Absolute Pyruvate Concentration
n
Labelled Pyruvate Concentraion
o
Pyruvate Fractional Labelling
p
Absolute Lactate Concentration
q
Labelled Lactate Concentration
r
Lactate Fractional Labelling
Intracellular Concentration (mM)
Fractional Labelling
Time (Hours)
ns

Figure 4.5: Amino acid treatments have no effect on glycolytic rate. LN229 cells were seeded at 800,000 cells per well and treated with either 5:1 or 1:5 alanine to serine ratio in the media. Metabolism was quenched and harvested after 15 minutes, 30 minutes, 1 hour, 2 hours, and 6 hours incubation before analysis via GC-MS. Data for activating 1:5 A:S condition is in red and inhibitory 5:1 condition in black. The absolute intracellular concentration of a) glucose, d) G6P, g) F6P, j) 3-PG, m) pyruvate, p) lactate. The labelled intracellular concentration of b) glucose, e) G6P, h) F6P, k) 3-PG, n) pyruvate, q) lactate. The fractional labelling for c) glucose, f) G6P, i) F6P, l) 3-PG, o) pyruvate, r) lactate. ns = not significant.

4.7 Amino acid ratios influence trends in serine production through the serine production pathway

There are some metabolites that are generated from glycolytic intermediates that we can also use to determine whether high activator or high inhibitor media conditions influence glycolysis. These include glycerol – 3 – phosphate (G3P), serine and alanine. The media condition that contains a high concentration of inhibitor, alanine, the rate of labelled alanine production is 0.55 ± 0.04 $hour^{-1}$, significantly higher than the low inhibitor, or high activator condition at 0.29 ± 0.04 $hour^{-1}$ (Figure 4.6b). However, the fractional labelling of alanine is not significantly different between the high activator and high inhibitor conditions (Figure 4.6c). This means that in the high inhibitor condition, there is a higher contribution of glucose carbons into the production of alanine, but the relative contribution of carbons from glucose and other, unlabelled pathways into the production of alanine do not change between the treatment conditions. To account for this non-significant change in fractional labelling, there is some dilution of the total alanine pool by the unlabelled alanine provided in the media. In this case, if the total pool of alanine were the same between the two conditions, we could expect the labelled fraction to be lower in the high inhibitor 5:1 A:S condition, due to the amount of unlabelled alanine diluting the total pool. However, the fraction of labelled alanine in these two conditions is very similar (Figure 4.6 c), suggesting that the alanine must be being used elsewhere to account for this change and decreasing the size of the pool. There is no evidence for this in a dilution of the pyruvate pool in this condition, therefore the unlabelled alanine is not being converted to pyruvate (Figure 4.5m). It is a possibility that the excess unlabelled alanine

is being exported from the cell, in exchange for transport of other amino acids. Export could be one of many explanations why the labelled alanine fraction is similar between the two conditions.

The serine production pathway (SPP) begins at the point of 3-PG and branches from the main glycolytic pathway. If there is a build-up of glycolytic intermediates that can be funnelled through different pathways in a high inhibitor condition, this might be evident in branching metabolites such as serine. The intracellular concentration of labelled serine increases over time in the high activator 1:5 A:S condition (Figure 4.6e). The intracellular concentration of labelled serine in the high inhibitor 5:1 A:S condition is variable and around the lower limit of detection. However, the fractional labelling of serine, which considers the size of the serine pool and contributions of other unlabelled carbon sources for serine, shows that in the high inhibitor 5:1 A:S condition, there is a higher labelled fraction of serine 0.44 ± 0.07 $hour^{-1}$, compared to the high activator condition at 0.56 ± 0.23 $hour^{-1}$ (Figure 4.6f). Although this difference is not significant, it indicates a trend at the highest time points. These data suggest that in the high inhibitor 5:1 A:S condition, there may be an increased contribution of glucose carbons through the SPP and into serine. Increasing the time course may improve this difference between conditions.

Another metabolite generated from glycolytic intermediates that can be measured is G3P. By 6 hours, 15 % of the G3P fractional labelling is achieved, and this does not reach an isotopic steady state (Figure 4.6i). There is also no significant difference in the labelled intracellular concentration of G3P, indicating that the treatment conditions do not influence the contribution of glucose carbons into the production of G3P (Figure 4.6h).

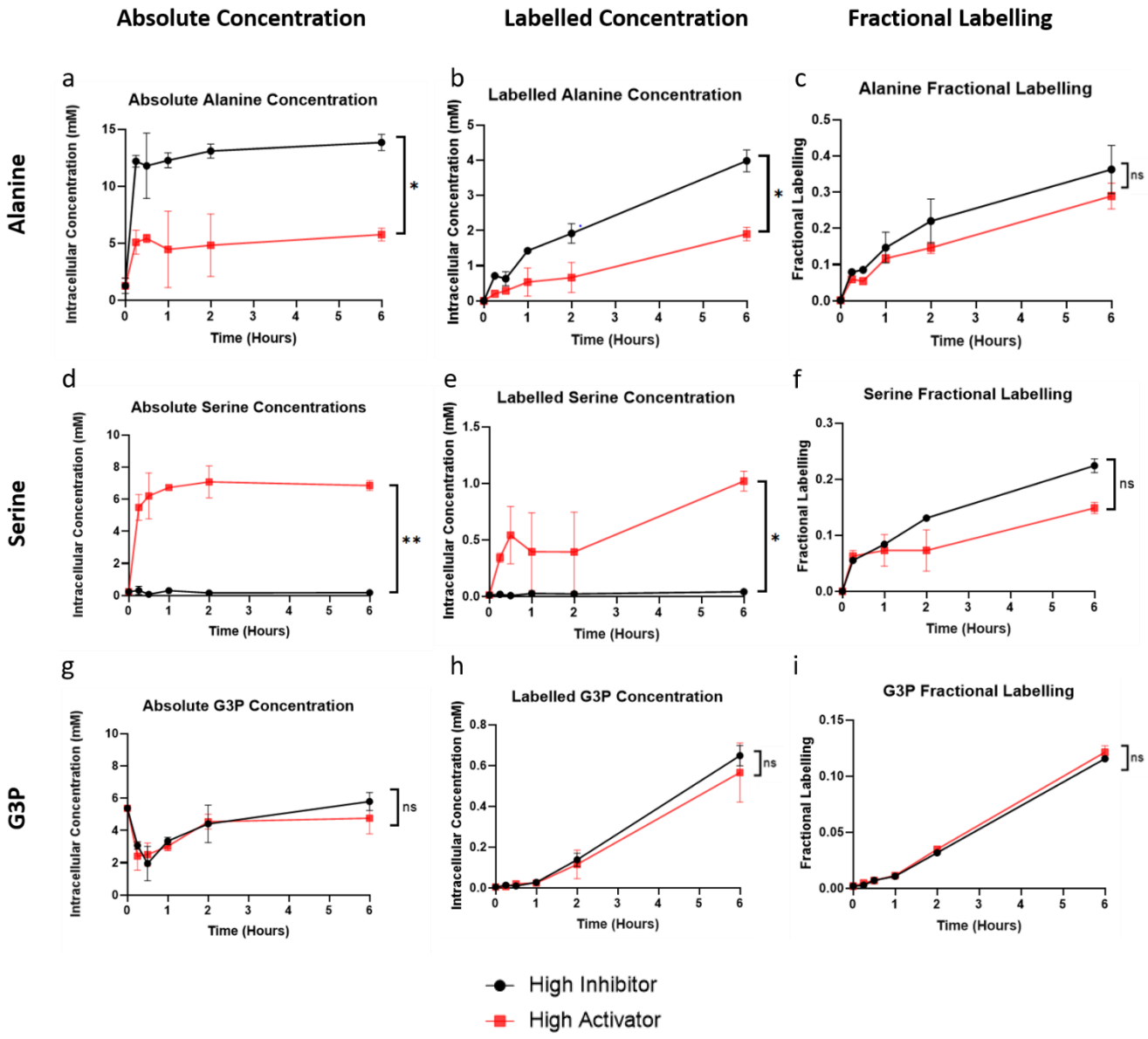

Figure 4.6: Intracellular concentration data of alanine, serine and G3P from the 6-hour time course. LN229 cells were seeded at 800,000 cells per well and treated with either 5:1 or 1:5 alanine to serine ratio in the media. Metabolism was quenched and harvested after 15 minutes, 30 minutes, 1 hour, 2 hours, and 6 hours incubation before analysis via GC-MS. Intracellular absolute concentration of a) alanine, d) serine and g) G3P. Intracellular concentration of labelled b) alanine, e) serine and h) G3P. The fractional labelling of c) alanine, f) serine and i) G3P. Data for activating 1:5 condition is in red and inhibitory 5:1 condition in black. * = p value < 0.05, ** = p value < 0.01. ns = not significant.

4.8 High activator amino acid ratios increase rate of labelled TCA cycle intermediate production

Another set of metabolites that can be investigated downstream of glycolysis are those in the tricarboxylic acid (TCA) cycle. The GC-MS method used in these experiments can quantify citrate, α-ketoglutarate (α-KG), succinate, fumarate and malate. Although the rate of labelled citrate production is not significantly different between the two treatment conditions (Figure 4.7b), the rate of fractional labelling was higher in the high activator 1:5 A:S treatment condition at 1.1 ± 0.25 $hour^{-1}$ compared to the high inhibitor 5:1 A:S condition at 0.59 ± 0.12 $hour^{-1}$ (Figure 4.7c). The labelled concentration of citrate increases and a difference between the condition emerges between the two treatment conditions over 6 hours. Citrate has not reached an isotopic steady state within 6 hours, suggesting that the time course should be extended.

Conversely to citrate, the rate of fractional labelling of α-KG does not show a significant difference between the two treatment conditions (Figure 4.7f). However, the rate of labelled α-KG generation is increased in the high activator 1:5 A:S treatment condition at 0.006 ± 0.0002 $hour^{-1}$ compared to the high inhibitor condition at 0.0035 ± 0.0002 $hour^{-1}$ (Figure 4.7e). The rate of absolute α-KG generation is increased in the high activator 1:5 A:S treatment condition at 0.017 ± 0.0012 $hour^{-1}$ compared to the high inhibitor condition at 0.0001 ± 0.0025 $hour^{-1}$ (Figure 4.7d). The fractional labelling of α-KG suggests an approach to an isotopic steady state, however these data cannot confirm whether an isotopic steady state is achieved. To confirm, a longer time course would be required.

Similar observations to α-KG are seen for succinate although the rate of labelled succinate production is not significantly different between the two conditions (Figure 4.7h). A trend can be observed in these labelled succinate data that there is an emerging difference between the two conditions at increasing time points. An isotopic steady state for succinate cannot be confirmed using these data and therefore an increased time point would be required (Figure 4.7i).

Data for fumarate follow the same pattern as other TCA cycle intermediates with a significantly higher rate of labelled intracellular concentration at 0.001 ± 0.0001 $hours^{-1}$

in the high activator treatment condition, compared to the high inhibitor condition at 0.0006 ± 0.00001 $hours^{-1}$ (Figure 4.7k). Although it is clear that within 6 hours an isotopic steady state of fumarate is not reached (Figure 4.7l). Similar data can be seen for malate. There is a higher rate of labelled malate generated in the high activator condition at 0.0087 ± 0.0007 $hours^{-1}$, compared to the high inhibitor condition at 0.0047 ± 0.0004 $hours^{-1}$ (Figure 4.7n) as well as an increased rate of absolute malate (Figure 4.7m) at 0.02 ± 0.0017 $hours^{-1}$ in the high inhibitor condition, compared to 0.033 ± 0.0039 $hours^{-1}$ in the high activator condition. However, malate does not reach an isotopic steady state in 6 hours, whereas other upstream TCA cycle do (Figure 4.7o).

These data presented in Figure 4.7 show that in the high activator treatment condition, there is a higher concentration of labelled TCA cycle intermediates than in the high inhibitor condition. In order to confirm these data, this experiment will be repeated using a longer time course of 24 hours, to ensure isotopic steady state of these analytes is achieved and allow any divergence between treatment conditions to increase.

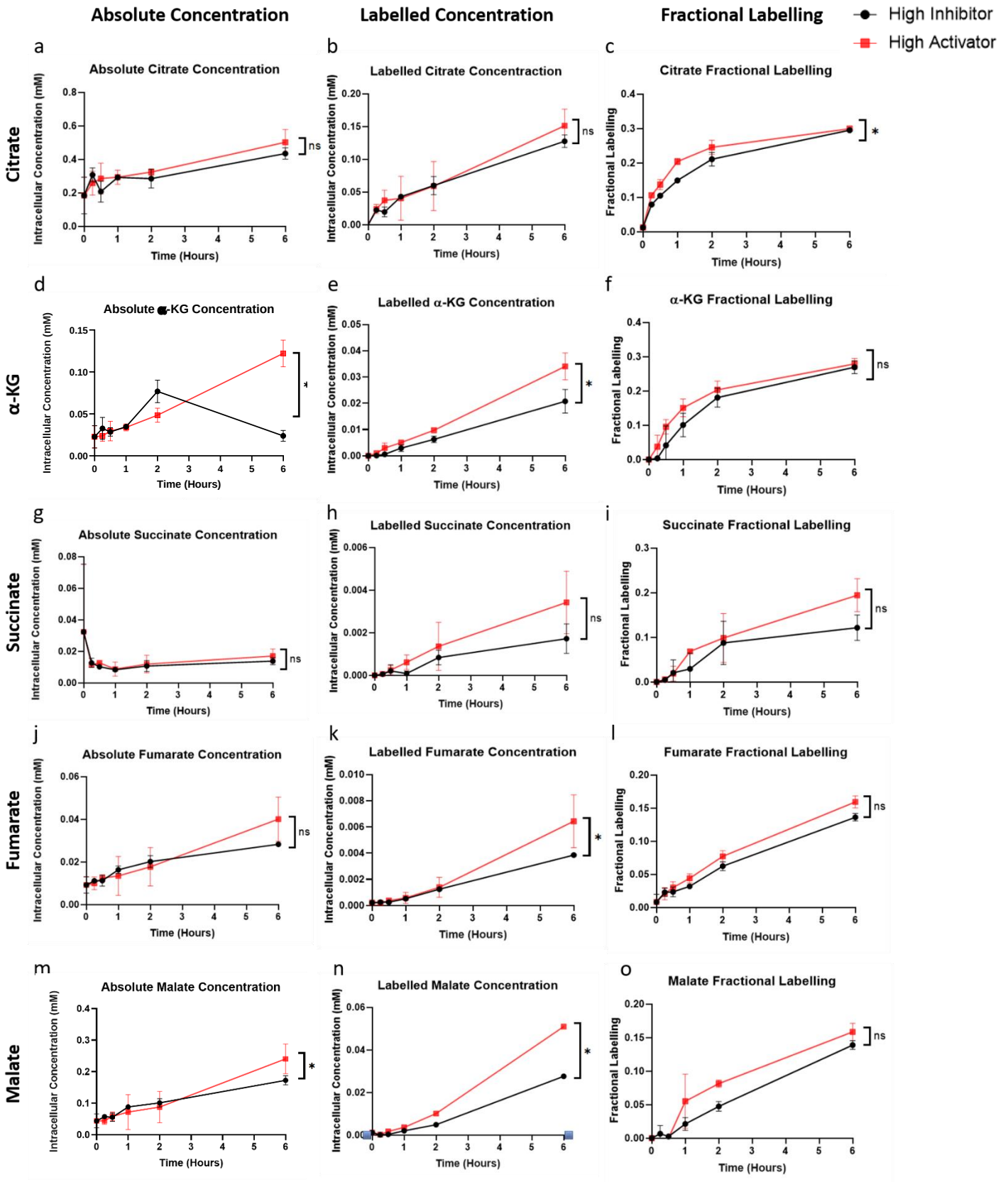
Absolute Concentration
Labelled Concentration
Fractional Labelling
High Inhibitor
High Activator
Citrate
α-KG
Succinate
Fumarate
Malate
a
Absolute Citrate Concentration
b
Labelled Citrate Concentraction
c
Citrate Fractional Labelling
d
Absolute α-KG Concentration
e
Labelled α-KG Concentration
f
α-KG Fractional Labelling
g
Absolute Succinate Concentration
h
Labelled Succinate Concentration
i
Succinate Fractional Labelling
j
Absolute Fumarate Concentration
k
Labelled Fumarate Concentration
l
Fumarate Fractional Labelling
m
Absolute Malate Concentration
n
Labelled Malate Concentration
o
Malate Fractional Labelling
Intracellular Concentration (mM)
Fractional Labelling
Time (Hours)
ns
*

Figure 4.7: Intracellular data for TCA cycle intermediates from 6-hour time course. LN229 cells were seeded at 800,000 cells per well and treated with either 5:1 or 1:5 alanine to serine ratio in the media. Metabolism was quenched and harvested after 15 minutes, 30 minutes, 1 hour, 2 hours, and 6 hours incubation before analysis via GC-MS. Data for activating 1:5 condition is in red and inhibitory 5:1 condition in black. The absolute concentration of a) citrate, d) α-KG, g) succinate, j) fumarate and m) malate. The labelled concentration of b) citrate, e) α-KG, h) succinate, k) fumarate and n) malate. The fractional labelling for c) citrate, f) α-KG, i) succinate, l) fumarate and o) malate. * = p value <0.05. ns = not significant.

4.9 An isotopic steady state is achieved for all glycolytic intermediates in 24 hours

In order to further investigate and confirm the data seen previously, the same experiment was completed but with an increased incubation time. Cells were incubated with ^{13}C-glucose in either high activator media; containing a 1:5 ratio of alanine to serine, or high inhibitor media containing a 5:1 ratio of alanine to serine. These cells were harvested at various time increments over 24 hours and metabolites measured by GC-MS.

The absolute glucose concentration, by the 10-hour time point, has depleted and therefore the cells are likely to be under significant stress after this point (Figure 4.8a). Data were collected for a 24-hour time point, however these data were omitted for plotting purposes and calculating production rates of each analyte due to a lack of glucose and therefore predicted cell stress. As per the 6-hour time course data for glucose in Figure 4.5c, glucose reaches a maximal fractional labelling at 75 % within 15 minutes and remains at steady state for 10 hours (Figure 4.8c). However, there is no significant difference between the two treatment media, confirming the observations from the 6-hour time course. There is also no difference between the two treatment conditions in the fractional labelling or rate of labelled 3-PG production (Figure 4.8e and Figure 4.8f). These data, similar to Figure 4.5l, observe a fractional labelling of 3-PG stable at 75 % within 15 minutes (Figure 4.8f). Unlike in the 6-hour time course, within 10 hours, pyruvate and lactate achieve an isotopic steady state at around 25 % (Figure 4.8i and Figure 4.8l). There is no significant difference between the two treatment conditions on the generation of labelled pyruvate and lactate (Figure 4.8h and Figure 4.8k).

Much like the previous iteration of this experiment, it appears that there is no discernible difference in glycolytic intermediates with high activator or high inhibitor media provided. All metabolites reached an isotopic steady state within 10 hours of incubation.

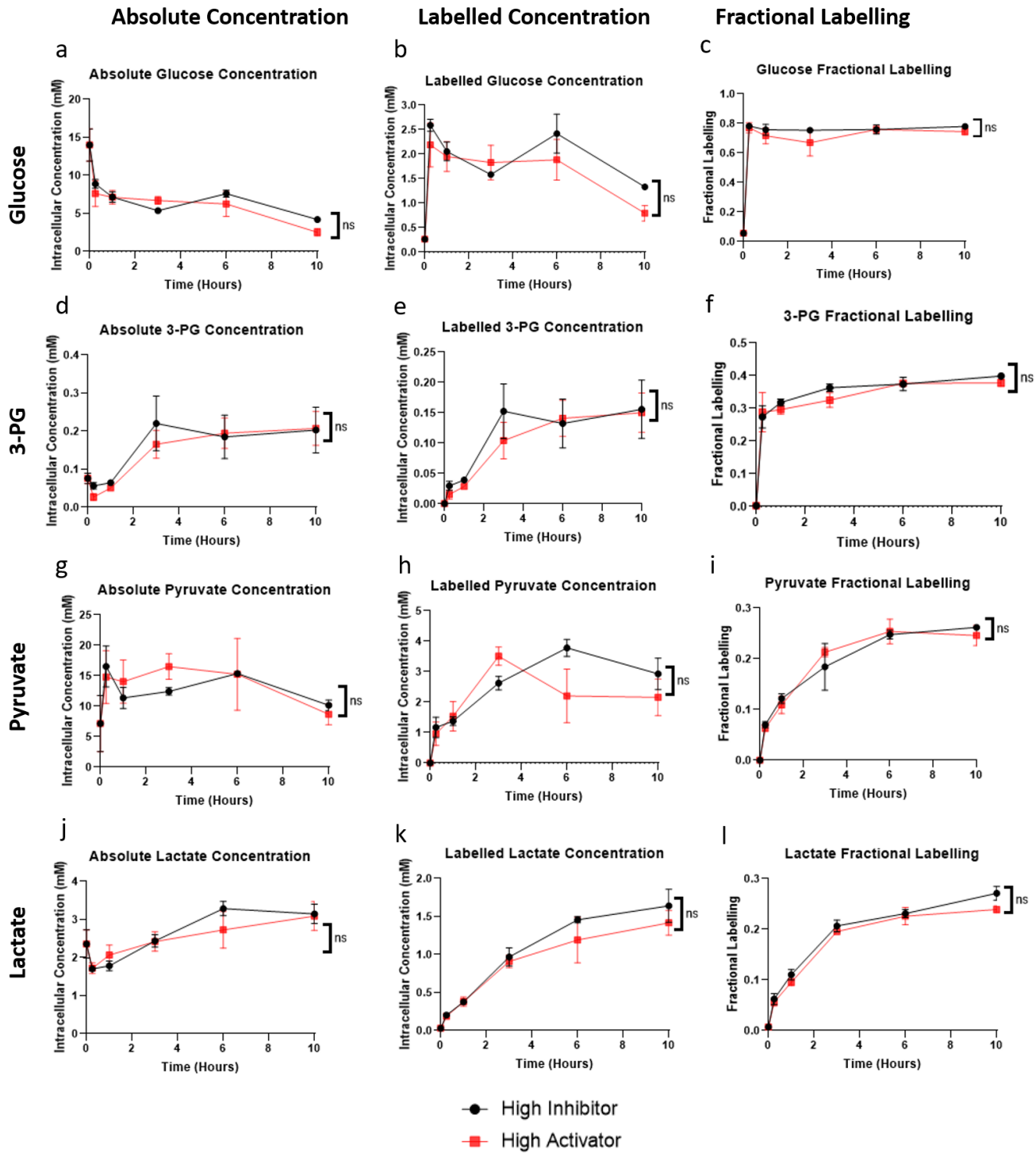
Absolute Concentration
Labelled Concentration
Fractional Labelling
Glucose
3-PG
Pyruvate
Lactate
a
Absolute Glucose Concentration
b
Labelled Glucose Concentration
c
Glucose Fractional Labelling
d
Absolute 3-PG Concentration
e
Labelled 3-PG Concentration
f
3-PG Fractional Labelling
g
Absolute Pyruvate Concentration
h
Labelled Pyruvate Concentraion
i
Pyruvate Fractional Labelling
j
Absolute Lactate Concentration
k
Labelled Lactate Concentration
l
Lactate Fractional Labelling
Intracellular Concentration (mM)
Fractional Labelling
Time (Hours)
ns
High Inhibitor
High Activator

Figure 4.8: Intracellular measurements of glycolytic intermediates over 24 hours. LN229 cells were seeded at 800,000 cells per well and treated with either 5:1 or 1:5 alanine to serine ratio in the media. Metabolism was quenched and harvested after 30 minutes, 1 hour, 3 hours, 6 hours and 24 hours incubation before analysis via GC-MS. Data for activating 1:5 condition is in red and inhibitory 5:1 condition in black. The absolute intracellular concentration of a) glucose, d) 3-PG, g) pyruvate and j) lactate. The labelled intracellular concentration of b) glucose, e) 3-PG, h) pyruvate, k) lactate. The fractional labelling data for c) glucose, f) 3-PG, j) pyruvate and m) lactate. ns = not significant.

4.10 24-hour data does not confirm trends seen in labelled serine generation

Metabolites that can be generated directly from glycolytic intermediates, such as alanine and serine, were investigated in the previous iteration of this experiment. As in the 6-hour time course, the rate at which labelled alanine is generated is higher in the high inhibitor treatment media at 0.94 ± 0.007 $hours^{-1}$, compared to the high activator condition at 0.68 ± 0.028 $hours^{-1}$ (Figure 4.9b). However, there is no difference between the two conditions in terms of fractional labelling (Figure 4.9c). As in Figure 3.6c, this means that the high inhibitor condition, there is a higher contribution of glucose carbons into alanine, but the relative contribution from other carbon sources do not change between the two conditions. This lack of significant difference in fractional labelling, could be as described in section 4.8.

Serine data observed in Figure 4.6f were not confirmed in the 24-hour time course (Figure 4.9f). The 6-hour data showed that there was a higher contribution of glucose carbons in terms of the entire cellular pool in the high inhibitor condition, although this observation was only a trend and the difference between conditions is not significant (Figure 4.6f). The fractional labelling of serine does not appear to be stable in the high activator condition and therefore it cannot be confirmed that the isotopic steady state of serine has been reached (Figure 4.9f). There is a significant difference in the rate of labelled serine generation favouring the high activator condition at 1.02 ± 0.35 $hours^{-1}$ compared to the high inhibitor condition at 0.08 ± 0.006 $hours^{-1}$ (Figure 4.9e). This confirms data in Figure 4.6f but raises questions about dilution of the labelled serine by the high concentration of serine given in the media. The trend observed at the 6-hour time course, where the rate of labelled serine generation was higher in the high inhibitor treatment condition was not corroborated in these 24-hour data.

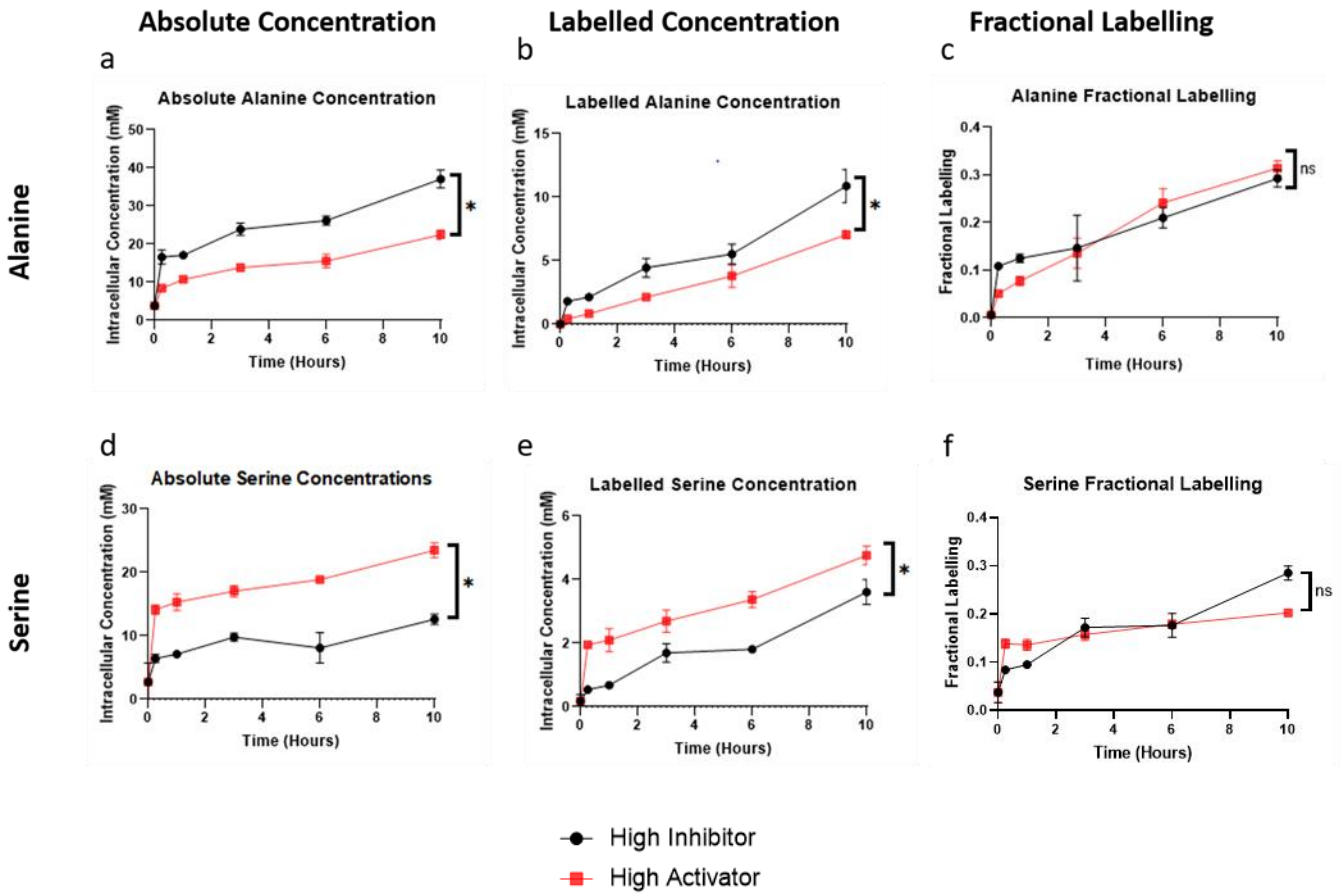

Figure 4.9: Intracellular data of alanine and serine over 24 hours. LN229 cells were seeded at 800,000 cells per well and treated with either 5:1 or 1:5 alanine to serine ratio in the media. Metabolism was quenched and harvested after 30 minutes, 1 hour, 3 hours, 6 hours and 24 hours incubation before analysis via GC-MS. The absolute concentrations of a) alanine and d) serine. The labelled concentration of b) alanine and e) serine. The fractional labelling data of c) alanine and f) serine. High activator condition depicted by red data points and high inhibitor by the black data point. * = p value <0.05. ns = not significant.

4.11 TCA cycle intermediates show trends of higher production in high activator conditions at 24 hours

Citrate reaches a steady state within 10 hours (Figure 4.10c), however there is no difference between the two treatment conditions. The amount of labelled citrate increases over time (Figure 4.10b), however unlike in the 6-hour data (Figure 4.7b), the trend of an increase rate of labelled citrate production was not as clear.

The fractional labelling data for α-KG cannot confirm whether α-KG has reached an isotopic steady state within 10 hours (Figure 4.10f). The labelling data from the 6-hour time course suggest that steady state is being reached, so the data in Figure 4.10f do not confirm this. Whereas the 6-hour time course showed a significant difference between the labelled α-KG production rate favouring the high activator condition, the 24-hour data did not confirm this and there was no significant difference between the two conditions (Figure 4.10e).

An isotopic steady state was reached for succinate (Figure 4.10i), and there is a trend, albeit not significant for an increased production of labelled succinate in the high activator treatment condition (Figure 4.10h). Similar observations can be made for malate and fumarate. They both reach an isotopic steady state within 10 hours (Figure 4.10l and Figure 4.10o), however, they both show a trend in increased labelled fumarate and malate production in the high activator condition although not significant (Figure 4.10k and Figure 4.10n).

These data for the 24-hour time course suggest that high PKM2-activator treatment conditions may increase the amount of labelled TCA cycle intermediates generated, however these data were not significant. It is possible that repeating this experiment with a more severe alanine to serine ratio in the treatment media may increase the differences seen in labelled TCA cycle intermediate production rates.

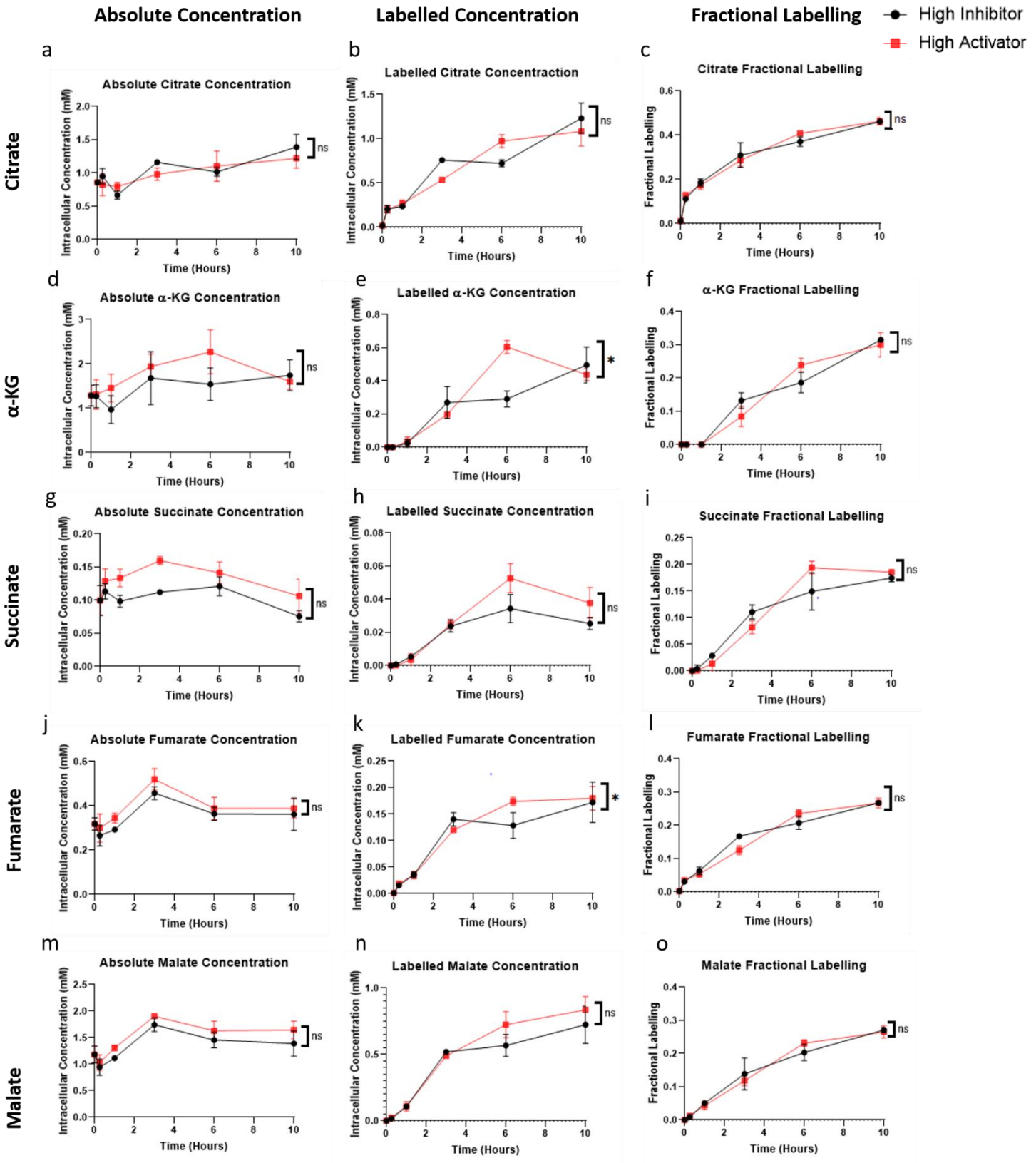
Absolute Concentration
Labelled Concentration
Fractional Labelling
High Inhibitor
High Activator
Citrate
α-KG
Succinate
Fumarate
Malate
a
Absolute Citrate Concentration
b
Labelled Citrate Concentraction
c
Citrate Fractional Labelling
d
Absolute α-KG Concentration
e
Labelled α-KG Concentration
f
α-KG Fractional Labelling
g
Absolute Succinate Concentration
h
Labelled Succinate Concentration
i
Succinate Fractional Labelling
j
Absolute Fumarate Concentration
k
Labelled Fumarate Concentration
l
Fumarate Fractional Labelling
m
Absolute Malate Concentration
n
Labelled Malate Concentration
o
Malate Fractional Labelling
Intracellular Concentration (mM)
Fractional Labelling
Time (Hours)
ns
*

Figure 4.10: Intracellular data for TCA cycle intermediates over 24 hours. LN229 cells were seeded at 800,000 cells per well and treated with either 5:1 or 1:5 alanine to serine ratio in the media. Metabolism was quenched and harvested after 30 minutes, 1 hour, 3 hours, 6 hours and 24 hours incubation before analysis via GC-MS. Data for activating 1:5 condition is in red and inhibitory 5:1 condition in black. The absolute concentration of a) citrate, d) α-KG, g) succinate, j) fumarate, m) malate. The labelled concentration of b) citrate, e) α-KG, h) succinate, k) fumarate, n) malate. The fractional labelling of c) citrate, f) α-KG, i) succinate, l) fumarate and o) malate. * = p value < 0.05. ns = not significant.

4.12 Discussion

The purpose of the experiments described in this chapter was to investigate how PKM2-activating and -inhibitory amino acid ratios within the cell affect glucose metabolism. LN229 cells were treated with a ratio of 5:1 alanine to serine, or vice versa to mimic a PKM2-inhibitory, or PKM2-activating environment within the cell. LN229 cells were chosen as they have been previously shown to have the well-known PKM2 allosteric activator F 1,6 BP, at saturating concentrations within the cell. These cells were also shown to have intracellular amino acid concentrations, specifically serine and phenylalanine around their respective K_D values for PKM2 [53]. The work in this study led to the hypothesis that instead of F 1,6 BP causing the small changes in PKM2 activity, it is the amino acids within the cell, which have their own allosteric binding pocket on PKM2, that give rise to this regulation. Not only the presence of that amino acid, but the ratio between activating and inhibitory amino acids achieve this fine-tuned regulation of PKM2 activity. Other studies have demonstrated, that ratios of activating and inhibitory amino acids can combine to regulate PKM2 in a biochemical study with isolated enzyme [37], however, this will be the first work to manipulate the intracellular amino acid concentration to create this amino acid ratio, and investigate the effects on wider metabolism. This aims to increase clarity on the effect PKM2 has in aerobic glycolysis and Warburg metabolism.

The first step was to confirm that by manipulating the media for cell treatment that the intracellular concentration of alanine and serine reflected this change. Figure 4.2 shows that the intracellular concentration of alanine and serine were changed from time zero, and achieved a steady state within 15 minutes incubation. The intracellular concentration ratio was not 5:1 or 1:5 as in the media. There was a calculated 10:1 alanine to serine ratio achieved in the intended 5:1 condition and 1:2 alanine to serine ratio achieved in the 1:5 intended condition. An intracellular concentration of each amino acid

was not expected to match the media concentration as amino acids do not pass freely through the membrane in equilibrium. Cells were given minimal amino acids in the seeding of the experiments to allow depletion of other amino acids. Many other amino acids have activating and inhibitory effects on PKM2, and therefore the purpose of depleting these amino acids and supplementing only alanine and serine, allows any changes in metabolism seen to be focussed towards effects of these two amino acids. The amino acid landscape at time zero was plotted in Figure 4.4 and shows that the intracellular concentration of alanine and serine reach their maximal concentration in the mM range within 15 minutes of treatment. As other amino acids are not supplemented, especially essential amino acids such as PKM2-inhibitor phenylalanine, these amino acids deplete over time, decreasing further any effects they may have on PKM2. Due to the lack of other amino acids in these experiments, a growth curve experiment was completed on LN229 cells using an Incucyte to monitor cell growth in different media conditions. PKM2-activating and -inhibitory alanine to serine ratios were given either with supplemented amino acids to the level of the usual culture media or without. The control of the normal culture media was used for comparison. As expected, the conditions with supplemented amino acids behaved similarly to the usual culture media. However, the conditions where alanine and serine were the only amino acids given, the cells did not reach 100 % confluency and reached a stationary growth phase faster than that of the supplemented conditions. These data suggest that the cells were depleted of nutrients in the conditions with only alanine and serine present from 24 hours and confirmed that a 24-hour time course could be used. However, metabolomics data after 24 hours incubation in treatment conditions showed that glucose becomes limiting, as do other amino acids and therefore likely cause cell stress. Most labelled metabolites at the 24-hour time point decrease significantly, and although this is not due to a lack of cells, as can be confirmed in Figure 4.2, it is likely the cells are stressed and are possibly in metabolic crisis [71], [72]. Therefore, for intracellular concentration measurements, the 24-hour time point was removed, and rate calculations generated with data up to the 10-hour time point.

Once it was established that the intracellular alanine and serine concentration were altered appropriately, LN229 cells were treated with ^{13}C-glucose and PKM2-activating or

-inhibitory alanine to serine ratios and their metabolism quenched at various time intervals. These samples were analysed by GC-MS and no significant difference in the consumption of glucose or production of glycolytic intermediates within 10 hours between the two treatment conditions was observed. Therefore, these data indicate that the treatment conditions used here were not sufficient to illicit a change in glycolytic flux.

It is understood that when glycolysis is slowed down, carbons are funnelled away from glycolysis through various branching pathways including the serine production pathway, the pentose phosphate pathway and the generation of alanine [58]. To determine if high inhibitor conditions increased the rate at which various metabolites are generated through pathways branching from glycolysis, the intracellular concentrations of labelled alanine, serine and G3P were calculated. In the 6-hour time course, serine was generated at a higher rate in the high inhibitor condition, compared to that of the high activator condition. This would suggest that the high inhibitor condition is causing an increase in carbons being metabolised through the serine production pathway. The generation of G3P was also measured to probe the pentose phosphate pathway, however there was no difference between the two treatment conditions. The other metabolite that can be synthesised from glycolytic intermediates that we can investigate is alanine. Although the concentration of labelled alanine was higher in the high inhibitor condition, the fraction of labelled alanine in relation to the total pool of alanine was the same between the two conditions. Using such a high concentration of alanine in the media, increases the amount of unlabelled alanine in the cell. If, between the two conditions, the alanine pool were the same, we would expect that the 5:1 high inhibitor condition would have a lower labelled fraction. However, in these data the labelled fraction is very similar between the two conditions, the absolute alanine concentration measurements confirm that the alanine pool in the 5:1 high inhibitor condition is not the same size, and therefore the unlabelled alanine from the media must be being used, consumed or effluxed from the cell. This complicates understanding the alanine data, however, there appears to be no difference in labelled alanine generation between the two conditions.

If carbons from glucose are routed through oxidative phosphorylation, rather than aerobic glycolysis, they pass through the TCA cycle, therefore TCA cycle intermediates were measured to determine if high activator and high inhibitor treatment conditions had

any influence. If amino acids within the cell are regulating PKM2 activity and by extension glycolysis, this might also encompass the TCA cycle. Data from both the 6-hour and 24-hour time course suggest that in the high activator media conditions, there is an increase in labelled TCA cycle intermediates.

Data presented here support the hypothesis that the high activator ratio of alanine and serine in cells increases the generation of pyruvate and other downstream TCA cycle intermediates. Data also support the hypothesis that high inhibitor ratios of alanine to serine in cells allows an increase in carbons through branching metabolic pathways, as seen in the increased serine generation in this condition at 6 hours. This system used to investigate glucose metabolism, in starving of most amino acids is not as phenotypically relevant as a system with all amino acids present, it can also induce metabolic stress. Starvation of amino acids, and glucose deprivation, as seen in these data at 24 hours, can inhibit mTORC1 activation and cause multiple downstream signalling cascades resulting in halted cell growth and proliferation [73], [74]. A solution to this is to supplement amino acids to their usual culture conditions to ensure amino acid starvation is not influencing general cell metabolism and glycolysis. However, concentrations of other PKM2-regulating amino acids should be monitored here to ensure the balance of PKM2-activating and inhibitory amino acids is understood. Another approach is to use a cancer cell line identified from the cancer cell line database such as LOUCY, which may have an appropriate endogenous intracellular A:S ratio due to the expression of enzymes involved in the production of alanine and serine. Although the cell lines identified in Figure 3.1 can be bucketed based on prediction of PKM2 activity, this would need to be confirmed experimentally using methods similar to presented section 4.3 to confirm the intracellular concentration of alanine and serine and calculate the ratio of those amino acids.

The data presented here demonstrate a correlation between a media condition that contains a high activator ratio of alanine and serine, and an increase in the TCA cycle. It also demonstrates an increase in serine generation through the PPP in a high inhibitor media condition. However, these data do not confirm that it is PKM2 regulation causing these effects. Using PKM2 small molecule activators such as TEPP-46 [23] or inhibitors such as shikonin [75], would build confidence in these data. Data in a study by Kung et al, 2012 [76] show that small molecule activation of PKM2 decreased serine production

through the SPP. Further confirmation of this phenomena could come from PKM2 mutants generated in a study by Macpherson et al 2018 [53]. These mutants A327S and C358A, were identified to retain the ability to be regulated by F 1,6 BP, but have lost the ability to be regulated by amino acids. Using these mutants expressed in cells to confirm this phenotype would give reason to believe PKM2 regulation is the cause of the phenotypes seen in these data.

6. Final summary and future directions

PKM2 and the association with glycolytic regulation implicates itself in Warburg metabolism. Aerobic glycolysis has long been a key area of research in the understanding of cancer and treatment discovery and therefore understanding how PKM2 fits into this complex landscape is important to identify it as a drug target for the treatment of cancers. As PKM2 is exclusively expressed, over its alternatively spliced isoform PKM1, in highly proliferative tissue like cancerous cells, PKM2 could provide a selectivity window in treatment between healthy differentiated tissues and cancer. However, the understanding of the metabolic role PKM2 plays in cancerous cells is not completely understood. There is vast literature encompassing PKM2, some of it contradictory. Therefore, the data presented in this thesis aims to create some clarity on the regulation of PKM2 and the relationship, in a whole-cell metabolism context, with amino acids. Literature shows that PKM2 can bind activating and inhibitory amino acids to a single allosteric binding pocket, and this affects PKM2 activity in a recombinant protein and cell-free system. The data in this thesis investigates the effects of activating amino acid serine, and inhibitory amino acid alanine, on endogenous PKM2 by measuring the intracellular concentration of glycolytic, TCA cycle and other related metabolites. These data suggest that although there is no effect in this system seen on glycolytic intermediates, the production of serine from glucose is increased when PKM2 is inhibited with high alanine concentrations. And conversely, TCA cycle intermediates are increased in the presence of more PKM2 activator, serine. The system used in these experiments are complex and can be better controlled, for example by maintaining the concentrations of other amino acids. However,

this comes with other complications, as it is not only alanine and serine that can influence PKM2 activity. The purpose of using a 1:5 or 5:1 ratio of alanine to serine has been shown in literature to shift PKM2 from high to low activity and with other amino acids present, this ratio will be difficult to control [30]. Due to the experimental setup conducted in this thesis, my hypothesis that it is the ratio of activating and inhibitory amino acids that regulate PKM2 and therefore glycolytic flux, remains unanswered. To answer this question there are multiple alternate routes that can be taken. These include using cells with an endogenous differences in their alanine to serine ratio that were identified in this thesis using the COSMIC cell line database, rather than attempting to induce an alternate amino acid ratio via the media. Another, is to use small molecules like PKM2 activator TEPP-46, or inhibitor Shikonin, to overcome any changes observed by an amino acid ratio, this would relate the phenotype observed specifically to PKM2. Finally, using mutants described in literature [30], that retain the ability to be regulated by FBP, but have lost the ability to be regulated by amino acids.

Bibliography

[1] D. Hanahan and R. A. Weinberg, “The hallmarks of cancer,” *Cell*. 2000. doi: 10.1016/S0092-8674(00)81683-9.

[2] D. Hanahan and R. A. Weinberg, “Hallmarks of Cancer: The Next Generation,” *Cell*, vol. 144, no. 5, pp. 646–674, 2011, doi: https://doi.org/10.1016/j.cell.2011.02.013.

[3] C. Marbaniang and L. Kma, “Dysregulation of glucose metabolism by oncogenes and tumor suppressors in cancer cells,” *Asian Pacific Journal of Cancer Prevention*, vol. 19, no. 9. Asian Pacific Organization for Cancer Prevention, pp. 2377–2390, Sep. 01, 2018. doi: 10.22034/APJCP.2018.19.9.2377.

[4] A. M. Otto, “Warburg effect(s)—a biographical sketch of Otto Warburg and his impacts on tumor metabolism,” *Cancer & Metabolism*, vol. 4, no. 1, Dec. 2016, doi: 10.1186/s40170-016-0145-9.

[5] V. R. Fantin, J. St-Pierre, and P. Leder, “Attenuation of LDH-A expression uncovers a link between glycolysis, mitochondrial physiology, and tumor maintenance,” *Cancer Cell*, vol. 9, no. 6, pp. 425–434, Jun. 2006, doi: 10.1016/j.ccr.2006.04.023.

[6] Y. S. eok Ju *et al.*, “Origins and functional consequences of somatic mitochondrial DNA mutations in human cancer,” *eLife*, vol. 3, 2014, doi: 10.7554/eLife.02935.

[7] X. D. Xu *et al.*, “Warburg effect or reverse warburg effect? a review of cancer metabolism,” *Oncology Research and Treatment*, vol. 38, no. 3. S. Karger AG, pp. 117–122, Mar. 24, 2015. doi: 10.1159/000375435.

[8] C. Jose, N. Bellance, and R. Rossignol, “Choosing between glycolysis and oxidative phosphorylation: A tumor’s dilemma?,” *Biochimica et Biophysica Acta - Bioenergetics*, vol. 1807, no. 6. Elsevier B.V., pp. 552–561, 2011. doi: 10.1016/j.bbabio.2010.10.012.

[9] E. Obre and R. Rossignol, “Emerging concepts in bioenergetics and cancer research: Metabolic flexibility, coupling, symbiosis, switch, oxidative tumors, metabolic remodeling, signaling and bioenergetic therapy,” *International Journal of Biochemistry and Cell Biology*, vol. 59. Elsevier Ltd, pp. 167–181, Feb. 01, 2015. doi: 10.1016/j.biocel.2014.12.008.

[10] X. L. Zu and M. Guppy, “Cancer metabolism: Facts, fantasy, and fiction,” *Biochemical and Biophysical Research Communications*, vol. 313, no. 3. Academic Press Inc., pp. 459–465, Jan. 16, 2004. doi: 10.1016/j.bbrc.2003.11.136.

[11] D. Goldman, “Theoretical models of microvascular oxygen transport to tissue,” *Microcirculation*, vol. 15, no. 8, pp. 795–811, 2008, doi: 10.1080/10739680801938289.

[12] R. H. Thomlinson and L. H. Gray, “The histological structure of some human lung cancers and the possible implications for radiotherapy,” *British Journal of Cancer*, vol. 9, no. 4, pp. 539–549, 1955, doi: 10.1038/bjc.1955.55.

[13] R. A. Gatenby and R. J. Gillies, “Why do cancers have high aerobic glycolysis?,” *Nature Reviews Cancer*, vol. 4, no. 11. Nature Publishing Group, pp. 891–899, Nov. 2004. doi: 10.1038/nrc1478.

[14] M. G. V. Heiden, L. C. Cantley, and C. B. Thompson, “Understanding the warburg effect: The metabolic requirements of cell proliferation,” in *Biochemistry*, 5th ed., NIH Public Access, 2002. doi: 10.1126/science.1160809.

[15] J. M. Berg, J. L. Tymoczko, and L. Stryer, “Gluconeogenesis and Glycolysis Are Reciprocally Regulated,” in *Biochemistry*, W H Freeman, 2002.

[16] J. M. Berg, J. L. Tymoczko, and L. Stryer, “The Glycolytic Pathway Is Tightly Controlled,” in *Biochemistry*, 5th ed., W H Freeman, 2002.

[17] L. B. Tanner *et al.*, “Four key steps control glycolytic flux in mammalian cells,” *Cell Systems*, vol. 7, no. 1, pp. 49–62, 2018, doi: 10.1016/j.cels.2018.06.003.Four.

[18] J. Monod, J. Wyman, and J. P. Changeux, “On the nature of allosteric transitions: A plausible model,” *Journal of Molecular Biology*, vol. 12, no. 1, pp. 88–118, May 1965, doi: 10.1016/S0022-2836(65)80285-6.

[19] I. Mor, E. C. Cheung, and K. H. Vousden, “Control of glycolysis through regulation of PFK1: Old friends and recent additions,” *Cold Spring Harbor Symposia on Quantitative Biology*, vol. 76, pp. 211–216, Jan. 2011, doi: 10.1101/sqb.2011.76.010868.

[20] Z. Zhang, X. Deng, Y. Liu, Y. Liu, L. Sun, and F. Chen, “PKM2, function and expression and regulation,” *Cell and Bioscience*, vol. 9, no. 1. BioMed Central Ltd., pp. 1–25, Jun. 26, 2019. doi: 10.1186/s13578-019-0317-8.

[21] H. R. Christofk *et al.*, “The M2 splice isoform of pyruvate kinase is important for cancer metabolism and tumour growth,” *Nature*, vol. 452, no. 7184, pp. 230–233, Mar. 2008, doi: 10.1038/nature06734.

[22] M. Cortés-Cros *et al.*, “M2 isoform of pyruvate kinase is dispensable for tumor maintenance and growth,” *Proceedings of the National Academy of Sciences of the United States of America*, vol. 110, no. 2, pp. 489–494, Jan. 2013, doi: 10.1073/pnas.1212780110.

[23] D. Anastasiou *et al.*, “Pyruvate kinase M2 activators promote tetramer formation and suppress tumorigenesis,” *Nature chemical biology*, vol. 8, no. 10, p. 839, 2012, doi: 10.1038/NCHEMBIO.1060.

[24] M. T. Snaebjornsson and A. Schulze, “Non-canonical functions of enzymes facilitate cross-talk between cell metabolic and regulatory pathways,” *Experimental and Molecular Medicine*, vol. 50, no. 4. Nature Publishing Group, p. 34, Apr. 01, 2018. doi: 10.1038/s12276-018-0065-6.

[25] D. Anastasiou *et al.*, “Inhibition of pyruvate kinase M2 by reactive oxygen species contributes to cellular antioxidant responses,” *Science (New York, N.Y.)*, vol. 334, no. 6060, p. 1278, Dec. 2011, doi: 10.1126/SCIENCE.1211485.

[26] B. M. Gassaway *et al.*, “Distinct Hepatic PKA and CDK Signaling Pathways Control Activity-Independent Pyruvate Kinase Phosphorylation and Hepatic Glucose Production,” *Cell reports*, vol. 29, no. 11, p. 3394, Dec. 2019, doi: 10.1016/J.CELREP.2019.11.009.

[27] G. Prakasam, M. A. Iqbal, R. N. K. Bamezai, and S. Mazurek, “Posttranslational Modifications of Pyruvate Kinase M2: Tweaks that Benefit Cancer,” *Frontiers in Oncology*, vol. 0, no. FEB, p. 22, Feb. 2018, doi: 10.3389/FONC.2018.00022.

[28] W. Yang, “Structural basis of PKM2 regulation,” *Protein and Cell*, vol. 6, no. 4, pp. 238–240, Apr. 2015, doi: 10.1007/s13238-015-0146-4.

[29] J. D. Dombrauckas, B. D. Santarsiero, and A. D. Mesecar, “Structural basis for tumor pyruvate kinase M2 allosteric regulation and catalysis,” *Biochemistry*, vol. 44, no. 27, pp. 9417–9429, Jun. 2005, doi: 10.1021/bi0474923.

[30] J. A. Macpherson *et al.*, “Functional cross-talk between allosteric effects of activating and inhibiting ligands underlies PKM2 regulation,” *eLife*, vol. 8, Jul. 2019, doi: 10.7554/eLife.45068.

[31] S. Fushinobu, H. Nishimasu, D. Hattori, H.-J. Song, and T. Wakagi, “Structural basis for the bifunctionality of fructose-1,6-bisphosphate aldolase/phosphatase,” *Nature 2011 478:7370*, vol. 478, no. 7370, pp. 538–541, Oct. 2011, doi: 10.1038/nature10457.

[32] P. Wang, C. Sun, T. Zhu, and Y. Xu, “Structural insight into mechanisms for dynamic regulation of PKM2,” *Protein and Cell*, vol. 6, no. 4, pp. 275–287, Apr. 2015, doi: 10.1007/s13238-015-0132-x.

[33] W. Yang, “Structural basis of PKM2 regulation,” *Protein and Cell*, vol. 6, no. 4, pp. 238–240, Apr. 2015, doi: 10.1007/s13238-015-0146-4.

[34] H. P. Morgan *et al.*, “M2 pyruvate kinase provides a mechanism for nutrient sensing and regulation of cell proliferation,” *Proceedings of the National Academy of Sciences of the United States of America*, vol. 110, no. 15, pp. 5881–5886, Apr. 2013, doi: 10.1073/PNAS.1217157110/-/DCSUPPLEMENTAL.

[35] M. Yuan *et al.*, “An allostatic mechanism for M2 pyruvate kinase as an amino-acid sensor,” *Biochemical Journal*, vol. 475, no. 10, pp. 1821–1837, May 2018, doi: 10.1042/BCJ20180171.

[36] M. Yuan *et al.*, “An allostatic mechanism for M2 pyruvate kinase as an amino-acid sensor,” *Biochemical Journal*, vol. 475, no. 10, p. 1821, May 2018, doi: 10.1042/BCJ20180171.

[37] M. Yuan *et al.*, “An allostatic mechanism for M2 pyruvate kinase as an amino-acid sensor,” *Biochemical Journal*, vol. 475, no. 10, pp. 1821–1837, May 2018, doi: 10.1042/BCJ20180171.

[38] S. Bröer and A. Bröer, “Amino acid homeostasis and signalling in mammalian cells and organisms,” *Biochemical Journal*, vol. 474, no. 12. Portland Press Ltd, pp. 1935–1963, Jun. 15, 2017. doi: 10.1042/BCJ20160822.

[39] D. Y. Boudko, “Molecular basis of essential amino acid transport from studies of insect nutrient amino acid transporters of the SLC6 family (NAT-SLC6),” *Journal of Insect Physiology*, vol. 58, no. 4. NIH Public Access, pp. 433–449, Apr. 2012. doi: 10.1016/j.jinsphys.2011.12.018.

[40] T. M. Hoffmann *et al.*, “Effects of Sodium and Amino Acid Substrate Availability upon the Expression and Stability of the SNAT2 (SLC38A2) Amino Acid Transporter,” *Frontiers in Pharmacology*, vol. 9, no. FEB, p. 63, Feb. 2018, doi: 10.3389/fphar.2018.00063.

[41] T. Takahara, Y. Amemiya, R. Sugiyama, M. Maki, and H. Shibata, “Amino acid-dependent control of mTORC1 signaling: a variety of regulatory modes,” *Journal of Biomedical Science 2020 27:1*, vol. 27, no. 1, pp. 1–16, Aug. 2020, doi: 10.1186/S12929-020-00679-2.

[42] I. Amelio, F. Cutruzzolá, A. Antonov, M. Agostini, and G. Melino, “Serine and glycine metabolism in cancer §,” *Trends in Biochemical Sciences*, vol. 39, pp. 191–198, 2014, doi: 10.1016/j.tibs.2014.02.004.

[43] G. Guiducci *et al.*, “The moonlighting RNA-binding activity of cytosolic serine hydroxymethyltransferase contributes to control compartmentalization of serine metabolism,” *Nucleic Acids Research*, vol. 47, no. 8, p. 4240, Aug. 2019, doi: 10.1093/NAR/GKZ129.

[44] L. R. Gray, S. C. Tompkins, and E. B. Taylor, “Regulation of pyruvate metabolism and human disease,” *Cellular and Molecular Life Sciences*, vol. 71, no. 14, p. 2577, Jul. 2014, doi: 10.1007/S00018-013-1539-2.

[45] X. Zhou, S. Curbo, F. Li, S. Krishnan, and A. Karlsson, “Inhibition of glutamate oxaloacetate transaminase 1 in cancer cell lines results in altered metabolism with increased dependency of glucose,” *BMC Cancer 2018 18:1*, vol. 18, no. 1, pp. 1–14, May 2018, doi: 10.1186/S12885-018-4443-1.

[46] M. J. Lukey, W. P. Katt, and R. A. Cerione, “Targeting amino acid metabolism for cancer therapy,” *Drug discovery today*, vol. 22, no. 5, p. 796, May 2017, doi: 10.1016/J.DRUDIS.2016.12.003.

[47] D. KH *et al.*, “Amino acids as signaling molecules modulating bone turnover,” *Bone*, vol. 115, pp. 15–24, Oct. 2018, doi: 10.1016/J.BONE.2018.02.028.

[48] B. Alberts, A. Johnson, J. Lewis, M. Raff, K. Roberts, and P. Walter, “From RNA to Protein,” in *Molecular Biology of the Cell*, 4th ed., Garland Science, 2002. Accessed: Oct. 07, 2021. [Online]. Available: https://www.ncbi.nlm.nih.gov/books/NBK26829/

[49] D. D. Church *et al.*, “Essential Amino Acids and Protein Synthesis: Insights into Maximizing the Muscle and Whole-Body Response to Feeding,” *Nutrients*, vol. 12, no. 12, pp. 1–14, Dec. 2020, doi: 10.3390/NU12123717.

[50] H. A. Hansen and C. Emborg, “Extra- and intracellular amino acid concentrations in continuous Chinese hamster ovary cell culture,” *Applied Microbiology and Biotechnology 1994 41:5*, vol. 41, no. 5, pp. 560–564, Jul. 1994, doi: 10.1007/BF00178489.

[51] H. Eagle, K. A. Piez, and M. Levy, “The Intracellular Amino Acid Concentrations Required for Protein Synthesis in Cultured Human Cells,” *Journal of Biological Chemistry*, vol. 236, no. 7, pp. 2039–2042, Jul. 1961, doi: 10.1016/S0021-9258(18)64126-2.

[52] R. J. DeBerardinis and N. S. Chandel, “Fundamentals of cancer metabolism,” *Science Advances*, vol. 2, no. 5, May 2016, doi: 10.1126/SCIADV.1600200.

[53] M. JA *et al.*, “Functional cross-talk between allosteric effects of activating and inhibiting ligands underlies PKM2 regulation,” *bioRxiv*, Jul. 2018, doi: 10.1101/378133.

[54] E. K. Wiese *et al.*, “Enzymatic activation of pyruvate kinase increases cytosolic oxaloacetate to inhibit the Warburg effect,” *Nature Metabolism*, vol. 3, no. 7, pp. 954–968, Jul. 2021, doi: 10.1038/s42255-021-00424-5.

[55] M. v. Liberti and J. W. Locasale, “The Warburg Effect: How Does it Benefit Cancer Cells?,” *Trends in Biochemical Sciences*, vol. 41, no. 3. Elsevier Ltd, pp. 211–218, Mar. 01, 2016. doi: 10.1016/j.tibs.2015.12.001.

[56] J. M. Berg, J. L. Tymoczko, and L. Stryer, “The Metabolism of Glucose 6-Phosphate by the Pentose Phosphate Pathway Is Coordinated with Glycolysis,” in *Biochemistry*, 5th ed., W H Freeman, 2002. Accessed: Oct. 07, 2021. [Online]. Available: https://www.ncbi.nlm.nih.gov/books/NBK22590/

[57] M. A. Reid *et al.*, “Serine synthesis through PHGDH coordinates nucleotide levels by maintaining central carbon metabolism,” *Nature Communications*, vol. 9, no. 1, pp. 1–11, Dec. 2018, doi: 10.1038/s41467-018-07868-6.

[58] Y. J. Chen, X. Huang, N. G. Mahieu, K. Cho, J. Schaefer, and G. J. Patti, “Differential incorporation of glucose into biomass during Warburg metabolism,” *Biochemistry*, vol. 53, no. 29, pp. 4755–4757, Jul. 2014, doi: 10.1021/bi500763u.

[59] T. Sunil, K. Reddy, G. Balammal, and A. Saravana Kumar, “ULTRA PERFORMANCE LIQUID CHROMATOGRAPHY: AN INTRODUCTION AND REVIEW,” pp. 24–31, Accessed: Dec. 10, 2021. [Online]. Available: www.ijpra.com

[60] S. Cubbon, C. Antonio, J. Wilson, and J. Thomas-Oates, “Metabolomic applications of HILIC-LC-MS,” *Mass spectrometry reviews*, vol. 29, no. 5, pp. 671–684, Sep. 2010, doi: 10.1002/MAS.20252.

[61] C. Lifshitz, “Basic aspects and principles of mass spectrometry applied to biomolecules,” *Mass Spectrometry Reviews*, vol. 22, no. 3, pp. 157–157, Jan. 2003, doi: 10.1002/MAS.10051.

[62] C. S. Ho *et al.*, “Electrospray Ionisation Mass Spectrometry: Principles and Clinical Applications,” *The Clinical Biochemist Reviews*, vol. 24, no. 1, p. 3, 2003, Accessed: Dec. 10, 2021. [Online]. Available: /pmc/articles/PMC1853331/

[63] J. J. Pitt, “Principles and Applications of Liquid Chromatography-Mass Spectrometry in Clinical Biochemistry,” *The Clinical Biochemist Reviews*, vol. 30, no. 1, p. 19, Feb. 2009, Accessed: Dec. 10, 2021. [Online]. Available: /pmc/articles/PMC2643089/

[64] A. Schreiber, “Higher Confidence in Identification with QTRAP ® LC/MS/MS Systems when Screening and Quantifying Pesticides in Fruit and Vegetable Samples.”

[65] H. Li *et al.*, “The landscape of cancer cell line metabolism,” *Nature medicine*, vol. 25, no. 5, pp. 850–860, May 2019, doi: 10.1038/S41591-019-0404-8.

[66] F. Grimm, L. Fets, and D. Anastasiou, “Gas Chromatography Coupled to Mass Spectrometry (GC–MS) to Study Metabolism in Cultured Cells,” Springer, Cham, 2016, pp. 59–88. doi: 10.1007/978-3-319-26666-4_5.

[67] B. Thiele, K. Füllner, N. Stein, M. Oldiges, A. J. Kuhn, and D. Hofmann, “Analysis of amino acids without derivatization in barley extracts by LC-MS-MS,” *Analytical and bioanalytical chemistry*, vol. 391, no. 7, pp. 2663–2672, Aug. 2008, doi: 10.1007/S00216-008-2167-9.

[68] A. Walvekar, Z. Rashida, H. Maddali, and S. Laxman, “A versatile LC-MS/MS approach for comprehensive, quantitative analysis of central metabolic pathways,” *Wellcome Open Research*, vol. 3, 2018, doi: 10.12688/WELLCOMEOPENRES.14832.1.

[69] S. A. Forbes *et al.*, “COSMIC: Somatic cancer genetics at high-resolution,” *Nucleic Acids Research*, vol. 45, no. D1, pp. D777–D783, Jan. 2017, doi: 10.1093/NAR/GKW1121.

[70] H. Kondo *et al.*, “Single-cell resolved imaging reveals intra-tumor heterogeneity in glycolysis, transitions between metabolic states, and their regulatory mechanisms,” *Cell reports*, vol. 34, no. 7, Feb. 2021, doi: 10.1016/J.CELREP.2021.108750.

[71] B. J. Altman and J. C. Rathmell, “Metabolic Stress in Autophagy and Cell Death Pathways,” *Cold Spring Harbor Perspectives in Biology*, vol. 4, no. 9, p. a008763, Sep. 2012, doi: 10.1101/CSHPERSPECT.A008763.

[72] D. Spitz, A. Simons, D. Mattson, and K. Dornfeld, “Glucose deprivation-induced metabolic oxidative stress and cancer therapy,” *Journal of cancer research and therapeutics*, vol. 5 Suppl 1, no. Suppl 1, p. 2, 2009, doi: 10.4103/0973-1482.55133.

[73] J. Liu, P. D. Stevens, X. Li, M. D. Schmidt, and T. Gao, “PHLPP-mediated dephosphorylation of S6K1 inhibits protein translation and cell growth.,” *Molecular and Cellular Biology*, vol. 31, no. 24, pp. 4917–4927, Oct. 2011, doi: 10.1128/MCB.05799-11.

[74] J. M. Orozco *et al.*, “Dihydroxyacetone phosphate signals glucose availability to mTORC1,” *Nature Metabolism 2020 2:9*, vol. 2, no. 9, pp. 893–901, Jul. 2020, doi: 10.1038/s42255-020-0250-5.

[75] X. Zhao *et al.*, “Shikonin Inhibits Tumor Growth in Mice by Suppressing Pyruvate Kinase M2-mediated Aerobic Glycolysis,” *Scientific Reports 2018 8:1*, vol. 8, no. 1, pp. 1–8, Sep. 2018, doi: 10.1038/s41598-018-31615-y.

[76] C. Kung *et al.*, “Small Molecule Activation of PKM2 in Cancer Cells Induces Serine Auxotrophy,” *Chemistry & biology*, vol. 19, no. 9, p. 1187, Sep. 2012, doi: 10.1016/J.CHEMBIOL.2012.07.021.

[77] Q. Su *et al.*, “The role of pyruvate kinase M2 in anticancer therapeutic treatments,” *Oncology Letters*, vol. 18, no. 6, p. 5663, 2019, doi: 10.3892/OL.2019.10948.